2012

Investigation of Colored Dissolved Organic Matter and Dissolved Organic Carbon Using Combination of Ocean Color Data and Numerical Model in the Northern Gulf of Mexico

Nazanin Chaichitehrani
Louisiana State University and Agricultural and Mechanical College

INVESTIGATION OF COLORED DISSOLVED ORGANIC MATTER AND DISSOLVED ORGANIC CARBON USING COMBINATION OF OCEAN COLOR DATA AND NUMERICAL MODEL IN THE NORTHERN GULF OF MEXICO

A Thesis

Submitted to the Graduate Faculty of the
Louisiana State University and
Agricultural and Mechanical College
in partial fulfillment of the
requirements for the degree of
Master of Science

in

The Department of Oceanography and Coastal Sciences

by
Nazanin Chaichitehrani
B.S., Karaj Azad University, 2001
M.S., Kish University, 2004
August 2012

ACKNOWLEDGEMENTS

I would like to express my sincere appreciation to my advisor, Dr. Eurico J. D'Sa, for his support and guidance throughout the research. I would also like to expand my gratitude to my committee members: Drs. Nan D. Walker and Kanchan Maiti for their constructive comments and helpful suggestions.

I would acknowledge support provided by a NASA grant NNX09AR7OG, and partial support from the Bureau of Ocean Energy Management Cooperative Agreement (1435-0104CA32806) and by a NASA grant (NNA07CN12A). I would also to thank Drs. Thomas Bianchi (Texas A&M University), Robert Chen (University of Massachusetts), Christopher Osburn (North Carolina State University), and Blake Schaffer (National Health and Environmental Effects Research Laboratory, FL, USA) for sharing CDOM and DOC through The Biological and Chemical Oceanography Data Management Office (BCO-DMO) website and personal communication. Also, I appreciate Dr. Dong S. KO (Naval Research Laboratory Stennis office, USA) for sharing NCOM data. I appreciate help from Dr. Seyed Mostafa Siadat Mousavi and Clint Edrington for their suggestions on my manuscript and their scientific comments.

Special thanks to my husband, Mohammad Nabi Allahdadi, my greatest source of encouragement and inspiration for all the support and endless patience. Last, but not least, my heartfelt gratitude goes to my mother, sister and brother for their love and support.

TABLE OF CONTENTS

ABSTRACT

The first part of this thesis includes evaluating and developing empirical band ratio algorithms for the estimation of colored dissolved organic matter (CDOM) and dissolved organic carbon (DOC) for SeaWiFS, MODIS and MERIS ocean color sensors for the northern Gulf of Mexico. For CDOM, matchup comparison between SeaWiFS-derived CDOM absorption coefficients and in situ absorption measurements at 412 nm ($a_{CDOM}(412)$) were examined using the D'Sa et al. (2006) and the Mannino et al. (2008) algorithms. These reflectance band ratio algorithms were also assessed to retrieve $a_{CDOM}(412)$ from MODIS and MERIS data using the $R_{rs}(488)/R_{rs}(555)$ and $R_{rs}(510)/R_{rs}(560)$ band ratios, respectively. Since DOC cannot be measured directly by remote sensors, CDOM as the colored component of DOC is utilized as a proxy to estimate DOC remotely. A seasonal relationship between CDOM and DOC was established for the summer and spring-winter with high correlation for both periods. Seasonal band ratio empirical algorithms to estimate DOC were thus developed. In the second part of this study, a numerical model to study CDOM dynamics in the northern Gulf of Mexico was examined. To derive surface CDOM concentration maps from simulated salinity output from the Navy Coastal Ocean Model (NCOM), a highly correlated linear inverse relationship between CDOM and salinity is required which was examined for both inner-shelf and outer-shelf areas for the spring-winter and the summer periods. Applying these relationships on NCOM simulated salinity resulted in hourly maps of CDOM exhibiting high consistency with CDOM patterns derived from SeaWiFS sensor. Overlaying the NCOM-derived CDOM maps on the simulated currents showed the profound effect of currents on CDOM advection. Cold fronts strongly impact CDOM advection in both the inner and outer shelves by flushing CDOM-laden waters out of the coastal bays.

CHAPTER 1: INTRODUCTION

1.1 Dissolved Organic Matter in Marine Environments

Dissolved organic matter (DOM) is considered as one the largest bioreactive and exchangeable reservoir of organic carbon on earth (Williams and Druffel, 1988, Carlson, 2002), and is recognized as organic matter which passes through a 0.45 µm filter (Figure1.1) (Carlson, 2002). DOM is a complex mixture of aromatic polymer and aliphatic organic compounds (Stedmon et al., 2003; Xing, 2010). These contain oxygen, nitrogen, and sulphur functional groups (Chen et al., 2003; Xing, 2010). This pool of organic carbon is comparable in size to the stock of CO_2 (inorganic carbon) in the atmosphere. Furthermore, DOM has a significant impact on marine food chains, as a substrate that supports heterotrophic bacterial growth (Azam, 1983; Wetzel et al. 1995; Hansell and Carlson, 2002). DOM serves as a biochemical buffer by immobilizing heavy metals, and changing their bioavailability and toxicity (Young et al., 2004; Laanen, 2007). In coastal environments, DOM originates from the biodegradation and breakdown of vascular or terrestrial plants, and is introduced into the ocean by rivers' runoff. Furthermore, primary production, zooplankton-related processes, such as grazing and excretion, cell lysis, and solubilization of particles are sources of DOM in marine systems (Stewart and Brown, 1969; Fogg, 1983; Jumars et al, 1989; Fuhrman, 1999; Carlson, 2002). DOM is removed through biotic consumption of DOM by free-living heterotrophic bacterioplankton, and abiotic removal processes (i.e., phototransformation and sorption onto particles) (Mopper et al., 1991; Keil and Kirchman, 1994; Moran and Zepp, 1997; Carlson, 2002). From early in the 20th century, many studies have been conducted to unfold the sources, chemical nature, and biogeochemical function of DOM in marine environments (Guo and Santschi, 1997; Hansell and Carlson, 2002; Ogawa and Tanoue, 2003; Conmy, 2008).

Regardless of DOM importance, there is a still little known about the chemical composition of DOM (Ogawa and Tanoue, 2003).

1.2 Determination of DOM

Since direct determination of the concentration each type of organic matter is challenging, DOM cannot be measured directly (Lannen, 2007). Thus, measurable quantity is needed to serve as a proxy for DOM abundance. Hence, dissolved organic carbon (DOC) which is a major element of organic matter is generally used to determine DOM (Ogawa and Tanoue 2003; Lannen, 2007). Since carbon makes up 60% of DOM, a positive linear relationship between DOC and DOM is assumed (Lannen, 2007). DOC can be measured via different methods (e.g., high temperature combustion) (Sugimura and Suzuki, 1988; Sharp, 1997). In addition, colored dissolved organic matter (CDOM) which makes up 60-80% of DOM is often used as an intermediary for estimation of DOM (Corbet, 2007; Lannen, 2007).

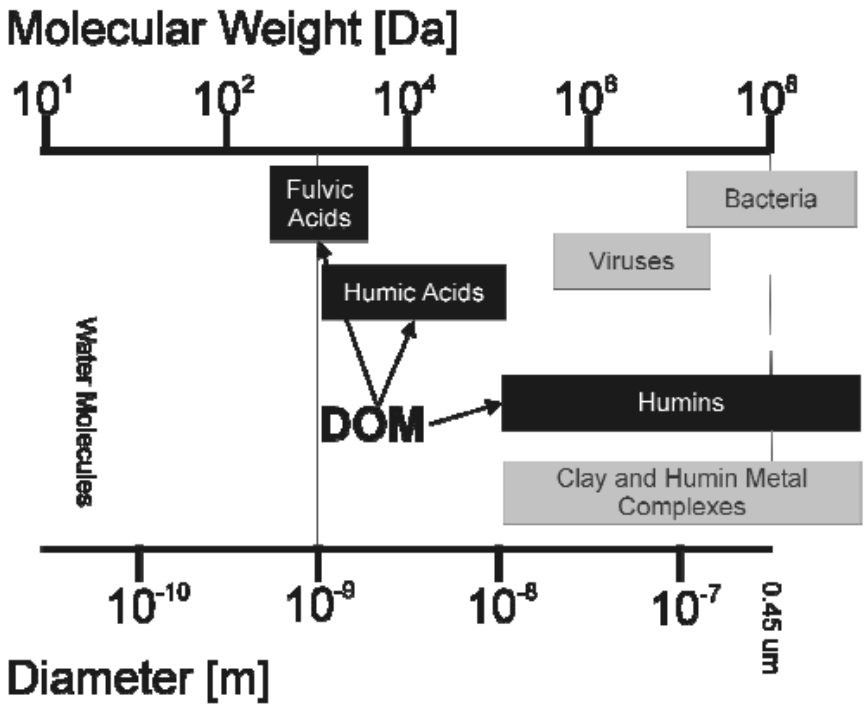

Figure1.1: The continuum of sizes and weights for DOM (after Steinberg 2003).

CDOM as a photoreactive portion of DOM is measured with optical techniques in laboratory, for example using a laboratory spectrometer (Corbet, 2007; Conmy, 2008). In addition, CDOM can also be retrieved from satellite ocean color sensor data directly (D'Sa and Miller, 2003; Kahru and Mitchell, 2001; Del Castillo and Miller, 2008). Of particular of interest is retrieving CDOM and DOC from satellite ocean color sensors to enhance our knowledge about carbon cycles, bulk DOM, and biogeochemical processes in aquatic environments.

1.3 Characteristic of Chromophoric Dissolved Organic Matter (CDOM)

1.3.1 Chemical Composition of CDOM

Colored organic compounds contain unsaturated groups, such as -C=C, -C=O, and -N=N-. Absorption of light in the ultraviolet (UV) and visible light is mainly due to double bonds between atoms of carbon (C=C) in aromatic phenolic and carboxylic moieties (Del Castillo, 2005; Shank et al., 2005). Double bonds are rich in electrons, and electrons in double bonds require less energy to excite than those in single bonds which increases the capability of molecules to absorb light (Del Castillo, 2005; Lannen, 2007). Since CDOM has multiple carbon bonds in the molecular structure, CDOM is considered as a major light-absorbing fraction of DOM pool in aquatic environments (Blough and Del Vecchio, 2002; Lannen, 2007). CDOM is described in the literature with different names. The term 'gelbstoff' was used by Kalle (1966) to describe yellow colored dissolved organic matter in water. Kirk (1976) used the phrase 'gilvin' to address yellow colored dissolved organic matter. Also, Humic substances (HS) is another term which is commonly used in limnology and soil sciences. The phrase CDOM (colored or chromophoric dissolved organic matter) is mostly used in remote sensing sciences (Conmy, 2008; Lannen, 2007). Humic and fulvic acids (Figure 1.2 and 1.3) are two major components of CDOM, and their different solubility characteristics at different pH, make them distinct from each other (Del Castillo, 2005).

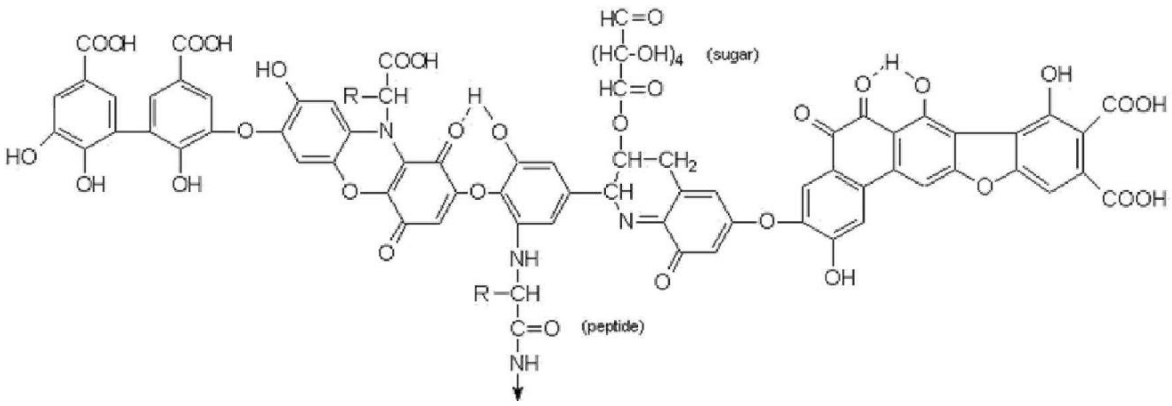

Figure 1.2: Model structure of humic acids (after Stevenson 1982).

Humic acids (HAs) are soluble at pH greater than 2, while fulvic acids (FAs) are soluble at any pH. Humic substances are characterized by higher molecular weight and higher aromatic content (carbon ring) (Blough and Del Vecchio, 2002). Humic acids have more double carbon bonds than the fulvic acids, which leads to high specific absorption. Humic acids are recognized as the refractory or recalcitrant compounds which are resistant to degradation by microbes and solar radiation, while fulvic acids are more labile with turn-over time of hours to days (Laanen, 2007).

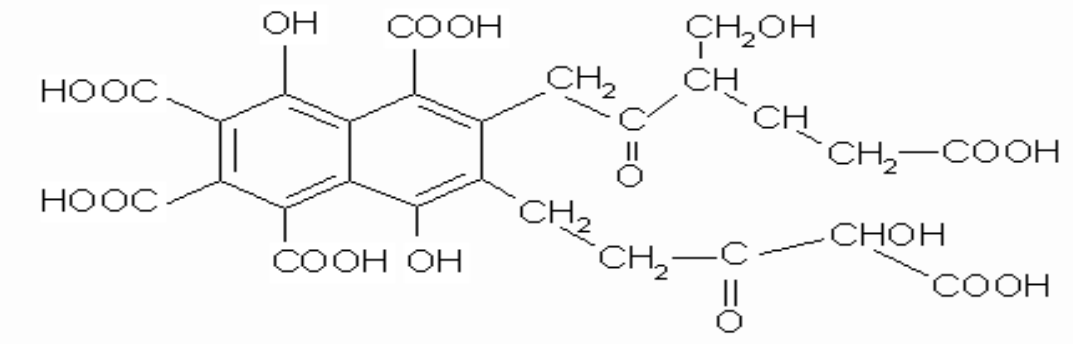

Figure 1.3: Model structure of fulvic acids (after McKnight and Aiken 1998).

Humic acids and fulvic acids are introduced into coastal water by river's runoffs which are leached from soils by precipitation (Coble et al., 2004; Nelson and Siegel, 2002). In the open ocean away from rivers' influence, humic and fulvic acids are released mostly by phytoplankton during cell autolysis (Nelson and Siegel, 2005; Lannen, 2007).

1.3.2 Optical properties of CDOM

CDOM absorbs visible light, UV-A (315 to 400 nm) and UV-B (280 to 315 nm) of the electromagnetic (EM) spectrum (Kirk, 1994). CDOM is defined operationally as organic matter that passes through 0.2 μm or 0.7 μm nominal pore sized filters, despite its origin and chemical composition (Blough and Del Vecchio, 2002). The absorption of light by CDOM ($a_{CDOM}(\lambda)$), phytoplankton ($a_{phy}(\lambda)$), non-algal particles (NAP) (or detrital), and by pure water (a_w) change the quality of light field in aquatic environments (Jerlov,1976; Kirk, 1994; Mobley, 1994). The total absorption (a) is modeled as (Equation 1.1):

$$a(\lambda) = a_w(\lambda) + a_{phy}(\lambda) + a_{nap}(\lambda) + a_{cdom}(\lambda) \quad (1.1)$$

Pure water absorbs light in the visible range strongly in the red and yellow. The absorption of light by pure water ($a_w(\lambda)$) is considered as a known constant (Pope and Fry, 1997; Nelson and Siegel, 2002). The green or golden green color of most phytoplankton is due to absorption of light by phytoplankton in blue, blue-green, as well as red (Nelson and Siegel, 2002). Non-algal particles (NAP; organic and inorganic matters) absorb light strongly in blue. NAP absorption decreases exponentially with increasing wavelengths. Since CDOM and NAP have similar composition, the shape of CDOM absorption spectrum is similar to that of NAP, and characterized by steeper exponential slope (Bricaud et al., 1981; Nelson and Siegel, 2002; D'Sa and Miller, 2005).

In general, the CDOM absorption spectrum (300-650 nm) is unstructured, and can be modeled using an exponential relationship (Equation 1.2) (Jerlov, 1968; Bricaud et al., 1981). Since chemical composition of CDOM varies spatially, the CDOM spectrum varies regionally (Gallegos, 2005; Conmy, 2008).

$$a(\lambda) = a(\lambda_\circ)e^{-s(\lambda-\lambda_\circ)} \quad (1.2)$$

where $a(\lambda)$ and $a(\lambda_o)$ are the absorption coefficient at wavelength λ and reference wavelength λ_o (m^{-1}), respectively. The spectral slope, S (nm^{-1}), provides us information about changes in the CDOM composition. The spectral slope also can be used to decipher the origin of CDOM (Nelson and Siegel, 2005). For examples, S decreases with increasing molecular weight, and increases with decreasing aromatic content (Blough and Green, 1995; Twardowski et al., 2004; Blough and Del Vecchio, 2002). Figure 1.4 shows CDOM absorption spectra for different regions (Corbett, 2007).

CDOM absorption coefficient has been used as a proxy to estimate CDOM concentration (Coble et al., 2004). Absorption coefficients ($a(\lambda)$) are calculated from following Equation (1.3) (Kirk, 1994) :

$$a(\lambda) = \frac{2.303A(\lambda)}{l} \qquad (1.3)$$

where A is the optical density or the absorbance (Log I_0/I), and l is the pathlength (m).

Optical properties of CDOM determine the quantity and quality of light field in natural waters. Branco and Kremer (2005) reported in the shallow estuaries over 70% of the variability in the diffuse attenuation coefficient of photosynthetically active radiation (K_{PAR}) can be attributed to CDOM. D'Sa et al. (2006) showed that CDOM plays a key role in regulating light attenuation in the northern Gulf of Mexico. In addition, CDOM may inhibit primary production by absorbing photosynthetically active radiation (PAR) mostly in estuarine and coastal waters. Furthermore, CDOM regulates the UV penetration, and protects phytoplankton and other biota from UV-induced DNA damage (Mopper et al., 1991; Zepp et al., 1995; D'Sa et al., 1999; Blough and Del Vecchio, 2002; Coble, 2007; Conmy et al., 2004) in marine environments, and alters structure and functioning of aquatic ecosystem (Klug and Cottingham, 2001). Moreover,

CDOM interferes with retrieval of chlorophyll-a by contaminating signals received by ocean color sensors (Carder et al., 1999; Siegel et al., 2002; Hu et al., 2006).

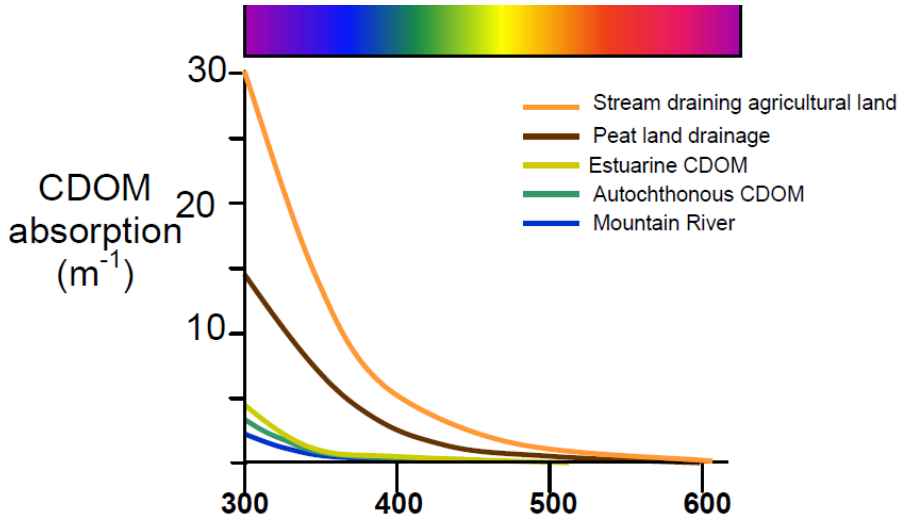

Figure 1.4: CDOM absorption spectra for different regions (adopted from Corbett 2007).

Since humic substances have negative charges, they make a complex with trace metals, such as iron and Copper (Corbett, 2007). In addition, CDOM reduces toxicity to phytoplankton and other biota by removing heavy metals and polyaromatic hydrocarbons (PAHs) (Coble et al., 2004). CDOM regulates bioavailability of nutrients, and may contribute to algal growth (Jolliff et al., 2003; Coble et al., 2004). Furthermore, CDOM can be served as a proxy for retrieving salinity using ocean color sensors (D'Sa et al., 2002; Hu et al., 2003, Bowers and Brett, 2008).

In the coastal environments, CDOM can be used as a tracer to track fresh water and circulation (Ferrari and Dowell, 1998; Stedmon et al., 2010; D'Sa and Korobkin, 2008; Conmy et al., 2004). In addition, CDOM absorption or fluorescence intensity can serve as an intermediary for dissolved organic carbon (DOC) (Vodacek et al., 1995; Ferrari, 2000; Rochelle-Newall and Fisher, 2002; Del Vecchio and Blough, 2004; Shank and Evans, 2011). Coble et al. (2004) suggested that CDOM can be utilized as an efficient tool for coastal resource

management. Hence, improving our knowledge about spatial distribution and temporal variations of CDOM is important.

1.4 Sources and Sinks of CDOM

1.4.1 Sources

In coastal environments, allochthonous CDOM originates mainly from the degradation of vascular or terrestrial plant. Terrestrial CDOM is introduced into the marine environment by river's runoff (Kirk, 1994; Coble et al., 2004; Stedmon et al., 2010). River borne CDOM is mainly composed of humic substances (Cauwet, 2002).

In the open ocean and regions away from the influences of rivers, autochthonous CDOM is released from phytoplankton during autolysis and viral lysis. In addition, CDOM is produced by zooplankton through grazing on phytoplankton, sloppy feeding, leaky fecal pellets, and excretion (Nelson et al., 1998; Urban-Rich, 1999; Steinberg et al., 2004; Del Castillo 2005; Lannen, 2007). High correlation between CDOM and chlorophyll has been reported in different aquatic environments (Kahru and Mitchell, 2001; Twardowski and Donaghay, 2001). Allochthonous or terrestrial CDOM generally consists of humic acids, while autochthonous CDOM contains fulvic acids (Lannen, 2007). Allochthonous CDOM is more complex than autochthonous CDOM, and is characterized by high molecular weight, more aromatic groups, and lower spectral slope (Del Castillo, 2005; Corbett, 2007). Sediment particles resuspension induced by wind, wave, and tidal mixing introduces CDOM into the water column (Boss et al., 2001; Burdige et al., 2004). In addition, anthropogenic inputs, sewage waters, and industrial waste can increase CDOM concentration (Corbett, 2007). Due to physical and complex mixing processes and biogeochemical transformation, it is challenging to clearly separate these various sources of CDOM in estuarine and coastal waters (Twardowsky and Donaghay et al., 2001; Chen et al., 2004)

1.4.2 Sinks

CDOM is removed from aquatic environments due to photodegradation, bacterial degradation, flocculation, and particles adsorption processes (Miller and Zepp, 1995; Opsahl and Benner, 1998; Moran et al., 2000; Uher et al., 2001).

Photodegradation or sunlight photobleaching is one of the major sinks of CDOM in aquatic environments (Miller and Zepp, 1995; Moran and Zepp, 1997; Vodacek et al., 1997; Osburn et al., 2009). CDOM photodegradation reduces CDOM capacity in light absorption through destruction of chromophoric groups (Shank et al., 2005). Absorption of light by CDOM results in production of reactive radical species such as hydrogen peroxide (H_2O_2), hydroxyl (-OH)), harmful reactive oxygen species, trace gases such as CO_2, CO, and COS, low molecular weight organic matters, and biologically organic labile compounds (Kieber et al., 1989; Blough and Zepp, 1995; Moran and Zepp, 1997; Gao and Zepp, 1998; Blough and Del Vecchio, 2002; Miller et al., 2002). Photo-induced low molecular weight organic matter and labile products can promote the growth of heterotrophic microbes (Moran and Zepp, 1997). In addition, photodegradation of CDOM leads to an increase in spectral slope (S) and loss of CDOM absorption (or fluorescence) (Vodacek et al., 1997; Blough and Del Vecchio, 2002; D'Sa and DiMarco, 2009). Photodegradation of CDOM has an impact on biogeochemical cycling of carbon and nitrogen (Moran and Zepp, 1997; Bushaw et al., 1996; Guo et al., 2007). In addition, CDOM photodegradation products react with trace metals, and alter their bioavailability (e.g., iron and copper) (Powell and Wilson-Finelli, 2003; Shank et al., 2005). Osburn and Morris (2003) reported an increase in CDOM photoreactivity with decrease in salinity across an estuarine gradient.

Flocculation removal process is common in low salinity regions, such as river plumes, estuarine and coastal environments. CDOM will be removed from water column during flocculation process when organic matters combine with particles (i.e., forming colloids) (Del Castillo, 2005).

In addition, high-molecular-weight (HMW) CDOM can be removed from the water column through preferential sorption to existing particles (Del Castillo, 2005; Shank et al., 2005). Adsorption and flocculation processes, have an influence on optical properties of CDOM (e.g., increasing S), and take place at low salinity regions. Reyes-Pesaresi (2010) reported removal of CDOM through flocculation and adsorption at low salinity (<8 psu) in Mayagüez Bay, Puerto Rico.

1.5 Dissolved Organic Carbon and Colored dissolved organic matter

Dissolved organic carbon (DOC) is recognized as the second largest bioreactive reservoirs of carbon in the ocean (H, 2002). Since DOC makes up approximately 60% of DOM, DOC can be used as a substitute for DOM, as mentioned in section 1.2 (Ogawa and Tanoue, 2003; Lannen, 2007). DOC plays a key role in the ocean carbon cycle, and contributes to the biological pump (Ducklow et al., 1995; Hansell, 2002). Maybeck (1982) estimated that that 0.25 $\times 10^{15}$ g dissolved organic carbon (DOC) is discharged to the ocean by rivers each year. DOC operationally is defined as organic carbon passing through 0.2 μm filters. Terrestrial DOC originates from decomposition of soil and plant materials (Thurman, 1985). In addition, in the upper ocean, DOC is produced by biological processes (Hansell and Carlson, 2001). In situ or autochthonous DOC is released by phytoplankton exudation of organic matter, zooplankton excretion, cell lysis and dissolution of fecal pellets (Carlson and Ducklow, 1995; Maier et al., 2009). Also, DOC is introduced into the water column from sediments through diffusive

transport (Swett, 2010). Photodegradation and particles sorption are the major processes of removal of DOC, (Benner and Opsahl 2001; Carlson, 2002). Moreover, microbial degradation removes DOC from water column (Moran et al., 1991).

DOC can be measured in field and laboratory measurements, but these procedures are expensive and time consuming. CDOM, as a colored fraction of DOC, contributes up to 70% to the total DOC in coastal regions, and stands for 20% of the total DOC pool in the open ocean (Coble, 2007; Kowalczuk et al., 2010). Since CDOM can be determined using ocean color sensors directly, CDOM absorption (or fluorescence) is used as a proxy to determine DOC through ocean color sensors (Del Castillo and Miller, 2008; Mannino et al., 2008; Griffin et al., 2011). A positive correlation between these two has been reported in the literature (Green and Blough, 1994; Ferrari et al., 1996; Vodacek et al., 1997; Ferrari, 2000; Chen et al., 2002). The high and positive correlation between these two properties indicates that the distribution of CDOM and DOC is controlled by the mixing between river end-member and seawater end-member (Coble, 2007). Ferrari et al. (1996) suggested the intercept value in the plot of CDOM versus DOC discloses a background of uncolored DOM component (Coble, 2007; Lannen, 2007). Furthermore, the seasonal variation in CDOM concentration may cause changes in y-intercept in the relation between these two parameters (Del Castillo, 2005). Hence, the relationship between these two properties must be examined seasonally (Del Castillo, 2005; Mannino et al., 2008). The negative correlation between these two properties is reported in open ocean and coastal regions away from river's influence (or terrestrial influence), where removal and addition processes that control these two properties are decoupled (Nelson and Siegel, 1998; Coble, 2007). For instance, Vodacek et al. (1997) reported loss of CDOM absorption due to photodegradation without any changes in DOC concentration. In addition, increases in DOC concentration due to biological activity without accompanying variation in CDOM distribution

has been reported (Del Castillo, 2005). DOC can be measured remotely and independently, when the high and positive correlation between CDOM and DOC is observed, or once DOC behaves conservatively (Del Castillo, 2005). The strong relationship between CDOM and DOC along with CDOM retrievals using bio-optical algorithms has been used to investigate the carbon cycles and to monitor transport of terrestrial organic carbon to the open oceans using ocean color sensors (Del Castillo, 2005; Del Castillo and Miller, 2008, Mannino et al., 2008).

1.6 Salinity and Colored dissolved organic matter

Salinity as a conservative tracer can be used to study CDOM sources and sinks (Del Vecchio and Blough, 2006). The negative correlation between CDOM absorption (or fluorescence) and salinity has been observed in coastal regions and many estuaries that are influenced by freshwater river discharge (Table 1.1) (Ferrari and Dowell et al., 1998; Carder et al., 1994; D'Sa et al., 2002; Stedmon and Markager, 2003). Figure 1.5 shows the absorption spectra of CDOM at different salinities in samples from the Mississippi River plume and the Gulf of Mexico. Linearly decreasing CDOM with increasing salinity suggests presence of CDOM-rich water, as well as lack of sources and sinks of CDOM (Del Vecchio and Blough, 2006). However, the non-linear relationship between a_{CDOM} and salinity has been reported in different aquatic environments, even in coastal regions not influenced by high riverine input (Blough et al., 1993; Højerslev et al., 1996; Kowalczuk, 1999; Uher et al., 2001). The inverse linear relationship between CDOM and salinity is disrupted by the addition or removal processes. Upward deviation from conservative mixing line indicates presence of CDOM sources (Figure 1.6). In contrast, depletion processes (e.g., photodegradation) lead to downward deviation from conservative mixing line (Figure 1.6) (Blough et al., 1993; Uher et al., 2001; Del Vecchio and Blough, 2006; D'Sa and DiMarco, 2009).

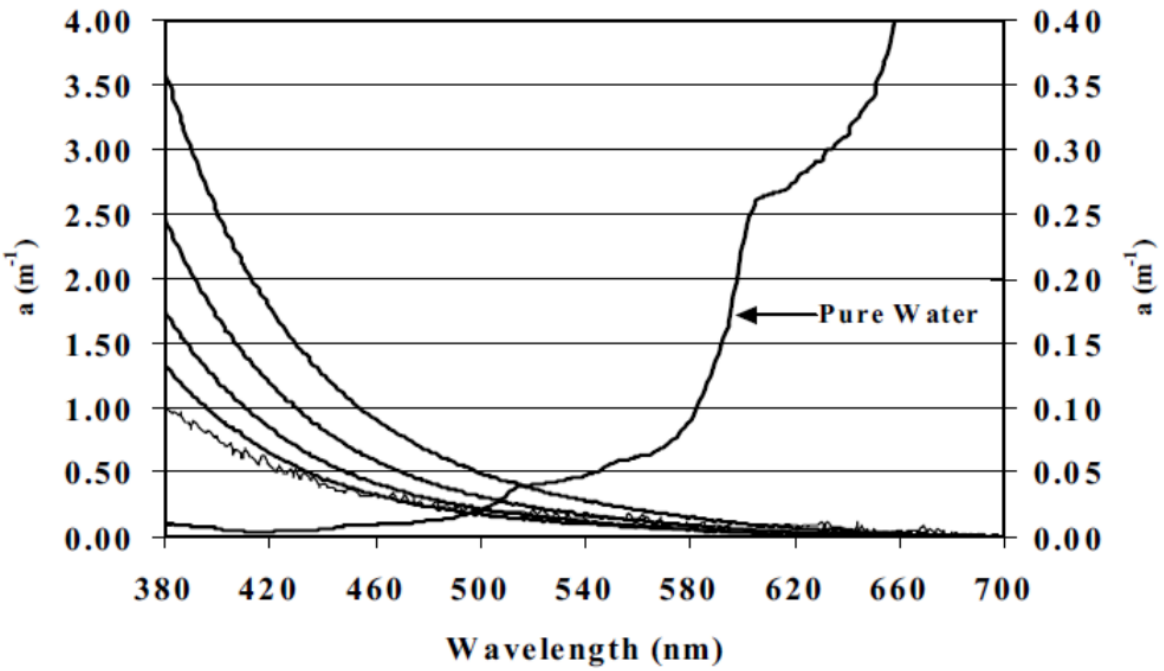

Figure 1.5: Absorption spectra of CDOM and pure water. CDOM spectra correspond to samples collected in the Mississippi River plume and Gulf of Mexico. From top to bottom, the salinities of the sample were 0, 5, 15, 19, and 35. The absorption scale for pure-water and for the blue-water sample (salinity =35, bottom curve) are in the Y-axis (Adopted from Del Castillo 2005).

Since CDOM concentration varies seasonally and spatially due to input (e.g. river discharge and in situ production) and removal (e.g. photodegradation and consumptopn) of CDOM, the seasonal and spatial correlation between these two properties should be examined (Blough and Del Vecchio, 2002). Guo et al. (2007) reported the linear dependence of CDOM on salinity was interrupted and CDOM removed due to particles sorption in low salinity regions in the Jiulong River Estuary. In addition, Højerslev et al. (1996) suggested the non-linear dependence of CDOM on salinity resulted from the quasi-conservative mixing of terrestrial CDOM from three water masses (North Sea water, Baltic Sea water, and German Bight/southern North Sea water).

Table 1.1: Correlation between CDOM absorption at 440 and salinity for different estuaries (adopted from Bower and Brett 2008).

Location	Number of Samples	R^2	Refrence
Pearl River, China	41	0.98	Hong et al. (2005)
St. Lawrence, Canada	16	0.99	Nieke et al. (1997)
Cape Fear River, USA	81	0.96	Kowalczuk et al. (2003)
Clyde Sea, Scotland	17	0.99	Binding and Bowers (2003)
Clyde Sea, Scotland	n/r	0.95	Mckee et al. (1999)
Conwy, Wales	29	0.98	Bowers et al. (2004)
Swan River, Australia	117	n/r	Kostoglidis et al. (2005)
Zambezi plume, Mozambique	26	0.76	Siddorn et al. (2001)
Baltic Sea	61	0.88	Kowalczuk et al. (2005)
Chesapeake Bay, USA	121	0.67	Rochelle-Newall and Fisher (2002)
Canadian Arctic	7	0.87	Retamal et al. (2007)
Galway Bay, Ireland	68	0.71-096	Goddijn (2007)

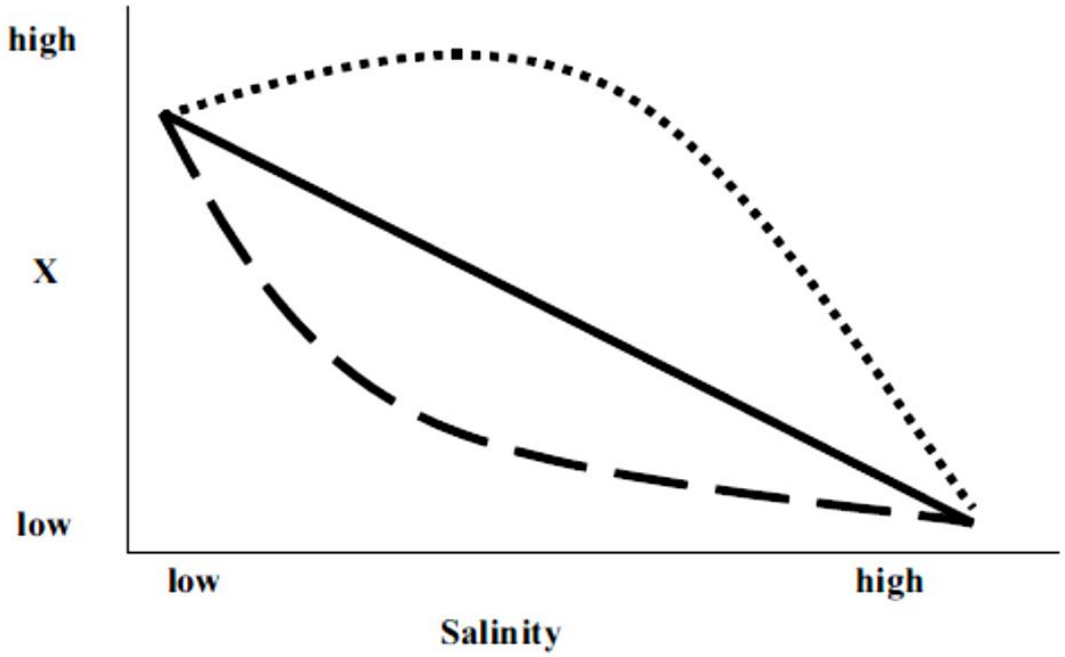

Figure 1.6: (——) indicates conservative behavior of CDOM (X); (— — —) suggests depletion of CDOM; (•••) denotes input of CDOM (adopted from Del Vecchio and Blough 2006).

1.7 Retrieval of CDOM from Ocean Color

1.7.1 Optical properties of Water

The inherent optical properties (IOPs) and the apparent optical properties (AOPs) are two types of optical properties of water. IOPs (e.g., absorption coefficient (a(λ)), scattering coefficient (b(λ)), and beam attenuation coefficient (c(λ)) are dependent on the concentration of water's constituents, and independent from the geometry of the ambient light field (Kirk, 1994). The optically active susbstances in water, such as chlorophyll, CDOM, and suspended particulate matter (SPM) define the IOPs of water. AOPs (e.g., irradiance reflectance ((R(λ,z), remote sensing reflectance (R_{rs}(θ,Ø,λ), and diffuse attenuation coefficient (K_d(λ)) are dependent on the concentration of water's constituents and the geometry of ambient light field. The AOPs can be determined from IOPs using (semi-)analytical models, which are the solution of radiative transfer equation (RTE) (Gordon et al., 1975; Kirk, 1984; Carder et al., 1999). Various simplification and assumption have been addressed in developing (semi-)analytical algorithm, because some parameters are unknown in RTE (Lannen, 2007). The following analytical model (Equation 1.4) relates the irradiance reflectance to the backscattering coefficient (b_b) and absorption coefficient (a) (Gordon et al, 1975):

$$R = f \frac{b_b}{a + b_b} \tag{1.4}$$

where f is a proportionality factor that is dependent on optical properties of water, the wavelength of ambient light, and solar zenith angle (Moler and Gentili, 1993; D'Sa and Miller, 2003). In addition, diffuse attenuation can be determined from IOPs (Gordon, 1989).

1.7.2 Classification of Water

Ocean waters have been divided into two types: Case I and Case II (Morel and Prieur, 1977; Gordon and Morel, 1983). In Case I waters, phytoplankton and their associated products (e.g., CDOM, detritus) control light filed, and have an influence on optical properties of water.

In Case II waters, phytoplankton and associated products along with other photoreactive water's constituents, such as CDOM (i.e., allochthonous CDOM) and suspended sediment, which may not co-vary with phytoplankton, have significant impacts on light field. Case II waters are recognized as complex water, where optical estimation of water's constituents is challenging (D'Sa and Miller, 2005). For example, retrieval of chlorophyll-a by ocean color remote sensing may not be accurate (e.g., overestimation of chlorophyll-a) in Case II due to interference of CDOM and contamination of signal received by satellite ocean color sensors (Carder et al., 1991; Hochman et al., 1994). In contrast, chlorophyll-a can be estimated with high accuracy from ocean color sensors using standard algorithms in case I waters (D'Sa and Miller, 2005). The definition of these tow concepts has been very helpful to predict the IOPs. However, a subtle line between these two concepts may lead to failure of some optical models to predict IOPs in marine environment due to ambiguity that these two concepts may cause (Bricaud et al., 1981; Mobley et al., 2004). Our study area, the northern Gulf of Mexico, is recognized as complex water, and water types change from Case I to Case II (Zhu et al., 2011). Hence, retrieving water's constituents would be challenging especially in turbid waters of the Mississippi and the Atchafalaya River plume regions.

1.7.3 Retrieval algorithms and CDOM

Remote sensing provides us unprecedented technique to understand and monitor coastal and ocean processes with repeated and synoptic coverage (Blough et al., 1993; Hodges et al.,

1995; Siegel et al., 2002; D'Sa and Miller, 2003). Concentration of photoreactive constituents of water, such as chlorophyll, CDOM and suspended particulate matter (SPM) in the upper ocean layer can be determined using empirical and semi-analytical algorithms. Retrieving CDOM from ocean color sensors is considered as an efficient method compared to time consuming and labor intensive field and laboratory procedures (Rayes-Pesaresi, 2010).

Historically, in the late 1970s, the coastal zone color scanner (CZCS) was launched to estimate the concentration of chlorophyll in Case I waters (Gorden and Morel, 1983; Hoge et al., 1995; IOCCG, 2006). In the past decades, the idea of retrieval of water constituents' concentration (e.g. Phytoplankton, CDOM/detritus) having their own major influence on water's IOPs has emerged (IOCCG, 2006). Semi-analytical inversion algorithms have been developed to estimate IOPs in Case I water (Roeseler and Perry, 1995; Garver and Siegel 1997; Carder et al., 1999; Maritorena et al., 2002, Siegel et al., 2002). Semi-analytical models (or algorithms) have been developed based on assumed relationship derived from RTE between normalized water-leaving radiance ($L_{wn}(\lambda)$) (or remote sensing reflectance (R_{rs})) and IOPs (e.g., absorption (a) and backscattering (b_b) coefficient) (Garver and Seigel, 1997; Carder et al., 1999). Various variables (e.g. chlorophyll a or CDOM concentration) can be retrieved by implementing semi-analytical models as inverse applications (Garver and Siegel, 1997). To retrieve CDOM and understand CDOM dynamics spatially and temporally, several models including empirical and semi-analytical models have been developed (Garver and Siegel, 1997; Lee et al., 2002; Kahru and Mitchell, 2001; D'Sa et al., 2006; Zhu et al., 2011). Garver and Siegel (1997) developed a semi-analytical ocean color model (GSM) that was then tuned by Maritorena et al. (2002). This model is not able to discriminate between CDOM and detritus (or nonalgal particles, NAP) due to similarity in shape of spectra. Hence, these two components are considered as a single product (a_{dg}) (IOCCG, 2006). Later, many semi-analytical models have been developed to invert CDOM

absorption coefficient exclusively and directly from SeaWiFS (Sea-viewing Wide Field-of-view sensors) using remote sensing reflectance band-ratio models (O'Reilly et al., 1998) and MODIS (Moderate Resolution Imaging Spectroradiometer) (Carder et al., 1999). Lee et al (2002) developed the Quasi-Analytical Algorithm to retrieve IOPs, and a_{dg} can be inverted from R_{rs} directly. QAA is recognized as a mathematically simple and computationally efficient model (IOCCG, 2006). Since CDOM plays a key role in biogeochemical processes in aquatic environments, it is imperative to investigate CDOM dynamics independently considering the fact that separating CDOM from detritus is very challenging (Zhu et al., 2011). Several empirical algorithms have been developed to retrieve absorption coefficient of colored dissolved organic matter independently (Kahru and Mitchell, 2001; Johannessen et al., 2003; D'Sa et al., 2006; Mannino et al., 2008). Empirical algorithms have been developed based on statistical relationship between optically active water's constituents (e.g., CDOM, chlorophyll, and SPM) and remote sensing reflectance band ratio. Empirical algorithms are easy to implement, and the robustness of these algorithms depends on the quality of in situ data utilized to develop these algorithms (Shanmugam et al., 2011). In addition, these algorithms do not need detailed knowledge of IOP relationships, and their application is confined to specific regions (Lee at al., 2002; Cui et al., 2010; Zhu et al., 2010). Kahru and Mitchell (2001) proposed an empirical algorithm to estimate CDOM absorption coefficient at 300 nm using normalized water leaving radiance (L_{wn}) ratio (433/510) for SeaWiFS in California coastal water. Also, Del Castillo (2004) developed a quantitative relationship between R_{rs} ratio (443/510) and CDOM absorption coefficient at 412 nm in the Mississippi River plume waters. Furthermore, computational intelligence-based techniques, such as neural networks methods and fuzzy logic algorithms have been proposed to estimate the absorption coefficient spectra of CDOM (D'Alimonte, 2004; Kishino et al., 2005; Yong Sun et al., 2011). Zhu et al. (2010) developed Extended Quasi-

Analytical Algorithm (QAA-E) to decompose CDOM absorption coefficient from nonpigmented particles in the Mississippi and Atchafalaya plume waters.

1.8 CDOM and Numerical Advection Model

The distribution of CDOM is generally controlled by physical advection and local mixing (Boss et al., 2001; Del Castillo, 2005). The influence of horizontal and vertical advection on CDOM has been studied for various regions (Boss et al., 2001; Acker et al., 2009). Acker et al. (2009) reported release of CDOM from suspended sediment induced by offshore advection. Numerical models provide us an effective tool to understand hydrodynamics, and other processes (e.g., sediment transport) affecting CDOM distribution. Jolliff et al. (2003) combined a circulation model with CDOM photolysis to study CDOM fate and transport on the west Florida shelf (WFS). Their model results estimated the optical and photochemical processes that occurred within Suwannee River plume, and showed that CDOM was entrained in a coastal jet extending south from the Suwannee River. In addition, Polimene et al. (2007) studied vertical and horizontal advection of DOC in the northern Adriatic Sea by numerical simulation. This study employed a three-dimensional ecosystem numerical model that was coupled to a biogeochemical-circulation model. The European Regional Sea Ecosystem Model (ERSEM) and the Adriatic Sea implementation of the Princeton Ocean Model were used as the biogeochemical model and the circulation model, respectively. The simulation results demonstrated the influence of circulation in regulating the DOC exchanges between regions with various trophic structures (Polimene et al., 2007). Georgas et al. (2010) interpreted CDOM dynamics in the New York/New Jersey Harbor and New York Bight system using high-resolution, four-dimensional predictive model of CDOM fate and transport. The simulated outputs were validated against SeaWiFS-derived surface CDOM. They upgraded the four-dimensional hydrodynamic model of New York Harbor using Observation and Prediction System (NYHOPS) to obtain a

hydrodynamic/CDOM forecasting model incorporating CDOM fluorescence source strength and first-order decay due to photodegradtion to investigate CDOM fate and transport. The model is providing 48hr forecast of allochthonous CDOM within NYHOPS regions (Georgas et al., 2010). Furthermore, Chai and Boss (2010) linked optical properties with the coupled physical-biological models to simulate and forecast optical properties for the Monterey Bay, California. To achieve their goals, they incorporated the Carbon, Silicate, and Nitrogen Ecosystem (CoSiNE) model into both the Navy Coastal Ocean Model (NCOM) and Regional Ocean Model System (ROMS); further inherent optical properties were also incorporated into the NCOM-CoSiNE and ROMS-CoSiNE (Chai and Boss, 2010). Shulman et al. (2011) utilized NCOM to model circulation associated with upwelling, then the model was coupled to the biochemical submodel of Chai et al. (2002) to study bio-optical properties. Cobb et al. (2008) used Navy Coastal Ocean Model (NCOM) to simulate the wind and tide induced circulation in the Atchafalaya Bay during cold front intrusions.

NCOM model is one of the most popular models employed for studying ocean and coastal circulation. This 3-dimensional, free surface baroclinic model was developed by Naval Research Laboratory (NRL) based on a finite difference numerical scheme. The model has been applied to different coastal and oceanic waters in order to Forecast/Nowcast circulation, salinity and temperature. Implementing a prediction model for Portuguese coast during MREA04 sea trial was one of the successful practical applications of model for coastal/ocean forecasting purposes (Ko et al., 2008). Assimilation of both CTD and satellite data into the model resulted in good accuracy for circulation parameters, temperature, and salinity. Model was also applied for studying Ocean/Atmosphere feedback at Ligurian Sea and Adriatic Sea (Jensen et al., 2010). Model accuracy in simulation of temperature and salinity was improved by enhancing vertical

mixing. Figure 1.7 shows comparison of NCOM-simulated temperatures with observed temperature values at Ocean Weather Station Papa (QWS Papa) located at 50° N and 145° W.

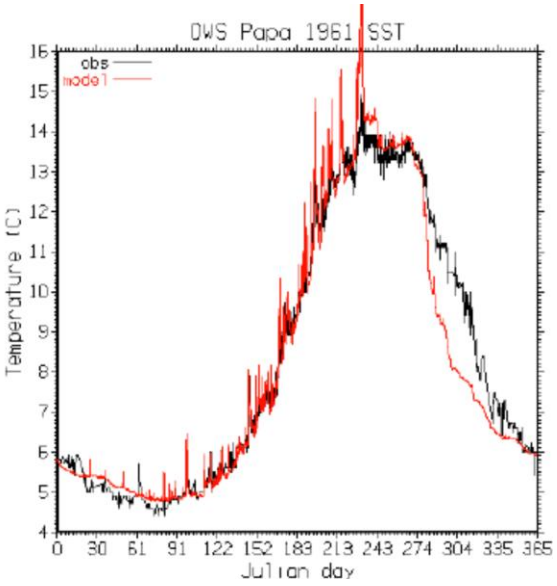

Figure 1.7: NCOM-simulated temperature based on enhanced mixing formulation in comparison to the observed values for OWS Papa.

Simulation results of NCOM for the Gulf of Mexico were provided by a model comprising Mississippi to Texas inner-shelves and some offshore area (27-30.5° N latitude and 88.2-95.5°W longitude) (Ko et al., 2003). The model was nested within a global model encompassing west of Atlantic as well as the Gulf of Mexico. The global model was forced by tide, wind, solar radiation, and river discharges (Ko et al., 2003). Model performance in simulating water level over the inner-shelf area of the northern Gulf of Mexico was evaluated by D'Sa and Ko (2008). Figure 1.8 shows the NCOM-simulated water level compared to the observed water level by tide gauges at three different stations: Galveston, Texas; Grand Isle, Louisiana, and Waveland, Mississippi which demonstrated satisfactory performance of NCOM model in simulating water level in the northern Gulf of Mexico. NCOM model as previously noted was applied for studying circulation, temperature, and salinity in different parts of the world including the northern Gulf of Mexico with quite accurate results. Hence, in this study

NCOM model simulation results were utilized for preparing synoptic CDOM maps based on CDOM-salinity relationship. Furthermore, current data obtained from NCOM simulation were employed to investigate advection effect on CDOM distribution.

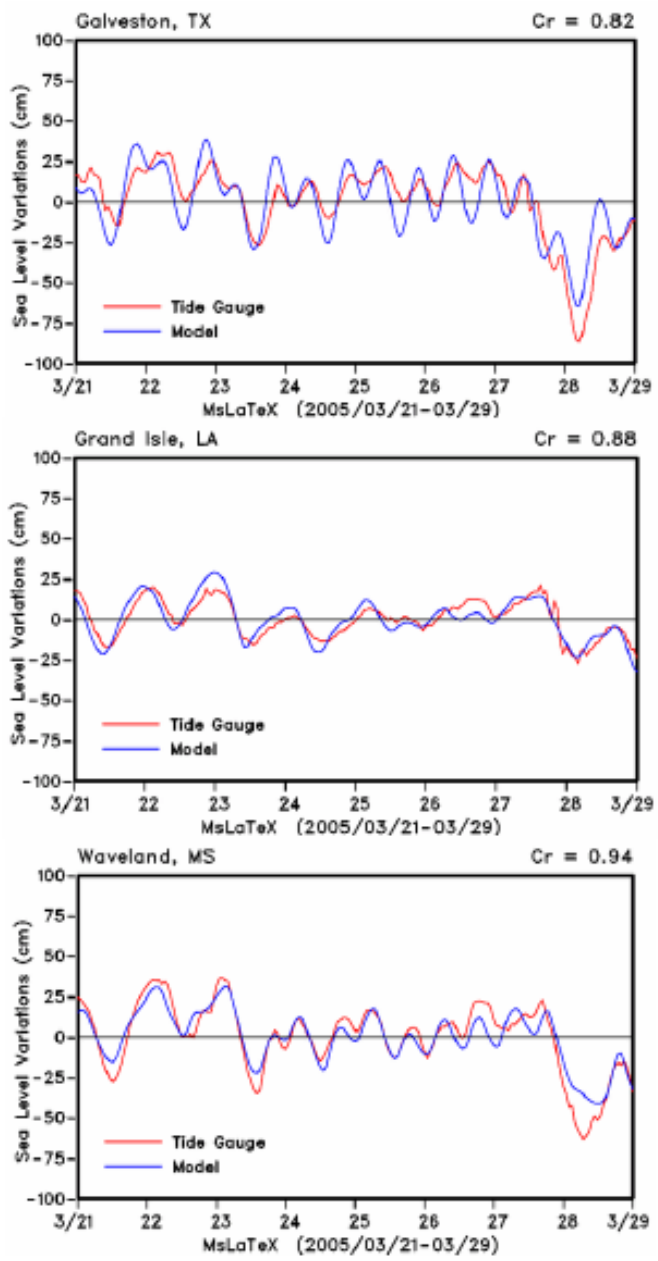

Figure 1.8: Water level simulated using NCOM and observed water level at tidal gauges for three different stations along Texas, Louisiana and Mississippi coasts.

1.9 Study Objectives

Since CDOM plays a critical role in biogeochemical cycles of aquatic environments, it is necessary to enhance our knowledge about CDOM dynamics. Fulfilling following objectives would help us to decipher the distribution of CDOM in our study:

1) Evaluating and developing empirical algorithms to retrieve CDOM from SeaWiFS, MODIS, and MERIS ocean color sensors.

2) Constructing empirical algorithms to derive DOC from SeaWiFS, MODIS, and MERIS.

3) Providing integrated surface CDOM concentration map using numerical model (NCOM)

4) Studying the impacts of horizontal advection on CDOM distribution.

1.10 Organization of thesis

To meet the main objectives of this thesis, 4 chapters are presented. Chapter 1 gives an introduction to DOM, CDOM, DOC, and numerical model to study CDOM, optical properties, and circulation in different aquatic regions, as well as the objectives of this study.

Chapter 2 mainly addresses the evaluation and development of empirical algorithms for deriving CDOM and DOC using satellite ocean color sensors. The available empirical algorithms for CDOM using SeaWiFS data (the D'Sa et al. (2006) and the Mannino et al. (2008) algorithms) were evaluated and the robust one was used to develop an algorithm for retrieving DOC. Empirical CDOM algorithms were also assessed and developed for the northern Gulf of Mexico using MODIS and MERIS data; these algorithms were developed and evaluated based on field data. CDOM algorithms further used to construct algorithms for DOC retrieval based on the conservative relationships between CDOM and DOC.

In chapter 3 efforts toward developing an approach for deriving CDOM from numerical modeling results are presented. An inverse linear relationship between surface CDOM and

surface salinity were examined for two different zones on the inner and outer-shelf for both summer and spring-winter periods. The relationships were applied to the NCOM-simulated salinity to convert salinity to CDOM. The advection effects on CDOM distribution was examined by comparing simultaneous NCOM-derived CDOM and currents over the study area. Different regimes of currents including down-coast and up-coast currents, as well as cold front outbreak were investigated to examine advection effects under different hydrodynamics conditions on CDOM dynamics.

Chapter 4 summarizes results in chapter 2 and chapter 3.

CHAPTER 2: CHROMOPHORIC DISSOLVED ORGANIC MATTER AND DISSOLVED ORGANIC CARBON IN THE NORTHERN GULF OF MEXICO FROM OCEAN COLOR SENSORS: EMPIRICAL ALGORITHMS FOR SEAWIFS, MODIS AND MERIS

2.1 Introduction

Dissolved organic matter (DOM) is the largest bioreactive inventory of carbon in the global ocean, and is comparable in size to the atmospheric CO2 stock (Hansell and Carlson, 2002; Jiao et al., 2010). Therefore, the DOM pool has a major impact on the global carbon cycle and climate change (Hansell and Carlson, 2002). Colored DOM, or chromophoric DOM (CDOM), also referred to as gelbstoff, yellow substances, and humic substances, primarily absorbs light ranging from UV (280 to 400 nm) to blue light (Kirk, 1994). Thus, CDOM can affect intensity and spectral quality of the light climate through attenuation of photosynthetically active radiation (PAR), which can adversely affect the ecosystem structure by inhibiting primary productivity (Arrigo and Brown, 1996; Vodacek et al., 1997; Blough and Del Vecchio, 2002; Chen and Gardner, 2004). Furthermore, CDOM is capable of protecting phytoplankton and other living organisms from DNA damage by providing a protective shield against harmful UV-B radiation (Blough and Zepp, 1990; Blough and Green 1995). High concentration of CDOM causes overestimation of satellite-derived chlorophyll-a (Morel and Prieur, 1977; Rochelle-Newall and Fisher, 2002; Siegel et al., 2002; D'Sa, 2008). The distribution of CDOM in the northern Gulf of Mexico is highly variable in space and time, which is mainly due to seasonal fluctuations of Mississippi-Atchafalaya River system (Chen and Gardner, 2004; D'Sa et al, 2006; D'Sa and Korobkin, 2008). Thus, it is imperative to monitor CDOM distribution spatially and temporally to improve our understanding of the carbon cycle, biogeochemical processes, and to advance retrieval of chlorophyll-a by remote sensors in coastal and estuarine waters (Chen et al.,

2004; D'Sa and Korobkin, 2008; Del Castillo and Miller, 2008; D'Sa and DiMarco, 2009; Singh et al., 2010).

Dissolved organic carbon (DOC) as an energy source for heterotrophic bacteria and as a pool of carbon on the time scale of ocean circulation plays a critical role in the biological pump and ocean carbon cycle (Benner et al., 1995; Zweifel et al., 1995; Hansell, 2002) and therefore has been a focus of many studies (Carlson et al., 1994; Ducklow et al., 1995; Hansell 2002; Cooper et al., 2005; Bianchi et al., 2009). As in situ measurement and analysis of DOC is time-consuming and expensive (Gandhi et al., 2004; Fichot and Benner, 2011), the potential for satellite estimates of DOC could provide an unprecedented tool with synoptic and repeated coverage. However, as DOC cannot be sensed directly by ocean color sensors, CDOM, the colored fraction of DOC, can be estimated remotely. Thus, CDOM can be utilized as an inexpensive intermediary to estimate the standing stock of DOC and the carbon cycle in aquatic environments. Coble (2007) reported CDOM's contribution to DOC ranged from 20% to 70% in the ocean. The optical signature of CDOM can be used as a proxy for DOC as long as these two parameters behave conservatively in marine environments (Del Castillo and Miller, 2008; Griffin et al., 2011). In addition, a robust bio-optical algorithm to retrieve CDOM from ocean color sensors must be available (Del Castillo and Miller, 2008). Conservative behavior between the CDOM absorption coefficient (or fluorescence) and DOC has been reported in different type of water bodies (Vodacek et al., 1995; Ferrari, 2000; Rochelle-Newall and Fisher, 2002; Del Vecchio and Blough, 2004; Gueguen et al., 2005; Griffin et al., 2011; Shank and Evans, 2011). CDOM absorption coefficient ($a_{CDOM}(\lambda)$) and DOC concentration are highly correlated with each other in regions where the mixing of fresh and oceanic waters control the variability of each parameter (Kowalczuk et al., 2010). CDOM as well as other photoreactive in-water constituents (e.g. chlorophyll-a, detritus or non-algal particles) affect the underwater light field and the

optical properties of water (Coble et al, 2004; D'Sa et al., 2007). Hence, several ocean color algorithms have been developed to study CDOM distribution both spatially and temporally (D'Sa er al., 2006; Mannino et al., 2008).

Historically, coastal zone color scanner (CZCS) algorithms were developed to estimate chlorophyll-a concentrations, but other photoreactive in-water constituents (e.g. CDOM and detritus) can be obtained as they co-vary with chlorophyll-a in aquatic environments (Case-1 waters) (Morel and Prieur, 1977; Gordon and Morel, 1983; Gordon et al., 1983). Semi-analytical (SA) inversion models have been developed for the Sea-viewing Wide Field-of-view Sensor (SeaWiFS) and Moderate Resolution Imaging Spectroradiometer (MODIS) to derive CDOM and detritus absorption coefficient as a single component (CDM) (Carder et al., 1999; Hodge et al., 2001; Maritorena et al., 2002; Siegel et al., 2002), as both exhibit similar spectral shape and slope in the visible light spectrum (Bricaud et al., 1981). The major shortcoming of these inversion algorithms is their weakness to discriminate between CDOM and detritus in marine environments. In order to investigate carbon cycling in coastal and estuarine waters (Case-2 Waters) where optically active constituents do not co-vary with chlorophyll-a, knowledge of CDOM's distribution and dynamics is required (Morel and Prieur, 1977; IOCCG, 2002; D'Sa et al., 2006). As decoupling CDOM from detrital absorption is challenging since both have a similar spectral shape and slope in the visible spectrum, several empirical ocean color algorithms have been developed to derive CDOM independently and directly from R_{rs} (Kahru and Mitchell, 2001; D'Sa and Miller 2003; Johannessen et al, 2003; Del Castillo and Miller, 2008;; Mannino et al., 2008). Empirical algorithms, also known as band ratio algorithms, are based on statistical relationships between R_{rs} band ratios and in water constituent's concentrations (Twardowski et al., 2005; D'Sa et al., 2006). For instance, D'Sa and Miller (2003) developed an algorithm for SeaWiFS to retrieve aCDOM(412) in the Mississippi River dominated coastal waters using a

relationship between aCDOM(412) and remote sensing reflectance band ratio, Rrs (510)/Rrs (555). Kahru and Mitchell (2001) developed a relationship between aCDOM(300) and SeaWiFS (Rrs 443/Rrs510) at the CalCOFI site in the southern California. For the coastal waters adjacent to the Chesapeake and Delaware, Johannessen et al. (2003) reported the relationship between ultraviolet (UV) attenuation coefficient (Kd) at 323 nm, 338 nm, and 380 nm and the Rrs(412)/Rrs(555) band ratio. Recently, Zhu et al. (2010) developed an Extended Quasi-Analytical Algorithm (QAA-E) to estimate CDOM in the Mississippi and Atchafalaya River plume regions using above-surface hyperspectral light measurements. In addition, there have been many attempts to derive DOC through the relationship between CDOM-DOC and CDOM-Rrs band ratios (Del Castillo and Miller, 2008; Mannino et al., 2008). Del Castillo and Miller (2008) applied the Rrs(510)/Rrs(670) band ratio to SeaWiFS imagery to retrieve DOC in the Mississippi River plume. Mannino et al. (2008) developed algorithms to derive DOC through the relationship between the a_{CDOM} at 412 nm, 355 nm, DOC, and Rrs ratios for MODIS/Aqua and SeaWiFS in coastal waters of the U.S. Middle Atlantic Bight.

The primary goal of this study is to evaluate existing and develop new ocean color algorithms for CDOM absorption and DOC concentrations in the northern Gulf of Mexico. An extended set of field CDOM absorption and DOC measurements collated for the northern Gulf of Mexico as part of a NASA funded project were used in this study. Algorithm assessment and development were based on two empirical band ratio CDOM algorithms, namely D'Sa et al. (2006) and the Mannino et al. (2008) for estimating $a_{CDOM}(412)$. These algorithms were extended to MODIS/Aqua and the MERIS/ENVISAT sensors. Further, DOC empirical algorithms were developed through the relationships between in situ $a_{CDOM}(412)$-in situ DOC and in situ aCDOM(412)-Rrs band ratios (satellite-derived) (Mannino et al. 2008). This approach was found to be an effective method to derive DOC concentration. The satellite-derived DOC concentration

enabled us to monitor DOC variations both spatially and temporally, and to enhance our understanding of the organic carbon processes in the northern Gulf of Mexico.

2.2. Materials and methods

2.2.1 Study area

The study area is located in the northern Gulf of Mexico on the Texas-Louisiana shelf, covering the region from latitude 28.0° to 30.5° N and longitude 88.0° to 93.0° W (Figure 2.1A). The study site is highly influenced by the discharge from the Mississippi River (MR) and its largest distributary, the Atchafalaya River (AR). The Mississippi River drains approximately 41% of the contiguous United States, making it the third largest drainage basin. The MR also ranks as the seventh largest river in terms of fresh water discharge (Van der Leeden et al., 1990; Milliman, 1991). The Mississippi-Atchafalaya river system (MARS) discharges two-thirds (~70%) of its total flow into the Gulf of Mexico through the MR birdfoot delta. The remainder (~30%) is diverted down the AR and discharged through the AR and Wax Lake outlets into the broad, shallow Atchafalaya bay (Wiseman and Garvine, 1995; Lohrenz et al., 1999; Walker and Rabalais, 2006). Seasonal variations and the large discharge of freshwater from the MR and AR profoundly influence the bio-optical properties of water, primary productivity, and the distribution of carbon flux in the region (Dinnel and Wiseman, 1986; Rabalais et al., 1996; Lohrenz et al., 1999; D'Sa and Miller, 2003; Walker and Rabalais 2006; D'Sa, 2008). Terrestrially-derived (riverine or allochthonous) CDOM introduced by the MR and AR predominates the northern Gulf of Mexico (Conmy et al., 2004). It is reported that the Mississippi River discharges 3.1×10^{-3} Pg of DOC into the Gulf of Mexico annually which accounts for about 1.2% of the total global input of DOC from rivers to the ocean (Bianchi et al., 2004). Decreases in suspended materials, and increases in nutrient load due to anthropogenic effects (e.g. construction of dams) along the Mississippi River, as well as temporal variability in

river discharge have affected primary production and riverine DOC cycling (Bianchi et al., 2004).

2.2.2 Field Sampling

Field data comprising of CDOM optical (spectral absorption coefficient) and DOC concentrations in conjunction with and physical (salinity) properties of water were obtained from the study area during 17 oceanographic cruises in 2005 and 2007 - 2009 (Table 2.1, Figure 2.1). Some of these field CDOM and DOC measurements were hosted as part of a NASA funded project by the Biological and Chemical Oceanography Data Management Office (BCO-DMO) as a data rescue effort. In the spring and summer (March, May, July, and August) of 2005, coastal waters influenced by the MR from Southwest Pass to the Atchafalaya Delta were sampled aboard the *RV Gyre*. Water samples were collected from the surface using Niskin bottles attached to the conductivity-temperature-depth (CTD) profiler (Sea-Bird Electronic, Inc., Bellevue, WA, USA). The samples were filtered through pre-rinsed 0.2(μm) Nuclepore membrane filters within three hours of collection, and were stored in pre-cleaned amber glass bottles in the refrigerator (~4ºC) until CDOM laboratory analysis was conducted (D'Sa and DiMarco, 2009). Field data collected in May 2007 were obtained from the Biological and Chemical Oceanography Data Management Office (BCO-DMO) website (http://data.bco-dmo.org/jg/serv/BCO/NACP_Coastal/GulfMexico). Field observations were made in the AR plume region onboard *RV Pelican.* Water samples for analysis of CDOM absorption and DOC concentration were collected at the water surface either by bucket grabs, from the Pelican's flow-through system, or by CTD. Samples were filtered through 0.2 (μm) Polyether sulfone filters into baked (550 degrees Celsius; 5 hr. minimum) collection vials and stored at 4 degrees Celsius in the dark until return to the laboratory. More information can be found at the BCO-DMO website. *In situ* data obtained during the 2007 (July, August, September) and 2008 (February, April, June) cruises were also used. Near-shore

sampling was conducted from a small boat in transects out of the Vermilion, Atchafalaya, Terrebonne, and Barataria Bays, and the Mississippi River's Southwest Pass.

Table 2.1: The list of cruises in the northern Gulf of Mexico, and averaged values for $a_{CDOM}(412)$ DOC concentration and salinity in each cruise. The sign (-) indicates no data is available.

Cruise	Date	$a_{CDOM}(412)$ (m^{-1})	DOC (μmol C L^{-1})	Salinity (psu)
1	March23-March29, 2005	0.47	n/a	27.07
2	May20-May25, 2005	0.43	n/a	25.96
3	July8-July12, 2005	0.23	n/a	29.27
4	August 18-August24, 2005	0.25	n/a	28.75
5	March23-March28, 2007	n/a	204.51	n/a
6	April16-April20, 2007	0.41	n/a	31.75
7	May7-May10, 2007	0.87	180.02	24.16
8	July 17and 19, 2007	1.43	288.23	15.12
9	July17-July 20, 2007	n/a	155.13	n/a
10	August 9, 2007	0.74	266.58	27.64
11	September11and13, 2007	1.97	509.74	11.33
12	February9-February12, 2008	1.72	361.68	11.28
13	April5-April8, 2008	3.72	664.30	2.60
14	April6-April8, 2008	0.82	n/a	22.33
15	April16-April18, 2008	n/a	226.69	n/a
16	June2, 2008	2.52	377.25	1.23
17	August18-Augus20, 2009	0.34	166.97	7.94

For determining CDOM absorption and DOC concentrations, discrete water samples were collected 0.5 m below the water surface using a Sea-Bird 25 CTD. Water samples were filtered through Whatman 47 mm GF/F filters, nominal pore size 0.7 μm, into combusted glass flasks for CDOM and DOC analysis (Schaeffer et al., 2011). Moreover, *in situ* DOC concentrations were measured on the Louisiana continental shelf, west of Southwest Pass exceeding to 10 and 20 m isobaths, from the *RV Pelican* in March and July of 2007 and April and July of 2008 as part of the Mechanisms Controlling Hypoxia (MCH) project. In August 2009, *in situ* observations were made onboard the RV pelican on the Louisiana continental shelf. In situ samples from the water surface were collected using Niskin bottles attached to CTD profiles. Samples were immediately

filtered under low vacuum through a Whatman GF/F filter (nominal pore size 0.2 µm) and then stored in pre-cleaned amber glass bottles and refrigerated until CDOM absorption and DOC concentration were measured in the laboratory.

2.2.3 CDOM absorption

Spectral CDOM absorption values from filtered water obtained in 2005 were determined onboard the ship using a capillary waveguide system (WPI, Inc.), a single-beam spectrophotometer (D'Sa et al. 1999; 2001). The optical absorbance spectra (A) were obtained between 250 nm to 722 nm from two scans, namely, a cell filled with blank solution (Milli-Q water), adjusted for the sample salinity followed by a water sample scan. The absorbance values at each wavelength were corrected for baseline fluctuation and scattering by subtracting the absorbance averaged between 715-722 nm. The absorption coefficients at each wavelength ($a_{CDOM}(\lambda)$) (m^{-1}) were calculated using the following equation :

$$a(\lambda) = \frac{2.303A(\lambda)}{l} \qquad (2.1)$$

where l, the optical path length (m) used for the absorbance measurements were 0.1 or 0.5 m, respectively (D'Sa and DiMarco, 2009).

CDOM absorption from filtered water samples obtained during 2007 (July, August, September) and 2008 (Feb, April, June) were obtained with a Shimadzu UV1700 dual-beam spectrophotometer using a 1-cm cuvette at 1 nm intervals between 350-700 nm. Then spectra were normalized by subtracting each wavelength from the measured value at 700 nm (Schaeffer et al., 2011).

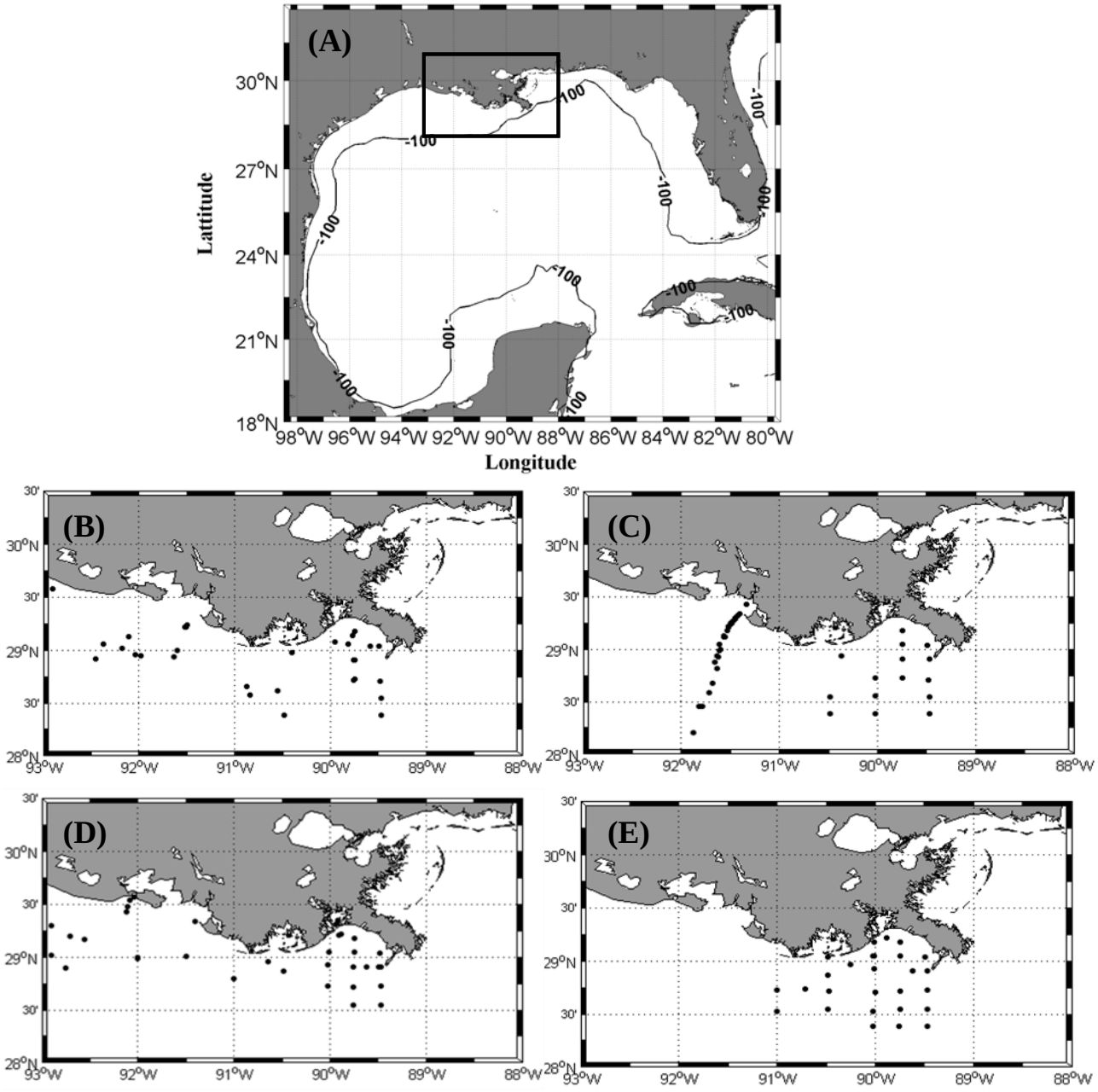

Figure 2.1: (A) Map of the study area in the northern Gulf of Mexico. Location of stations in (B) March, May, July and August 2005, (C) March, April, May, July 2007, (D) February, April, June 2008, (E) August 2009.

The CDOM absorption measurement method used to analyze the May 2007 water samples is documented at BCO-DMO website (http://data.bco-dmo.org/jg/serv/BCO/ NACP_Coastal). Filtered samples from the August 2009 survey were processed in the laboratory on a double beam Perkin Elmer Lambda 850 spectrophotometer between 190-750 nm at 2 nm intervals.

Samples were brought to room temperature before measuring the absorbance spectra of CDOM. Before determining $a_{CDOM}(\lambda)$, absorbance data were corrected by subtracting the mean absorbance from 700-750 nm from each wavelength. The CDOM absorption coefficient at each wavelength was derived using Equation 1.1.

2.2.4 DOC concentration

The DOC concentration of filtered-water samples obtained in 2007 (July, August, September) and in 2008 (Feb, April, June) was measured using a Shimadzu TOC–VCSN analyzer, calibrated with potassium biphthalate (Shaeffer et al., 2011). Samples collected in 2007 (March, July) and 2008 (April, July) were filtered through GF/F filters and then acidified (100 μL of 2 N HCl was added in order to remove inorganic carbon). The DOC concentration was then measured with the Shimadzu TOC-VCSH/CSN by using high-temperature catalytic oxidation (HTCO). The DOC concentrations used for this study from the May 2007 cruise were measured by wet chemical oxidation with high–amplification isotope ratio mass spectrometry (WCO-IRMS) using WCO-modified OI Analytical Model 1010 TOC analyzer (more information can be found on the BCO-DMO website, (http://bco-dmo.org/ under GMx label). For the August 2009 samples, DOC concentrations were obtained using a Shimadzu TOC-5000A (with ASI-5000A autosampler) using a high temperature combustion method.

2.2.5 Satellite data

Satellite data from the SeaWiFS, MODIS, and MERIS sensors were used to evaluate and parameterize CDOM and DOC empirical algorithms using R_{rs} visible bands from these sensors; specifically, the performance of two empirical algorithms, namely the D'Sa et al. (2006) algorithm using the $R_{rs}(510)/R_{rs}(555)$ band ratio and the Maninno et al. (2008) algorithm using the $R_{rs}(490)/R_{rs}(555)$ band ratios were used to derive $a_{CDOM}(412)$. Level 1A SeaWiFS LAC

(local area coverage) data with spatial resolution of 1.1 km at nadir, and with daily temporal resolution were acquired from NASA Goddard Space Flight Center (http://oceancolor.gsfc.nasa.gov/). Level 1A data were processed up to Level 2 (L2) using the SeaWiFS Data Analysis System (SeaDAS) developed by NASA's Ocean Biology Processing Group (OBPG) version 6.0 and IDL 6.3 to derive R_{rs} bands at 490, 510 and 555 nm. As the field data set spanned the period corresponding to the operational period of three ocean color sensors, the empirical algorithms were evaluated for SeaWiFS as well as the MODIS/Aqua and MERIS/ENVISAT sensors. MODIS/Aqua Level 1A LAC (~ 1 km at nadir, daily temporal resolution) were obtained from the NASA's Ocean Color website and processed to Level 2 (L2) to retrieve R_{rs} bands at 488nm and 555nm using SeaDAS 6.0 software package. The atmospheric correction algorithm developed by Gordon and Wang (1994) was used for SeaWiFS and MODIS to derive R_{rs} bands. Furthermore, R_{rs} bands using 1×1 and 3×3 pixel box size (1km/pixel at nadir) centered on the position of field measurements were chosen. Due to paucity of data points, a time window of ± 14 hours between satellite match-ups and field sampling was set. R_{rs} bands extracted from a 5×5 pixel box for both SeaWiFS and MODIS were also examined, but this pixel box size was not used because of the spatial heterogeneity in coastal waters; therefore, a 3×3 pixel box was applied for extracting most data. In order to develop an empirical algorithm to retrieve CDOM and DOC with MERIS/ENVISAT (European Space Agency (ESA)), Level 1 reduced resolution (RR) data, with a spatial resolution of ~1.2 km and daily temporal resolution, were obtained from ESA (http://merci-srv.eo.esa.int/merci/welcome.do) and processed to Level 2 using SeaDAS 6.0 software package. R_{rs} bands at 510 nm and 560 nm were extracted from 1×1 and 3×3 pixel box size (1.2 km/pixel at nadir) with ±24 hr temporal window between satellite overpass and the time of field sampling for obtaining sufficient data points.

2.3 Results

2.3.1 CDOM, DOC and salinity relationships

In developing an empirical ocean color DOC algorithm using CDOM's optical signature as a proxy for DOC, a prerequisite is a conservative behavior between DOC and CDOM (Del Castillo and Miller, 2008). The seasonal variation in MR and AR discharges along with effects of mixing caused by energetic atmospheric events (i.e., intrusion of cold fronts or storms) likely induces variability in CDOM optical properties and DOC concentration in the northern Gulf of Mexico (Chen and Gardner, 2004; Green et al., 2006; D'Sa and Korobkin, 2008) affecting biogeochemical cycles and the relationship between these two properties and salinity. Therefore, these relationships were examined seasonally (i.e., for summer and spring-winter periods) (Table 2.2). Based on the location of the field measurements, it was observed that MR discharge strongly influenced the relationships between DOC, CDOM and salinity during summer (August 2007, September 2007, August 2009), while spring-winter data (May 2007, February 2008) were significantly affected by the AR discharge. In summer, $a_{CDOM}(412)$, DOC concentration and salinity in surface waters ranged from 0.09 to 2.45 m^{-1} (mean= 1.23±1.21 m^{-1}, n=40), 117.16 to 487.50 μmol C L^{-1} (mean= 302.33±185.16 μmol C L^{-1}, n=40), and 4.39 to 33.14 psu (mean=19.39 ± 15 psu), respectively. During spring-winter study period, the DOC concentration ranged from 56.4 to 739.25 μmol C L^{-1} (mean= 397.82± 341.42 μmol C L^{-1}; n=40), $a_{CDOM}(412)$ varied from 0.011m^{-1} to 5.47m^{-1} (mean= 2.74±2.72; n=40), and salinity exhibited a range from 0.43 to 35.9 psu (mean=18.16±17.73). Elevated values for DOC and CDOM observed in spring-winter period were likely due to outwelled CDOM-laden water from productive wetlands adjacent to the AR plume (Chen and Gardner, 2004).

DOC concentrations were regressed against $a_{CDOM}(412)$ for spring-winter and summer periods to assess the seasonal relationship between DOC and CDOM. Results indicated strong conservative behavior between the two properties with high correlation for both time periods (Equations 2.2 and 2.3.; Figure 2.2A and 2.2B, respectively). Regression analyses between a_{CDOM} (412) and DOC concentration) indicated high R^2 values (0.9) for both seasons, while the intercept for the summer relationship (Equation 2.3) was higher than that of spring-winter relationship (Equation 2.2) (see Table 2.2).

$$DOC\,(\mu molCL^{-1}) = 127.027 a_{cdom}(412) + 77.97 \quad (2.2)$$

$$DOC\,(\mu molCL^{-1}) = 137.22 a_{cdom}(412) + 124.20 \quad (2.3)$$

The high positive correlation between a_{CDOM} (412) and DOC concentration suggests that these two properties behaved conservatively for the two time periods with mixing between the river and marine end members playing a critical role in the distribution of both CDOM and DOC.

Table 2.2: Coefficients resulting from regression analysis between $a_{CDOM}(412)$, DOC, and salinity.

Parameter	Season	Slope (a)	Intercept (b)	R^2	N
DOC vs. a_{CDOM} (412)	Summer	137.22	124.20	0.90	39
DOC vs. a_{CDOM} (412)	Spring-winter	127.02	77.97	0.90	40
$a_{CDOM}(412)$ vs. salinity	Summer	-0.079	2.62	0.7	39
$a_{CDOM}(412)$ vs. salinity	Spring-winter	-0.076	2.78	0.86	40
DOC vs. salinity	Summer	-11.48	497.82	0.77	39
DOC vs. salinity	Spring-winter	-11.84	482.64	0.8	40

Linear equations were fitted to all variables (y= a*x+b). In the DOC- CDOM relationship, y= DOC and x= aCDOM (412); in the CDOM-salinity relationship, y= aCDOM (412) and x=salinity; and in the DOC-salinity relationship, y=DOC and x=salinity.

Seasonal relationships between CDOM absorption coefficient at 412 nm and salinity (Table 2.2; Figure 2.2C and 2.2D) as well as between DOC concentration and salinity (Table 2.2; Figure 2.2E and 2.2F) exhibited strong linear inverse correlations for the summer and spring-winter periods. The inverse linear correlation between $a_{CDOM}(412)$ and salinity (R^2=0.77 in summer; R^2=0.86 in spring-winter) suggests that CDOM originated from terrestrial allochthonous sources; however, high CDOM and DOC concentrations due to riverine influences could be masking any significant autochthonous sources (e.g. in situ primary production) or any noticeable removal processes (e.g. photooxidation, flocculation and sorption). These results indicate similar trends and consistency as with previous studies (e.g., in the northern Gulf of Mexico, D'Sa and DiMarco (2009) observed a conservative behavior between CDOM and salinity (salinity= 1.37-0.036 a_{CDOM} (412), R^2= 0.93, n=51).

A strong negative correlation (Table 2.2; Figures 2.2C and 2.2F) exhibited between DOC and salinity indicates that terrestrial-derived DOC was conserved during the mixing of fresh river and saline end member waters. The strong correlations between these three properties show the persistent influence of the MR and AR discharges on the CDOM distribution and geochemical cycle in the northern Gulf of Mexico (Coble, 2007). These results (Figure 2.2) indicate that the first condition to derive DOC remotely and exclusively was met here. The data utilized to examine conservative behavior of DOC and CDOM were not used to evaluate and develop empirical algorithms in the following sections.

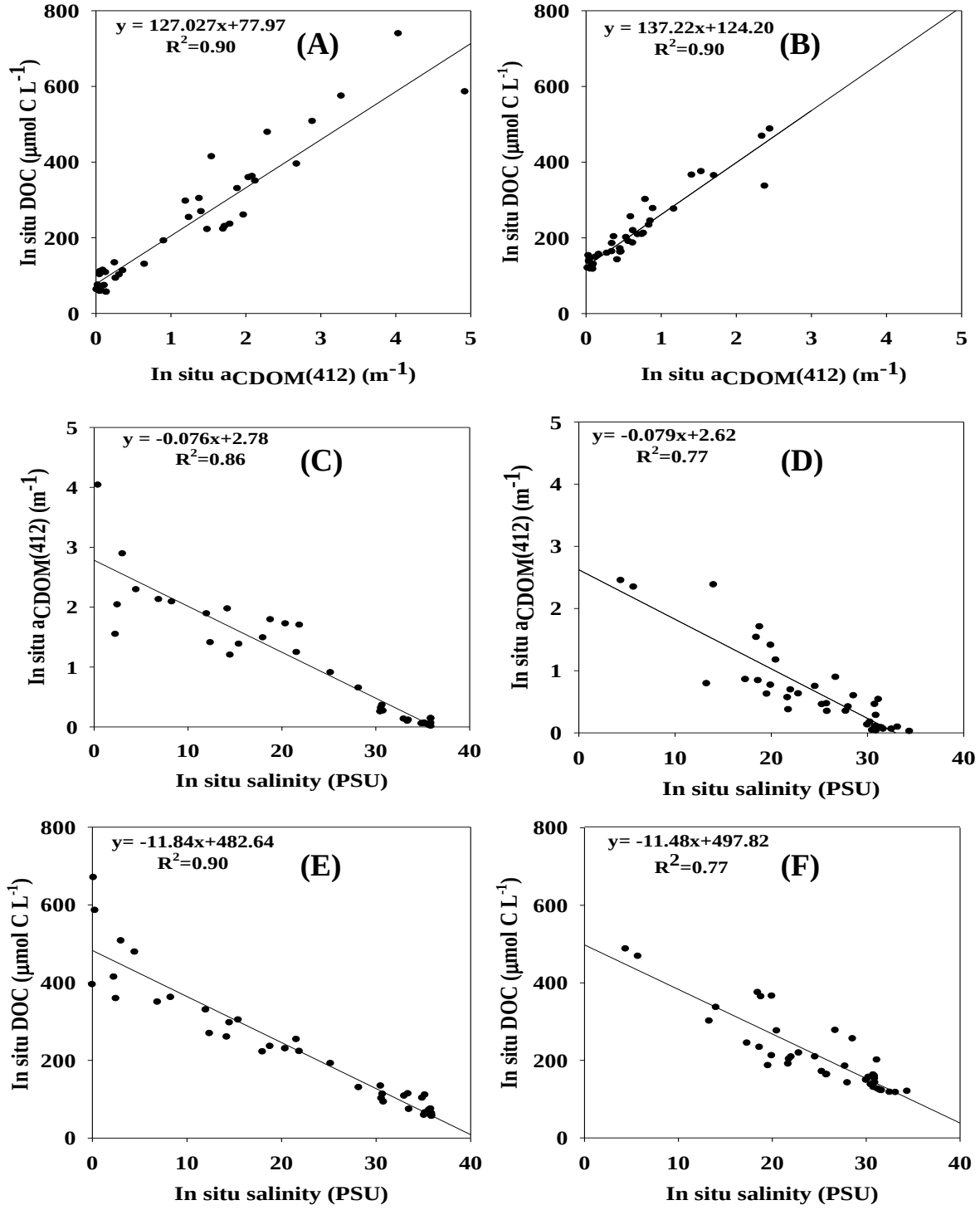

Figure 2.2: Relationship between (A) in situ $a_{CDOM}(412)$ and in situ DOC in spring-winter, (B) in situ a_{CDOM} (412) and in situ DOC in summer, (C) in situ a_{CDOM} (412) and in situ salinity in spring-winter, (D) $a_{CDOM}(412)$ and salinity in summer, (E) in situ DOC and in situ salinity in spring-winter, (F) in situ DOC and in situ salinity in summer.

2.3.2 CDOM and DOC empirical algorithms: validation and development

2. 3.2.1 Validation of D'Sa et al. (2006) and Mannino et al. (2008) empirical algorithms to derive CDOM and DOC

The second condition for estimating DOC concentration exclusively using satellite ocean color sensors is to provide a robust relationship between R_{rs} band ratio and CDOM absorption coefficient to retrieve CDOM remotely. Then DOC concentration can be derived through this relationship and the CDOM-DOC relationship. The D'Sa et al. (2006) regional empirical algorithm was developed through the relationship between in situ R_{rs} ratio band (R_{rs} (510)/ R_{rs} (555)) and in situ $a_{CDOM}(412)$ measurements sampled during three field cruises in spring and fall 2000 and March 2002 in the northern Gulf of Mexico (Equation 2.4).

$$a_{cdom}(412) = 0.227[(R_{rs}(510) / R_{rs}(555)]^{-2.022} \quad (2.4)$$

Equation 2.4 was applied to SeaWiFS imagery (Figure 2.3) to obtain an $a_{CDOM}(412)$ image. The robustness of this algorithm was assessed by comparing satellite-estimated $a_{CDOM}(412)$ with in situ measured a_{CDOM} (412) within ±14 hr of the satellite overpass. Matchup comparison illustrates a satisfactory trend and close agreement between satellite-derived and in situ measured a_{CDOM} (412) in our study region (Figure 2.4A), and shows that data were distributed uniformly along the one-to-one line. The algorithm was further quantified using bias function, root mean square error (RMSE), scatter-index (SI) and coefficient of determination (R^2) (Kowalczuk et al., 2010). The formulas used for calculating statistical quantities are presented in Table 2.3. The statistical analysis revealed that the D'Sa et al. (2006) algorithm performed well in our study area, according to relatively high R^2 (0.66), low RMSE (0.23), and low Bias (-0.045) (Table 2.4). In addition to the D'Sa et al. (2006) empirical algorithm, we examined R_{rs} band ratio as proposed by Mannino et al. (2008) to estimate $a_{CDOM}(412)$. Mannino et al. (2008) proposed an empirical algorithm using Rrs band ratio (Rrs490/Rrs555) to retrieve $a_{CDOM}(412)$ in the U.S. Middle

Atlantic Bight. We parameterized and updated the Mannino et al. (2008) algorithm by regional data by constructing the relationship between satellite-derived R_{rs} band ratio (Rrs490/Rrs555) and in situ measured $a_{CDOM}(412)$ sampled in the northern Gulf of Mexico. The new relationship was applied to SeaWiFS imagery using the SeaDAS 6.0 software package to derive $a_{CDOM}(412)$. To validate the relationship, in situ measured $a_{CDOM}(412)$ values were compared with satellite-derived $a_{CDOM}(412)$ values within ±14 hr of the satellite overpass. This yielded R^2=0.41, RMSE=0.4, and Bias= -0.21 (Table 2.4; Figure 2.4B). The in situ $a_{CDOM}(412)$ data used for matchup analysis were independent from the data utilized in the construction of the ($R_{rs}490/R_{rs}555$)-a_{CDOM} (412) relationship, and were similar to the data used in the D'Sa et al. (2006) algorithm validation analysis. The matchup comparison results (Table 2.4; Figure 2.4A and B) indicate that the performance of an empirical algorithm utilizing $R_{rs}(490)/R_{rs}(555)$ for estimation of $a_{CDOM}(412)$ was less satisfactory as the D'Sa et al. (2006) algorithm within our study region.

Table 2.3: Equations used for calculating error statistics for evaluation of algorithms.

Statistical estimator	Formula
Bias	$\frac{1}{N}\sum_{i=1}^{N}(y_i - x_i)$
Root mean square error	$\sqrt{\frac{1}{N}\sum_{i=1}^{N}(y_i - x_i)^2}$
Scatter-Index	$\frac{1}{\bar{x}}\sqrt{\frac{1}{N}\sum_{i=1}^{N}[(y_i - \bar{y}) - (x_i - \bar{x})]^2}$

where y_i is satellite-derived values and x_i is field-measured values.

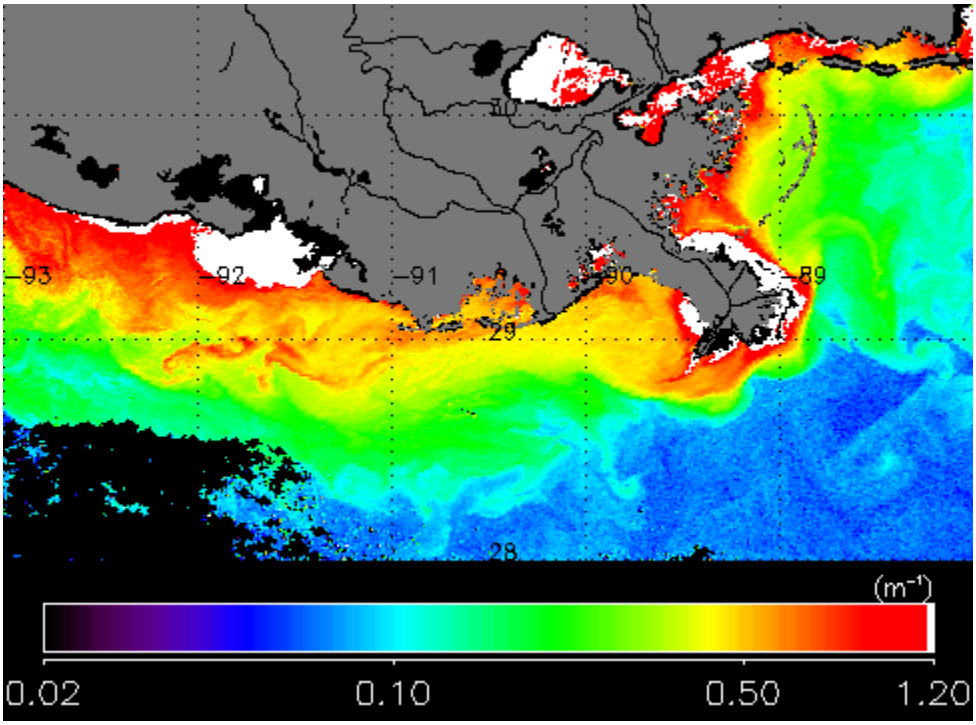

Figure 2.3: Surface CDOM absorption coefficient imagery ($a_{CDOM}(412)$) obtained using the D'Sa et al. (2006) algorithm from SeaWiFS for 6 February 2007.

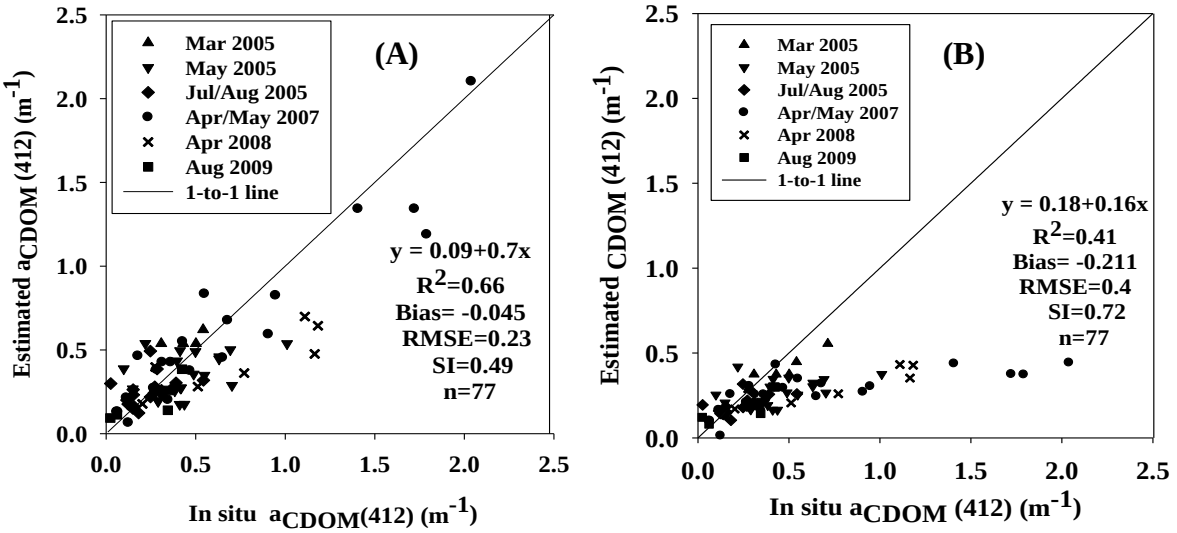

Figure 2.4: Matchup comparison between in situ $a_{CDOM}(412)$ and SeaWiFS-derived $a_{CDOM}(412)$ obtained from the D'Sa et al. (2006) algorithm (A) and from the empirical algorithm using R_{rs} band ratio proposed by Mannino et al. (2008) (B), in the northern Gulf of Mexico. The diagonal solid line shows the 1-to-1 line.

Table 2.4: Summary of error statistics derived from matchup comparisons between in situ and satellite-derived $a_{CDOM}(412)$ obtained from D'Sa et al. (2006) and parameterized Mannino et al. (2008) algorithms.

Rrs band ratio	R^2	RMSE	Bias	SI	Slope	Intercept	N*
Rrs510/Rrs555-D'Sa et al.(2006)	0.66	0.23	-0.045	0.49	0.70	0.09	77
Rrs490/Rrs555-Mannino et al.(2008)	0.41	0.40	-0.211	0.72	0.16	0.18	77

*N is the number of matchup observation.

Since the D'Sa et al. (2006) SeaWiFS CDOM algorithm was found to be more robust for the estimation of $a_{CDOM}(412)$ in the northern Gulf of Mexico, this algorithm along with the CDOM-DOC relationship was used to derive DOC concentration remotely. The seasonal DOC algorithms were developed simply through the CDOM-DOC seasonal relationships (Equations 2.2 and 2.3) and the D'Sa et al. (2006) algorithm (Equation 2.4). The DOC algorithms for the spring-winter and summer periods are given by the following two equations:

$$DOC = 28.835\left[R_{rs}(510)/R_{rs}(555)\right]^{-2.022} + 77.97 \quad (2.5)$$

$$DOC = 31.148\left[R_{rs}(510)/R_{rs}(555)\right]^{-2.022} + 124.20 \quad (2.6)$$

These algorithms were applied to SeaWiFS data to generate surface DOC concentration image (Figure 2.5). The performance of the newly developed DOC algorithm was examined just for the spring-winter period (Figure 2.6) due to the paucity of satellite-derived R_{rs} data in summer. The results of statistical analysis indicate that retrieval of DOC concentration (μmol C L^{-1}) was quite good with Bias=-10.38, RMSE= 27.45, SI=0.15, R^2= 0.5, and N=22. Moreover, surface DOC concentration was obtained remotely through this algorithm (Equation 2.5) with an average accuracy of 93% in spring-winter period.

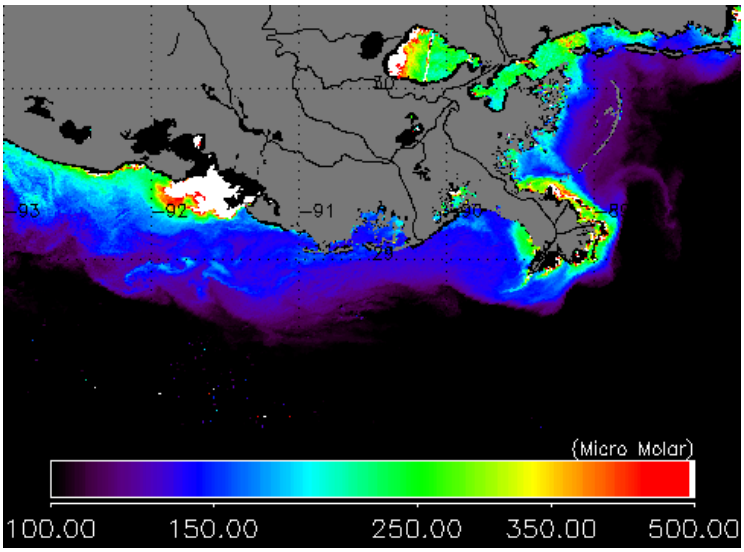

Figure 2.5: SeaWiFS-derived surface DOC concentration (µM) map for 6 February 2007.

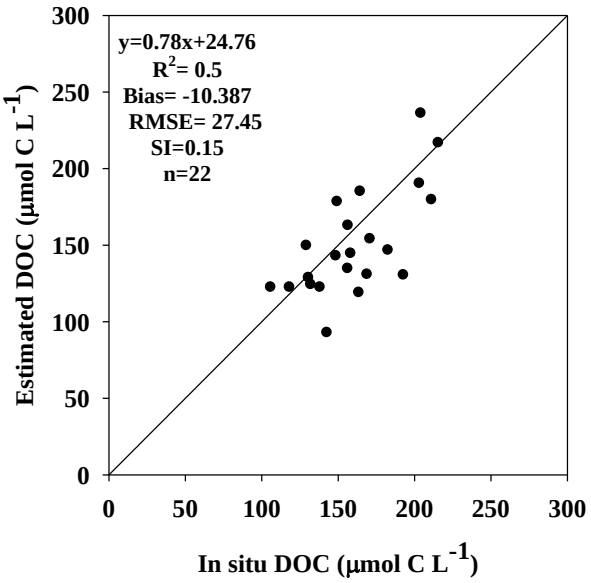

Figure 2.6: Matchup comparison between the SeaWiFS-derived DOC and in situ measured DOC for the spring-winter period. The diagonal line is one-one line.

2.3.2.2 CDOM and DOC empirical algorithms for MODIS and MERIS sensors

R_{rs} values at visible bands were derived from MODIS and MERIS to use as inputs to the empirical algorithms for CDOM and DOC. The R_{rs} band ratios used were $R_{rs}(488)/R_{rs}(555)$ for MODIS-Aqua and $R_{rs}(510)/R_{rs}(560)$ for MERIS-Envisat. Since the study region is an optically complex environment (D'Sa and Miller, 2003; Naik et al., 2010), we avoided using R_{rs} at 412

and 433 due to errors associated with atmospheric correction (Barnard et al. 1998; D'Sa and Miller, 2003). As CDOM absorption was high at 488 nm and even 510 nm in our region due to CDOM-rich water discharge from the MR and the AR (D'Sa and Miller, 2003; Chen and Gardner, 2004), the R_{rs} at these two bands (488nm and 510 nm) were set in the numerator of the empirical algorithms for MODIS and MERIS, respectively. Here, R_{rs} at 555nm and 560nm were chosen as a denominator in band ratio for MODIS and MERIS, respectively because of low CDOM absorption coefficient at these two wavelengths as well as their availability in the MODIS and MERIS ocean color wavelengths. To construct empirical algorithms, MODIS-derived $R_{rs}(488)/R_{rs}(555)$ and MERIS-derived $R_{rs}(510)/R_{rs}(560)$ band ratio were regressed with in situ measured $a_{CDOM}(412)$ through a non-linear three-parameter exponential decay curve (R^2 =0.67 for MODIS, R^2= 0.62 for MERIS) within ±14 hr and ±24 hr time difference between MODIS and MERIS overpasses and field measurements, respectively (Figure 2.7A and 2.8A). In addition, the log-transformed values of these two R_{rs} band ratios were correlated linearly with log-transformed values of in situ $a_{CDOM}(412)$ coefficients (R^2= 0.66 for MODIS, R^2=0.5 for MERIS) (Figures 2.7B and 2.8B). The exponential decay model exhibited higher correlation than the linear model for both sensors. CDOM absorption coefficient can be retrieved using the R_{rs} band ratios through the equation given by:

$$a_{cdom}(412) = \ln[(R_{rs}ratio - A) / B] / (-C) \quad (2.7)$$

Table 2.5 presents R_{rs} ratio and coefficient values (A, B, and C) for MODIS and MERIS. The regional CDOM empirical algorithms were applied to MODIS and MERIS data (Figures 2.9A and 2.9B) to provide a surface CDOM concentration map. The newly developed CDOM empirical algorithms were evaluated using in situ $a_{CDOM}(412)$ data which were independent from the data utilized for algorithm development (Figures 2.9C and 2.9D). The validation matchup

comparison between in situ and satellite-derived $a_{CDOM}(412)$ illustrates estimation of $a_{CDOM}(412)$ with Bias = 0.093, RMSE= 0.176, and R^2 = 0.4 for MODIS, and Bias= 0.089, RMSE= 0.3, R^2= 0.42 for MERIS (Table 2.6). We excluded outliers to improve the evaluation analyses. The time window and geographical position of outliers are discussed in the discussion section. The DOC retrieval algorithms for both MODIS and MERIS were constructed through combining the $a_{CDOM}(412)$-R_{rs} relationship (Equation 2.7) with seasonal $a_{CDOM}(412)$-DOC relationships (Equations 2.5 and 2.6). The resulting seasonal DOC-R_{rs} relationships for the spring-winter and the summer seasons respectively are given as:

$$DOC = 127.027 \ln[(R_{rs}ratio - A)/B]/(-C) + 77 \quad (2.8)$$

$$DOC = 137.22 \ln[(R_{rs}ratio - A)/B]/(-C) + 124.20 \quad (2.9)$$

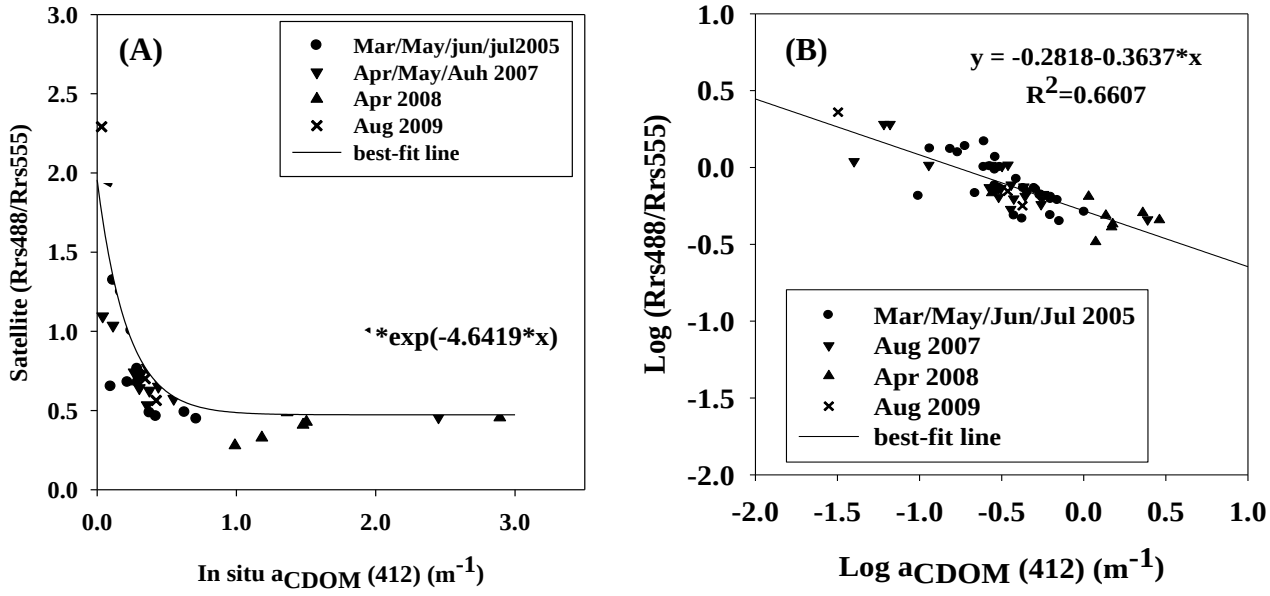

Figure 2.7: MODIS-derived R_{rs} band ratio (488nm and 555 nm) plotted against in situ surface CDOM absorption at 412 nm (A) exponential decay model and (B) logarithmic model.

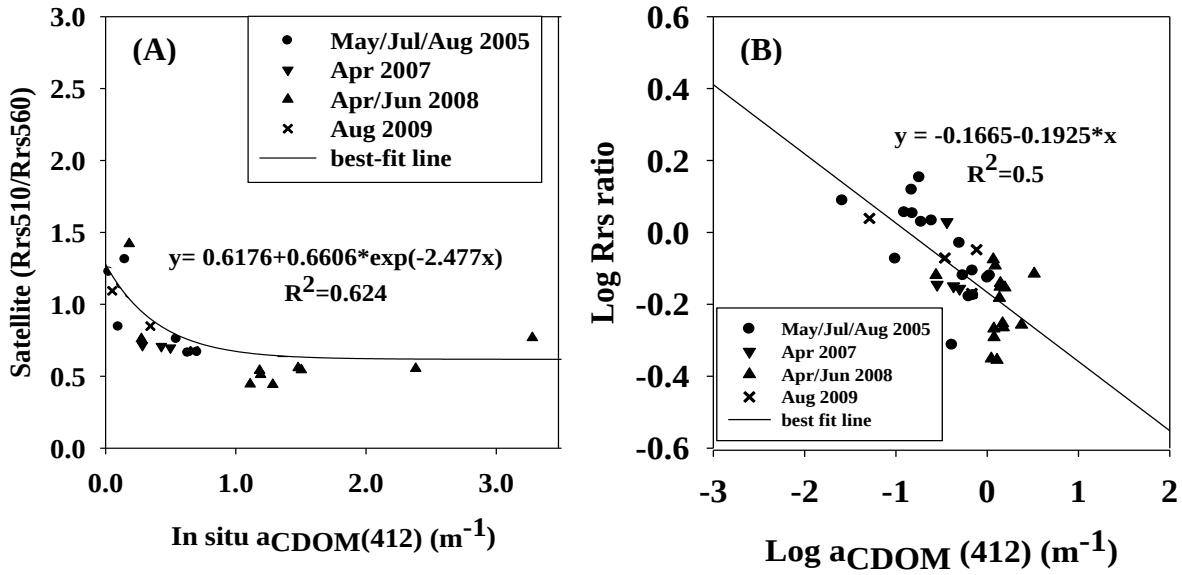

Figure 2.8: MERIS-derived Rrs band ratio (510 nm and 560 nm) plotted against in situ surface CDOM absorption at 412 nm (A) exponential decay model and (B) logarithmic model.

The R_{rs} band ratios and coefficients for both MODIS and MERIS are presented in Table 2.5. Surface DOC concentration maps were generated by applying the newly developed DOC algorithms to MODIS and MERIS data (Figure 2.10A and 2.10B). To test the performance of the DOC algorithms for each sensor, the in situ measured DOC concentrations (μmol C L^{-1}) were compared with MODIS and MERIS-derived DOC (μmol C L^{-1}) (Figure 2.11A-2.11D). The matchup comparisons showed estimation of DOC with Bias= -13.67, RMSE= 32.29, SI= 0.22, R^2=0.4, and N=25 for MODIS, and Bias= -3.5, RMSE= 44.22, SI=0.21, R^2=0.72, and N=7 for MERIS during the spring-winter period (Table 2.6). Furthermore, the statistical parameters obtained from validation of DOC for MODIS (Bias=2.42, RMSE=26.59, SI=0.15, R^2=0.52, and N=25) and for MERIS (Bias= 5.3, RMSE= 30.02, SI=0.17, R^2= 0.58, and N= 19) during the summer period are demonstrated in Table 2.6. The statistical analysis verifies acceptable performance of the DOC algorithm for MERIS in the northern Gulf of Mexico in both the summer and spring-winter periods.

Table 2.5: Summary of fitted coefficients for the regional MODIS and MERIS empirical algorithm illustrated in Figures 2.6 and 2.7 for CDOM and DOC retrievals. Presented coefficients are fitted in the seasonal DOC algorithm.

Product	Satellite	Fitting Curve	R_{rs} Band Ratio	A	B	C	R^2
$a_{CDOM}(412)$	MODIS	3 parameter exponential decay	488/555	0.472	1.48	4.64	0.67
$a_{CDOM}(412)$	MERIS	3 parameter exponential decay	510/560	0.617	0.66	2.47	0.62

The regional empirical algorithm for CDOM is: $a_{CDOM}(412) = \ln[(R_{rs}\text{ ratio} - A)/B]/(-C)$, and the equations for seasonal DOC are: DOC= 127.027 ln $[(R_{rs}$ ratio $-A)/B]/(-C)$ +77 for the spring-winter season, DOC= 137.22 ln $[(R_{rs}$ ratio $-A)/B]/(-C)$ +124.20 for summer. The coefficients are presented in Table 2.5.

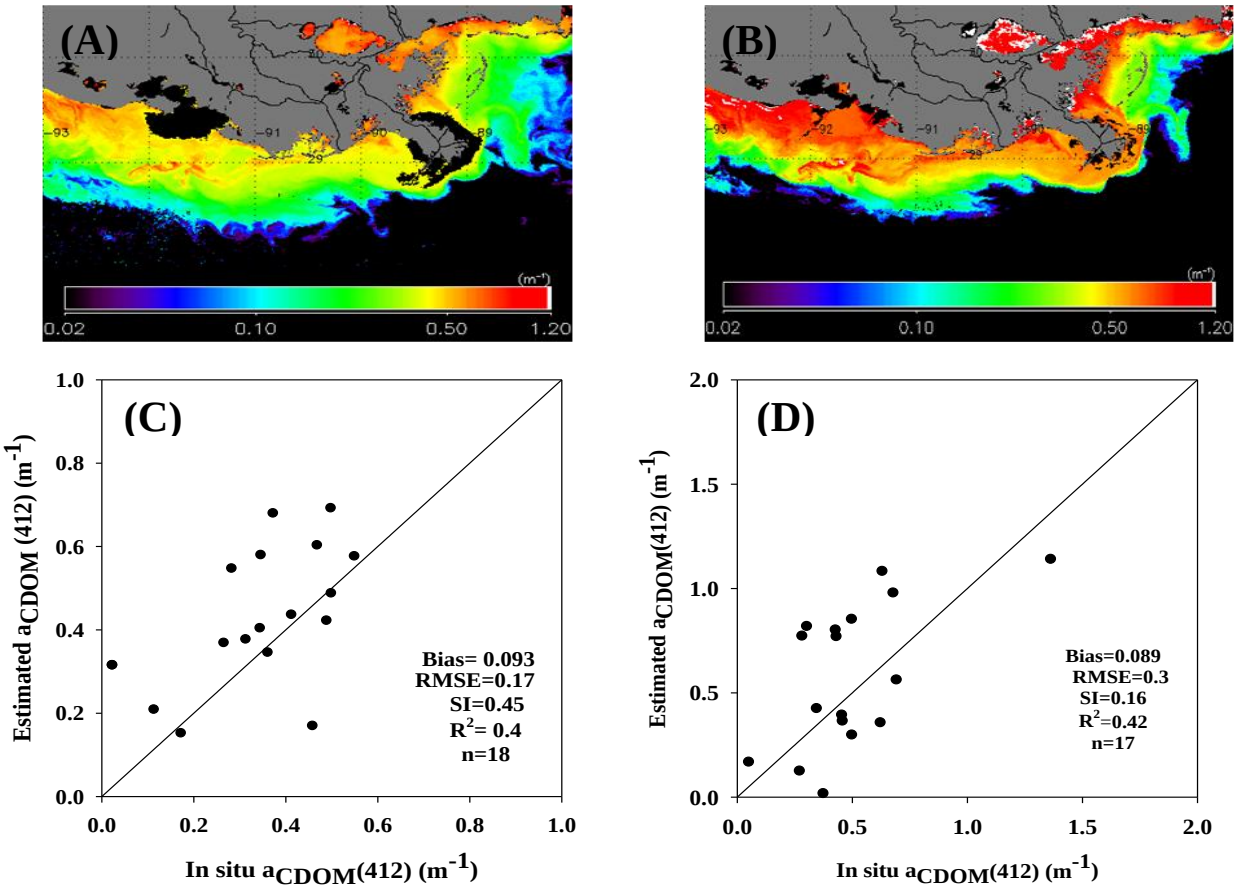

Figure 2.9: (A) CDOM absorption map ($a_{CDOM}(412)$) using the MODIS algorithm for 6 February 2007, (B) CDOM absorption map ($a_{CDOM}(412)$) using the MERIS algorithm for 6 February 2007, (C) matchup comparison between MODIS-derived $a_{CDOM}(412)$ and in situ surface $a_{CDOM}(412)$, (D) matchup comparison between MERIS-derived $a_{CDOM}(412)$ and in situ surface $a_{CDOM}(412)$.

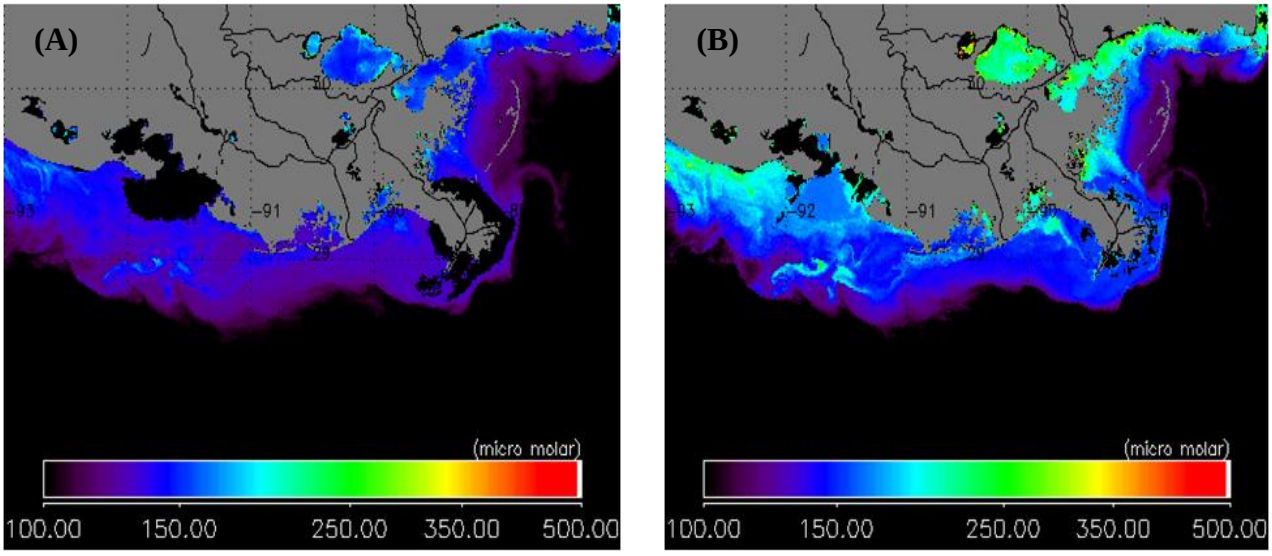

Figure 2.10: (A) MODIS-derived surface DOC (µmol C L^{-1}) concentration for 6 February 2007, (B) MERIS-derived surface DOC (µmol C L^{-1}) for the same date

Table 2.6: Summary of error statistics obtained from validation matchup comparisons for $a_{CDOM}(412)$ and DOC derived from MODIS and MERIS for the summer and spring-winter seasons.

Products	Bias	RMSE	SI	R^2	Slope	Intercept	N
$a_{CDOM}(412)$_MODIS	0.093	0.176	0.45	0.40	0.55	0.24	18
$a_{CDOM}(412)$_MERIS	0.089	0.300	0.16	0.40	0.70	0.23	17
DOC_MODIS_summer	2.420	26.69	0.15	0.52	0.61	66.18	25
DOC_MERIS_summer	5.300	30.02	0.17	0.58	0.39	109.15	19
DOC_MODIS_spring-winter	-13.67	32.29	0.22	0.40	0.43	56.96	25
DOC_MERIS_spring-winter	-3.500	44.22	0.21	0.72	0.99	-2.39	7

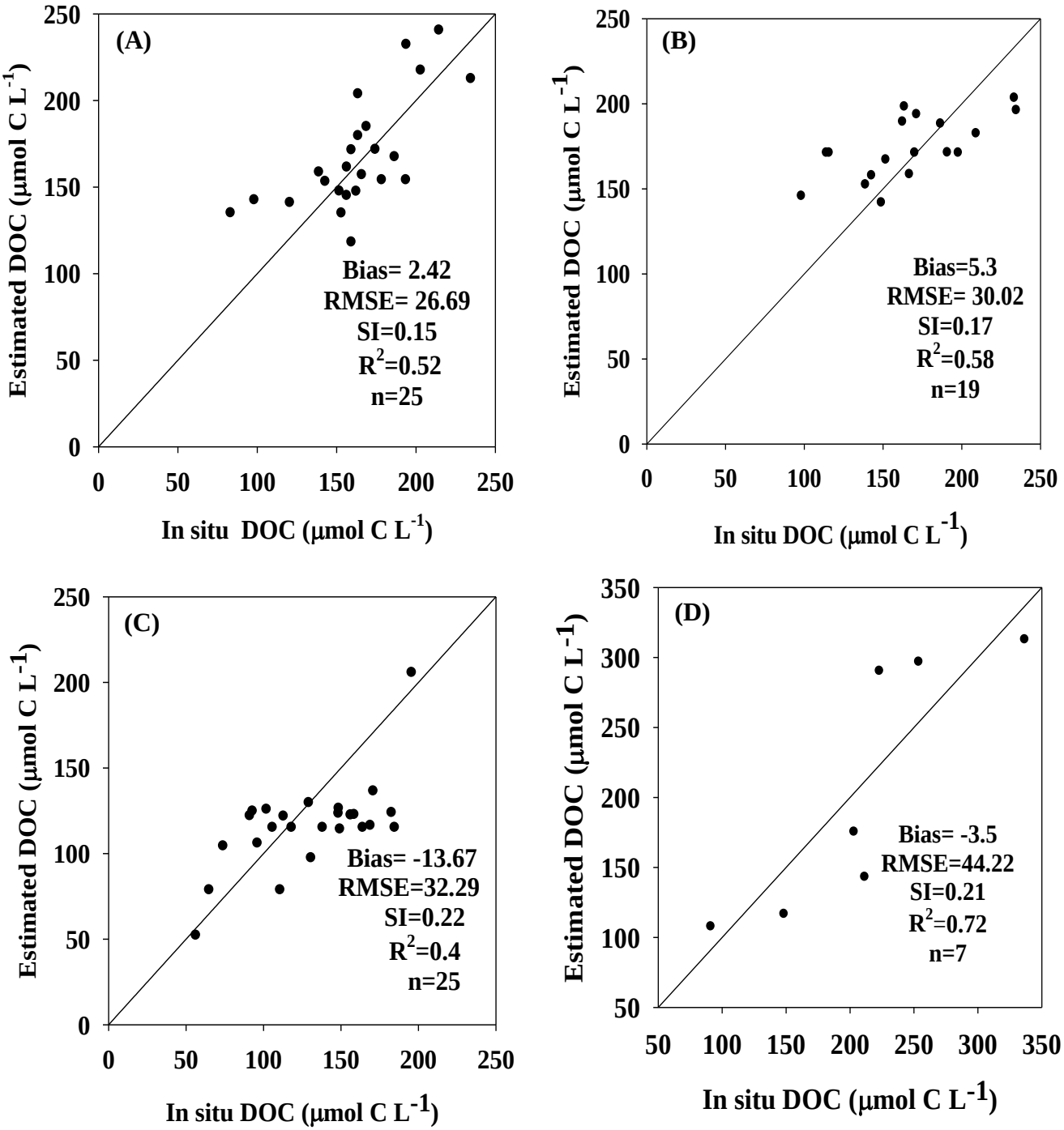

Figure 2.11: Matchup comparison (A) between MODIS-derived DOC (µmol C L^{-1}) and in situ DOC (µmol C L^{-1}) in summer, (B) between MERIS-derived DOC (µmol C L^{-1}) and in situ DOC (µmol C L^{-1}) in summer, (C) between MODIS-derived DOC (µmol C L^{-1}) and in situ DOC (µM C L^{-1}) n the spring-winter season, (D) between MERIS-derived DOC (µmol C L^{-1}) and in situ DOC (µmol C L^{-1}) in the spring-winter season.

2.4 Discussion

2.4.1 CDOM, Salinity and DOC relationship

The conservative behavior of CDOM and DOC were examined through the correlations between DOC, CDOM, and salinity. Seasonal variability in CDOM and DOC concentration is highly dependent on the MR and AR discharges (Chen and Gardner, 2004; D'Sa et al., 2006; D'Sa et al., 2008; Naik et al., 2011). Naik et al. (2011) reported that on the Atchafalaya shelf, CDOM dominates the total light absorption when Atchafalaya River flow is high, while non-algal particles (NAP) play a more important role contributing to total light absorption during low-flow conditions. Chen and Gardner (2004) observed high concentrations of CDOM and DOC during high-flow conditions in the Mississippi and Atchafalaya River plume regions, as well as their seasonal variability linked to water's residence time and plant growth cycles in the watershed. We observed that in situ measured DOC concentration in the lower Atchafalaya River was on average ~ 35% higher than DOC concentration in the lower Mississippi River during the spring-winter period. This is consistent with the results reported by Wang et al. (2004) that DOC concentration in the lower Atchafalaya River was 20-30% higher than in the lower Mississippi River for April 2001. The elevated DOC and CDOM in the lower Atchafalaya River plume is likely due to the interaction of the Atchafalaya River with the adjacent productive and extensive salt marshes, wetlands and bayous, while in comparison such interactions are less for the Mississippi River (Chen and Gardner, 2004; D'Sa, 2008). The strong inverse linear correlation between $a_{CDOM}(412)$ and salinity observed in summer (R^2=0.77), and in the spring-winter period (R^2=0.86) suggests that terrestrial allochthonous CDOM, resulting from biodegradation of terrestrial vegetation, behaved conservatively in our study area. Sampling in low salinity, high CDOM waters during summer likely masked the effects of light-induced photobleaching. The strong correlation between CDOM absorption coefficient at 412 nm and DOC concentration

shows that the distribution of DOC was also highly influenced by physical mixing between two-end members, indicating conservative behavior of DOC. However, the relationship during summer suggests loss of CDOM in comparison to DOC.

2.4.2 CDOM and DOC retrieval algorithms

In assessing the performance of two empirical CDOM algorithms for SeaWiFS, it was found that the average errors associated with the D'Sa et al. (2006) and the parameterized Mannino et al. (2008) algorithm for CDOM retrieval were 10% and 61%, respectively. Poor performance of the parameterized Mannino et al. (2008) algorithm could be that the algorithm was tuned to data from the U.S. Atlantic coast and the $R_{rs}(490)/R_{rs}(555)$ ratio is affected by greater interference from chlorophyll-a and particulate organic carbon (POC) in our study area. In comparison, the R_{rs} band ratio (Rrs(510)/Rrs(555)) proposed by D'Sa et al. (2006) is less affected by chlorophyll-a and POC (O'Reilly et al., 2000; Stramski et al., 2008; Allison et al., 2010). Regarding the robustness of the D'Sa et al. (2006) algorithm for CDOM retrieval, SeaWiFS-derived DOC concentration exhibited high accuracy (3% average error for summer, while spring-winter was not evaluated due to lack of data). In addition, this indicates that the newly developed DOC algorithm based on R_{rs} band ratio proposed by D'Sa et al. (2006) performs well in our study region.

The matchup comparison between in situ $a_{CDOM}(412)$ and MODIS-derived CDOM showed an overestimation of CDOM by MODIS (24% average error) which could due to interference by chlorophyll-a on the $R_{rs}(488)/R_{rs}(555)$ band ratio used for $a_{CDOM}(412)$ retrieval. In addition, other factors such as the time difference between satellite overpass and field measurement, pixel box size, and errors and uncertainties associated with satellite-derived R_{rs} used to develop an empirical algorithm can accentuate these discrepancies. Since CDOM

concentration is highly variable spatially and temporally in our study area, appropriate available time difference (less than 5hr) and pixel box size (1×1) could improve these disparities.

The empirical algorithm developed for MODIS failed for $a_{CDOM}(412)$ values larger than 1.5 (m^{-1}) in CDOM-rich coastal and estuarine waters. Strong underestimation of MODIS-derived CDOM values (for values larger than $1.5m^{-1}$) in coastal waters could be related to the sediment resuspension and errors associated with atmospheric correction algorithms in turbid waters (D'Sa et al., 2002). Furthermore, it is more likely that the selected pixel box size and time difference, which were limited by cloud coverage, sun glint, and lack of swath, exacerbated the inaccuracy of CDOM retrieval. Table 2.7 presents the stations' information along with selected pixel box size and time difference for some stations that were excluded as outliers for the validation analysis. These outlier points were located at the mouth of Barataria Bay and Vermilion Bay.

Table 2.7: Summary of outlier stations excluded from CDOM matchup comparison for MODIS.

Station#	1	2	3	4	5
Date	20080209	20080602	20080209	20070913	20080602
Latitude	29.573	29.352	29.539	29.350	29.316
Longitude	-92.043	-89.913	-92.080	-89.910	-89.942
In situ $a_{CDOM}(412)$	2.292	2.660	1.529	1.706	2.381
MODIS-derived $a_{CDOM}(412)$	0.812	0.869	0.623	0.425	0.777
Pixel Box size	3×3	3×3	1×1	3×3	3×3
Time difference(hr)	+10	- 5	+7	- 4	-12

As illustrated in figure (2.11A), the algorithm proposed for DOC retrieval with MODIS performs relatively well for summer, while MODIS-estimated DOC concentration was underestimated (11% in average) during the spring-winter period. Considering the locations of stations during the spring-winter period which were mainly in shallow waters, this underestimation could be attributed to the sediment resuspension associated with cold front passage during spring-winter season (Walker and Hammack, 2000). The sediment resuspension process contaminates remote

sensing reflectance and affects light availability leading to the underestimation of DOC concentration. Since the spring-winter field data were sampled mostly from shallow areas, the effects of sediment resuspension could have been enhanced. Also, the optically inactive fraction of DOC that cannot be measured by satellite could have contributed to the elevated DOC concentration leading to further underestimation of DOC by MODIS.

The influence of cold front passage on DOC concentration has been further examined by comparing the occurrence time of cold fronts and the time of DOC measurements. The information about cold front passage was obtained from the National Oceanic and Atmospheric Administration (NOAA), http://www.hpc.ncep.noaa.gov/html. It appears that cold front intrusion increases DOC concentration resulting in less agreement between measured and satellite-derived DOC concentration, while the DOC field measurement corresponding to the time when no cold front occurred exhibited higher agreement. For example on 18 April 2008, for the station located at Tiger Shoal off the Atchafalaya Bay, the in situ DOC sampling coincided with the passage of a cold front. The measured DOC concentration was 218.50 μmol C L^{-1}, while MODIS-derived DOC concentration was 125.84 μmol C L^{-1} (53% underestimation). In contrast, on 16 April 2008 no cold front was observed, and in situ measured DOC concentration at a station close to the former station was 170.9 μmol C L^{-1}, while MODIS-derived DOC concentration was 136.55 μmol C L^{-1} (17% underestimation).

The retrieval of $a_{CDOM}(412)$ using Rrs(510)/Rrs(560) for MERIS resulted in acceptable CDOM estimation. The algorithm performed better than MODIS (average error 16% for MERIS and 24% for MODIS). Better performance of the MERIS algorithm could be attributed to the use of the 510nm band in constructing the CDOM algorithm which is less affected by chlorophyll-a than the 488 nm band used in the MODIS CDOM algorithm. However, the algorithm overestimated CDOM values by 16% (average error). This overestimation could be attributed to

some factors including sediment resuspension over the shallow area, presence of chlorophyll-a, time gap, and pixel box size. Figure (2.12) shows the location of stations excluded from the MERIS CDOM algorithm evaluation as outliers. Station geographical coordinates for five selected stations have been presented in Table 2.8. Stations located at Louisiana Bight are highly affected by MR sediment plume as a result of westward coastal current and clockwise gyre formed in this region (Rouse and Coleman, 1976; Wiseman et al., 1976; Rouse, 1998; Walker et al., 2005), whereas stations located in the Atchafalaya-Vermilion Bay region are influenced by AR sediment plume. Optical interference of suspended sediments and other photoreactive water's constituents can interfere with the CDOM signal received by the sensor, and lead to significant errors in CDOM estimation by MERIS sensor. In addition, inappropriate time gaps between satellite overpasses and pixel box size are likely to deteriorate further the performance of the CDOM algorithm in coastal and estuarine waters. Table 2.8 illustrates the outliers' time gap and pixel box size information for selected stations.

Table 2.8: Summary of outlier stations excluded from CDOM matchup comparison for MERIS.

Station#	1	2	3	4	5
Date	20090819	20080406	20080407	20070717	20050523
Latitude	28.90	29.573	29.05	29.57	29.03
Longitude	- 89.47	-92.04	-90.01	-92.04	89.58
In situ $a_{CDOM}(412)$	0.74	3.27	1.22	1.53	0.09
MERIS-derived $a_{CDOM}(412)$	0.31	0.59	0.50	0.83	0.43
Pixel Box size	3×3	3×3	1×1	3×3	1×1
Time difference(hr)	10	24	6	14	8

MERIS estimates of DOC shows 3% and 1.7% average error for summer and spring-winter respectively, and in comparison to the error associated with MODIS, MERIS estimation shows higher accuracy. This could be due to the geographical location of stations used for MERIS DOC algorithm evaluation. While the stations used for evaluation of the DOC algorithm for MODIS

were mostly located in shallow water, the stations used for testing the DOC algorithm for MERIS were located mostly in deeper water (Figure 2.12, for summer time). The stations' location in deep water suggests that satellite derived band ratios were less affected by coastal water turbidity. Similar to MODIS, outlier points located in estuarine and coastal areas were excluded from DOC algorithm evaluation analysis. The DOC algorithm failed at these stations due to the effect of the same factors that caused MODIS DOC algorithm failure.

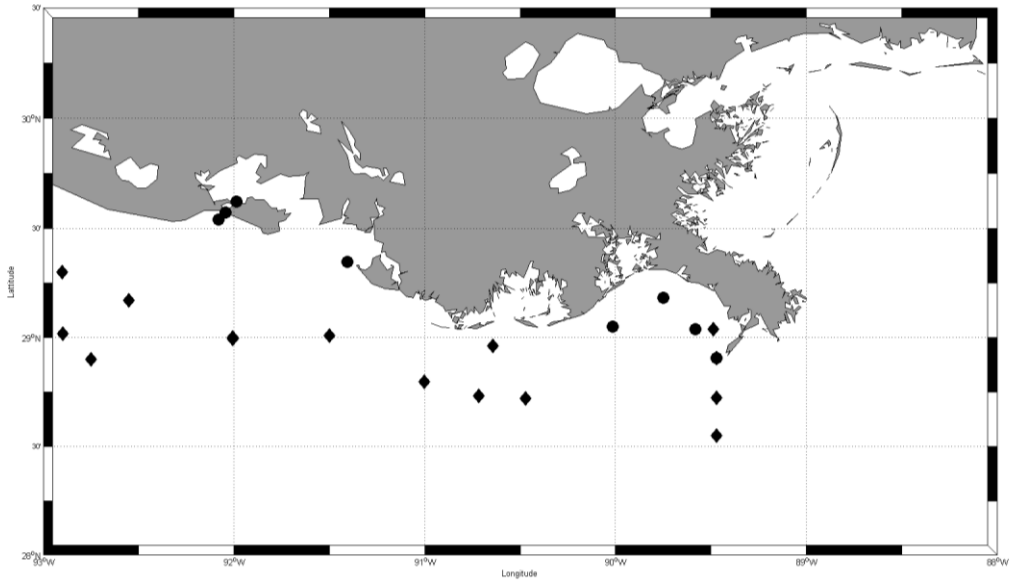

Figure 2.12: (●) indicates location of outliers excluded from CDOM matchup comparison for MERIS, and (♦) denotes location of stations used for evaluation of MERIS DOC algorithm.

2.5 Summary and Conclusion

The relationship between CDOM and DOC, as well as an assessment of CDOM and DOC retrieval algorithms using SeaWiFS, MODIS, and MERIS were addressed in this study. Field measured CDOM and DOC obtained from different research cruises covering areas over the Louisiana shelf in 2005 and from 2007 to 2009 were employed to evaluate and develop CDOM and DOC retrieval algorithms. Conservative DOC and CDOM behavior for both summer and spring-winter periods were observed in the study area. These conservative relationships were

used to develop empirical algorithms to derive DOC concentration from satellite ocean color sensors.

In comparing the D'Sa et al. (2006) algorithm with the parameterized Mannino et al. (2008) algorithm for CDOM estimation and further for DOC estimation, the D'Sa et al. (2006) SeaWiFS algorithm performed relatively well. Similar processes were followed to develop a DOC algorithm for MODIS and MERIS sensors. Since no empirical CDOM algorithms were available for MODIS and MERIS in our study area, relationships were developed between in situ measured $a_{CDOM}(412)$ and satellite-derived R_{rs} ratio for each sensor. For MODIS, $R_{rs}(488)/R_{rs}(555)$ values were obtained from satellite data and correlated with $a_{CDOM}(412)$, while for MERIS, $R_{rs}(510)/R_{rs}(560)$ values were used to construct a band ratio empirical algorithm. To evaluate the performance of each sensor, satellite-derived $a_{CDOM}(412)$ were compared with in situ match-up points. Our analysis revealed that both MODIS and MERIS tend to overestimate CDOM values less than 1.5 m^{-1}, and both algorithms failed for CDOM values greater than 1.5 m^{-1}. Several factors may contribute to these discrepancies such as optical interference of chlorophyll-a, time difference between satellite overpass and field measurement, and selected pixel box size. In addition, the seasonal relationship between a_{CDOM} (412) and DOC was combined with the $a_{CDOM}(412)$-R_{rs} ratio to construct DOC seasonal empirical algorithms. Then satellite-derived DOC values were correlated against in situ DOC values to test their performance. In summer, both sensors performed reasonably well, while in the spring-winter period there was a tendency for underestimation of DOC particularly for MODIS, likely due to sediment resuspension by cold front intrusion in the spring-winter period or time difference between in situ and satellite passes.

The approach followed in this study was based on available field and satellite data. As mentioned in the discussion section, some spatial and temporal limitations associated with

available data introduced significant errors and uncertainties. In order to develop robust empirical algorithms to estimate DOC concentration and gain insight about DOC dynamics, future measurements of physical and optical properties with high temporal and spatial resolutions is imperative in our study site.

CHAPTER 3: COLORED DISSOLVED ORGANIC MATTER DYNAMICS IN THE NORTHERN GULF OF MEXICO USING OCEAN COLOR AND NUMERICAL MODEL RESULTS

3.1 Introduction

The colored component of dissolved organic matter (CDOM) in natural waters absorbs light in the ultraviolet (UV) and visible wavelength range and plays a key role in regulating light attenuation in the northern Gulf of Mexico. The featureless absorption spectrum of CDOM decreases exponentially with increasing wavelength from the UV to visible domain (Jerlov, 1976; Twardowski et al., 2004; Del Vecchio and Blough, 2006). In coastal waters, river-borne CDOM which is a mixture of humic and fulvic acids is introduced to coastal systems by river runoff (Carder et al., 1989; McKnight and Aiken, 1998; Nelson and Siegel, 2002) whereas in open ocean autochthonous sources, such as phytoplankton and heterotrophic processes (Nelson et al., 2007, and references therein) contribute to CDOM. There is increasing interest in monitoring CDOM due to its numerous influences and applications. Its light absorbing properties can significantly impact primary productivity by limiting light while also blocking harmful UV radiation (Stedmon et al 2000). CDOM has been used as an intermediary for determination of dissolved organic carbon (DOC) (Del Castillo and Miller, 2008; Griffin et al., 2011). In coastal waters, CDOM has been employed as a semi-conservative water mass tracer, as an indicator of water mass mixing, and as an index to measure water quality (Ferrari and Dowell 1998; Blough and Del Vecchio, 2002; Coble et al., 2004; Le Fouest et al., 2006; D'Sa and Korobkin, 2008; Stedmon et al., 2010). Moreover, CDOM can be used as a proxy for retrieving salinity using ocean color sensors, and providing synoptic maps of salinity (D'Sa et al., 2002; Hu et al., 2003, Bowers and Brett, 2008). Since CDOM plays an important role in various biogeochemical cycles

and microbial ecology in natural waters (Moran and Zepp, 1997; Floge and Wells, 2007), it is critical to study its distribution and fate in the aquatic environment.

Although satellite ocean color data have been utilized to retrieve and monitor CDOM (Kahru and Mitchell, 2001; D'Sa et al., 2006; Mannino et al., 2008), their more regular use in monitoring and applications are hampered by cloud coverage, sun glint, and temporal resolution associated with the time and passage of the satellite. Obtaining clear imagery is often constrained by cloud coverage while sun glint can confound precise retrieval of water's constituents from remote sensors (IOCCG, 1999). Temporal resolution of ocean color sensors (e.g. daily resolution for SeaWiFS) further limits its application to the passing time of the satellite. In contrast, numerical circulation model outputs that can be directly (e.g., temperature) or indirectly (e.g., salinity) linked to satellite products can be generated at much higher temporal and spatial resolution. Hence, it would be desirable to find an approach to extract CDOM from the outputs of a numerical model. The strong linkage between salinity and CDOM reported in many studies especially in coastal waters suggest that salinity could be used as a proxy to derive CDOM from simulated salinity by model. However, in order to use numerical models to derive an ocean color product such as CDOM implement the above procedure successfully there is a requirement for: 1) a strong inverse linear relationship between CDOM and salinity, and 2) a reliable numerical model to simulate salinity.

The relationship between absorption coefficients of CDOM (a_{CDOM}) with salinity has been studied for different regions (Ferrari and Dowell et al., 1998; D'Sa et al., 2002; Stedmon et al., 2003). In coastal regions highly influenced by CDOM-laden river runoff, a_{CDOM} often declines linearly with increasing salinity indicating that CDOM behaves conservatively with respect to salinity. It also suggests that there is neither addition nor removal of terrestrial CDOM.

In other words, it is a pure dilution processes (Del Vecchio and Blough 2006; Blough et al., 1993; Blough and Del Vecchio, 2002; Vodacek et al., 1997; Ferrari and Dowell, 1998; Kowalczuk, 1999). The non-linear relationship between a_{CDOM} and salinity has been reported in different aquatic environments, even in coastal regions not influenced by high riverine input (Blough et al., 1993; Højerslev et al., 1996; Kowalczuk 1999). An upward and a downward deviation from an inverse linear relationship between CDOM and salinity suggest an addition (e.g. autochthonous production) or removal (e.g. photodegradation, adsorption) of CDOM, respectively (Uher et al., 2001; Stedmon et al., 2003; D'Sa and DiMarco 2009). Another possibility is the mixing of water masses with different CDOM end-members (Ferrari and Dowell, 1998; Uher et al., 2001; Stedmon et al., 2003; Del Vecchio and Blough, 2005). In such cases, caution should be taken in using salinity as a proxy for CDOM.

An important output of numerical models such as the Navy Coastal Ocean Model (NCOM) used in this study are the currents that can be used to in conjunction with derived CDOM to investigate the physical influences on CDOM distribution. Advection of CDOM by currents is an important physical process that could affect CDOM distribution in the northern Gulf of Mexico. Hitchcock et al. (2004) described a Lagrangian study of CDOM distribution within the Mississippi River plume. Swan et al. (2009) reported the effect of upwelling induced by a tropical current system on CDOM distribution in equatorial Pacific Ocean. Jolliff et al. (2003) combined a circulation model with CDOM photolysis to study CDOM transport over the west Florida shelf (WFS). Their circulation model included the advection-dispersion equations of pollutant transport with modified source terms to include CDOM transport. Following model verification with in-situ measurements and satellite data, simulation results were employed to study CDOM distribution pattern over WFS. Shulman et al. (2011) combined the remotely

sensed parameters and the navy coastal ocean model (NCOM) to study the effect of the California current system on optical parameters. In the northern Gulf of Mexico, better insights on the spatial and temporal distribution and fate of CDOM could be obtained by understanding the current patterns and use of model simulations.

Although factors such as winds, river discharge, and detached eddies from the Loop Current contribute to the generation of currents over the Louisiana-Texas shelf (Oey, 1995; Walker, 1996), currents are primarily produced by winds and enhanced by river's discharge and eddies (Oey, 1995; Li et al, 1997). A modeling study by Oey (1995) showed that a large component of transport over the inner-shelf is produced by wind (40-48%), while river discharge and loop current eddies account for 28-33% and 19-33%, respectively. Tidal induced currents are relatively small in this area due to the small tidal range (micro-tidal) (Wright, 1997). Two seasonal current patterns are distinguishable over the shelf that depends on wind characteristics (Cochrane and Kelly, 1986; Walker, 2005). During non-summer months (from September to May) due to persistent easterly and southeasterly winds and the resulting Ekman transport, a westward current is produced. The westward current is modulated by the Mississippi and Atchafalaya Rivers' discharge, and forms the Louisiana coastal current (LCC) (Cochrane and Kelly, 1986). This shelf current also known as down-coast current, is well developed with a clear westward direction, from Louisiana to Texas and southward along the Texas coast (Wiseman and Kelly, 1994). Concurrently, currents at the shelf break often flow east due to anticyclonic eddies. This eastward current forms a cyclonic gyre when it combines with westward currents on the inner-shelf. The inner limb of the cyclonic gyre is the down-coast current and the outer limb is the eastward current along the shelf break (Cochrane and Kelly, 1986). Currents southwest of this gyre are seaward, while currents flow shoreward at the southeast margin of the gyre. The

down-coast current weakens and disappears during summer month (June, July, and August) (Cochrane and Kelly, 1986; Nowlin et al., 1999) due the easterly and southeasterly winds shifting to southerly and southwesterly. This change in the wind direction generates an up-coast current that is generally directed eastward (Jarosz, 1997). The up-coast current is not as developed as the down-coast current and exhibits a disorganized pattern (Crout et al., 1984). Shelf break currents are still directed to the east, and no gyre is formed. The down-coast current is re-established at the end of August and becomes predominant by May (Cochrane and Kelly, 1986). The seasonal patterns of currents as well as the seasonality of rivers' discharge are likely to strongly contribute to the formation of distinct patterns of CDOM distribution over the shelf.

The main objective of the present study thus is to examine CDOM absorption coefficient distribution maps derived from NCOM numerical model salinity outputs and in conjunction with model current outputs to study its dynamics. The study includes two parts; the first part addresses the relationship between CDOM and salinity over the study area to derive CDOM from NCOM simulated salinity. CDOM-salinity relationships were determined for different zones and seasons, and then were applied to the simulated salinity maps. The second part investigates the application of current patterns simulated by the model to study CDOM distribution caused by horizontal advection. Here, currents simulated by the NCOM numerical model were superimposed on model-derived CDOM maps to investigate CDOM dynamics in the northern Gulf of Mexico.

3.2 Method and Data

3.2.1 Study area

The Northern Gulf of Mexico comprising both the inner and outer shelf areas between 88.2º W to 95.5º W and latitude 27ºN to 30.5º N were studied using field and satellite ocean color data along with the outputs of the NCOM numerical model (Figure 3.1).

The inner-shelf region of this area is characterized by high amounts of discharge from the Mississippi and the Atchafalaya Rivers. This large volume discharge of freshwater strongly affects the physical and biogeochemical processes over the study area (Lohrenz et al., 1990; Pakulski et al., 1995; Rabalais et al., 1996; D'Sa and Miller, 2003). Although the river discharge increases CDOM and decreases salinity in the coastal waters, they can both be modulated by shelf hydrodynamics.

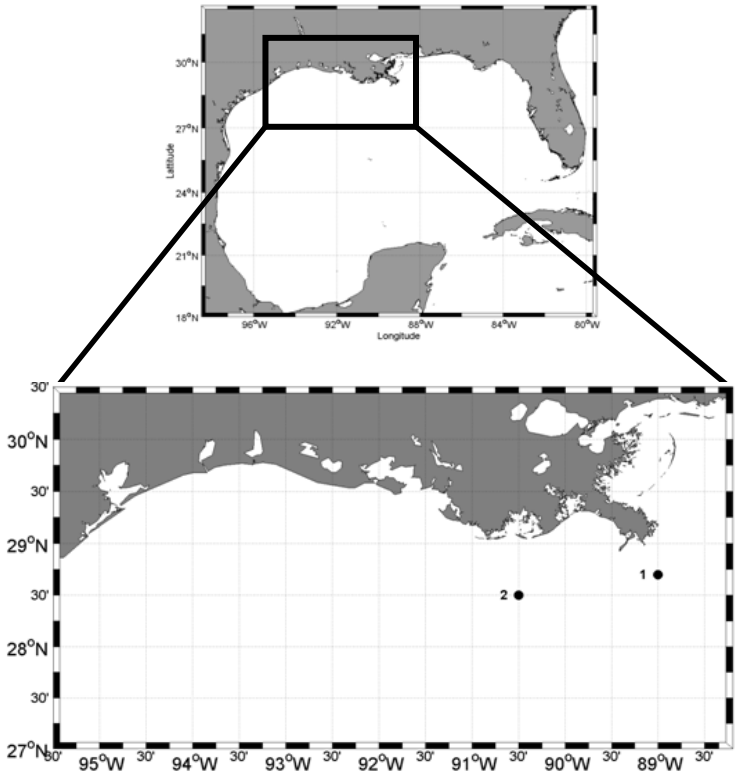

Figure 3.1: Map of the study region in the northern Gulf of Mexico encompassing the Mississippi, Louisiana and parts of Texas coast. Black circles show the locations for which NCOM-simulated current velocities were acquired for March and June 2005.

3.2.2 Data

3.2.2.1 Field data

CDOM and salinity data were obtained from 9 oceanographic cruises carried out in 2001 (April), 2005 (March, May, July and August), 2006 (January), 2007 (April and May), and 2009 (August) (Table 3.1). The sampling locations are shown for the spring-winter (Figure 3.2A) and

the summer (Figure 3.2B) periods. In 2005 (March, May, July and August), water samples were obtained from the nearshore coastal waters strongly influenced by the Mississippi and Atchafalaya Rivers (West of Southwest Pass, off the Terrebonne Bay, and Atchafalaya shelf) aboard the R/V Gyre.

Table 3.1: Summary of cruises undertaken in the northern Gulf of Mexico showing periods when samples were acquired for this study. Average values for $a_{CDOM}(412)$ and salinity shown for each cruise.

Cruise	Date	$a_{CDOM}(412)$ (m^{-1})	Salinity (psu)
1	April l2- l6, 2001	0.23	30.20
2	March 23-29, 2005	0.47	27.07
3	May 20-25, 2005	0.43	25.96
4	July 8-12, 2005	0.23	29.27
5	August 18-24, 2005	0.25	28.75
6	January 1- 4, 2006	0.43	23.50
7	May 7-10, 2007	0.87	24.16
8	April 16-20, 2007	0.41	31.75
9	August 18-20, 2009	0.34	7.94

Water salinity was measured using a conductivity-temperature-depth (CTD) profiler (Sea-Bird Electronic, Inc., Bellevue, WA, USA) during all cruises. Water samples were filtered through pre-rinsed 0.2-µm Nuclepore membrane filters. Filtered-samples were kept refrigerated at 4° C, and absorption coefficients measured on a single-beam or dual beam spectrophotometers. Optical absorbance spectra (A) measured from 250 nm to 722 nm using Milli-Q water as a reference were further corrected for baseline fluctuation by subtracting the average absorbance at the 715-722 nm (D'Sa and DiMarco, 2009). Absorption coefficient (m^{-1}) for each wavelength was obtained using the expression (3.1):

$$a(\lambda) = \frac{2.303A(\lambda)}{l} \tag{3.1}$$

where, A is the absorbance, λ is the wavelength and l is the optical path length in meters (0.1m or 0.5 m). Similar methods for field sampling and data analysis were utilized to obtain CDOM

and salinity data for samples acquired from other field campaigns. More detailed information can be found in the Biological and Chemical Oceanography Data Management Office (BCO-DMO) website (http://data.bco-dmo.org/jg/serv/BCO/NACP_Coastal/GulfMexico/CDOM.html0).

3.2.2.2 Satellite Data

Data from the SeaWiFS ocean color sensor aboard the Geoeye satellite (August 1997 to December 2010) were used to derive CDOM absorption coefficient at 412 nm ($a_{cdom}(412)$). Daily SeaWiFS Level-1 merged local area coverage (MLAC) data with 1 km resolution were obtained from NASA's Ocean Color website (www.oceancolor.gsfc.nasa.gov) and processed using SeaWiFS Data Analysis System (SeaDAS) into Level-2 to obtain CDOM absorption by applying the (D'Sa et al. 2006) empirical algorithm given by the equation:

$$a_{cdom}(412) = 0.227[R(510)/R(555)]^{-2.512} \quad (3.2)$$

where $R_{rs}(510)$ and $R_{rs}(555)$ are remote sensing reflectances at 510 and 555 nm wavelength bands, respectively. The robustness of this algorithm was demonstrated based on matchup comparisons with field data (Chaichi Tehrani et al., 2012, unpublished data). The SeaWiFS derived surface CDOM absorption imagery was used in this study to compare with NCOM-derived CDOM maps.

3.2.2.3 NCOM Data

A high-resolution (spatial resolution of ~1.9 km) nested (372 × 200 grid) Navy Coastal Model (NCOM) known as Mississippi-Louisiana-Texas (MsLaTex) developed as part of a NASA funded project were used in this study (D'Sa and Ko 2008). NCOM MsLaTex coastal model covers the region between 27º-30.5° N latitude and 88.2º-95.5°W longitude that includes the Mississippi, Louisiana and Texas shelves and oceanic waters in the northern Gulf of Mexico. The MsLaTex model is nested within Intra-Americas Sea Nowcast Forcast System (IASNF)

which has been developed at Naval Research Laboratory (NRL). NCOM is based on the Princeton Ocean Model (POM) and the Sigma/Z-level Model which implements the hydrostatic primitive equation (Martin 2000; Barron et al., 2006). Furthermore, the boundary conditions are imported from IASNF into the nested MsLaTex model. IASNFS includes Gulf of Mexico, the Caribbean, and parts of the western North Atlantic with horizontal resolution of ~6 km. The IASNFS regional model assimilates real-time sea surface height anomaly data from three satellites (GFO, Jason-1 and ERS-2), daily assimilation of river discharge data, sea surface temperature data from AVHRR, and topography from NRL DBDB2 and NGDC hydrographic data to produce ocean circulation and sea level variations in the Gulf of Mexico and adjacent oceanic regions (Ko et al., 2008; D'Sa and Ko, 2008).

3.3 Results

3.3.1 CDOM-salinity relationship

A conservative behavior between CDOM absorption and salinity is essential to employ salinity as a proxy for the determination of CDOM. For the study area, the inverse linear relationship between CDOM absorption and salinity was found to vary seasonally and spatially; seasonal discharge by the Mississippi and Atchafalaya Rivers, enhanced water column mixing during winter-spring season, and elevated CDOM photobleaching and stratification during summer likely contributed to this variability. Field data collected during various cruises (Table 3.1) were examined and CDOM-salinity relationships were established for the spring-winter and summer periods spatially partitioned into two zones (Figure 3.2A and 3.2B; Table 3.2). Zone 1 comprises the shallow areas east of the birdfoot delta and the inner-shelf west of the delta. Zone 2 comprises the deeper outer-shelf extending from Mississippi to the east Texas shelf. Zone 1 is directly affected by the discharge from the Mississippi and the Atchafalaya Rivers. In zone 1,

effects due to photobleaching are mostly likely masked by the lower salinity waters containing elevated levels of CDOM (D'Sa and DiMarco, 2009). In contrast, zone 2 is less affected by the rivers' fresh water and therefore less conservative behavior of CDOM and salinity is expected. This is generally in accordance to the shelf division suggested by Nowlin et al. (2005) in connection with studies of the long-term flow along the Texas-Louisiana shelf.

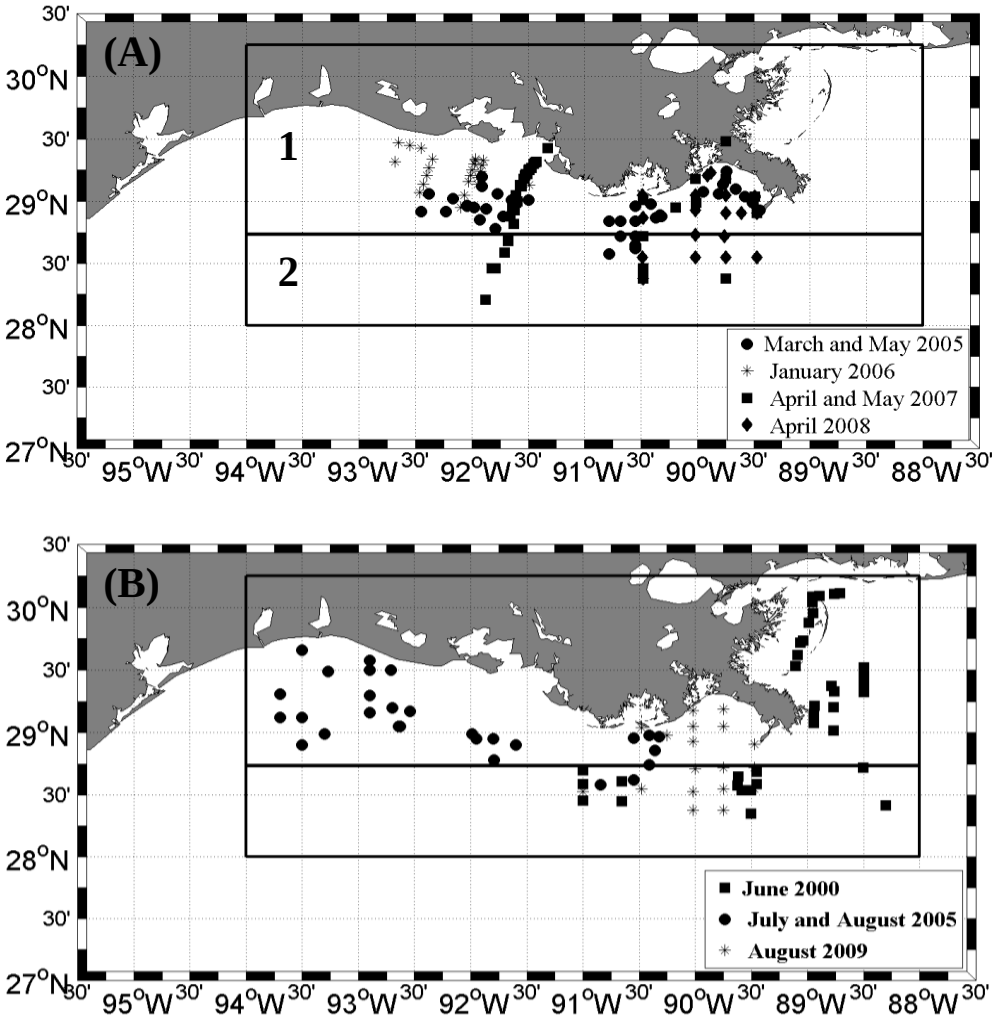

Figure 3.2: Station locations of cruises conducted during (A) spring-winter, and (B) summer periods.

Table 3.2: Geographical extension of the zone 1 and the zone 2.

Subset region	Latitude range	Longitude range
Zone 1	28.73ºN-30.25ºN	88.00 º W-94.00 º W
Zone 2	28.00 ºN-28.729ºN	88.00 º W-94.00 º W

Surface CDOM absorption coefficient at 412 nm was 0.61± 0. 57 m^{-1} at an average surface salinity of 26.06±8.22 during winter-spring in zone 1 indicating the strong river influence on the CDOM and salinity fields in the nearshore waters. During the same period, zone 2 exhibited an average surface salinity of 32.66±4.47, and an average CDOM absorption of 0.203±0.18 m^{-1}, which was three times less than that of the zone 1. During summer, surface CDOM in zone 1 (0.32 ±0.22 m^{-1}) was almost two times less than the spring-winter period, while the mean surface salinity over this zone increased slightly to 27.47± 3.62. Lower CDOM in zone 1 during the summer could be attributed to the low flow of the Mississippi and the Atchafalaya Rivers, and photobleaching effects aided by stratification and high solar insolation (Boss et al., 2001; D'Sa and DiMarco, 2009). Zone 2 during summer exhibited the lowest CDOM absorption (0.064±0.103 m^{-1}) and highest salinity (32.84 ±2.72) suggesting loss of CDOM due to photochemical decomposition (Opsahl and Benner, 1998; Chen and Gardner, 2004).

For each season and each zone, CDOM absorption coefficient at 412 nm, $a_{CDOM}(412)$, were plotted as a function of salinity (Figures 3.3A to 3.3D; Table 3.3). High correlations between CDOM and salinity were obtained for the spring-winter and the summer periods for zone 1 (R^2= 0.88, n=117; R^2= 0.92, n= 39, respectively) (Figure 3.3A and 3.3C) suggesting conservative mixing between coastal and oceanic waters (D'Sa and DiMarco, 2009). Similarly, for zone 2, CDOM and salinity were highly dependent during the spring-winter period (R^2=0.93, n=22) (Figure 3.3B), likely due to mixing associated with frontal passages during the period. In contrast, during summer, $a_{CDOM}(412)$ exhibited low dependency of on salinity (Figure 3.3D), which could be attributed to photooxidation and loss of CDOM during the summer.

Table 3.3: Results showing the slope (a), intercept (b) and correlation coeff. R^2 of the regression equation* between $a_{CDOM}(412)$ and salinity for the two zones.

Subset region	Season	Number of Samples	a	b	R^2
Zone 1	Spring-winter	117	-0.066	2.35	0.88
Zone 2	Spring-winter	22	-0.039	1.49	0.93
Zone 1	Summer	39	-0.060	1.98	0.92
Zone 2	Summer	25	-0.028	0.98	0.54

* An inverse (negative) linear relationship was fitted between $a_{CDOM}(412)$ (m^{-1}) and salinity in form of $a_{CDOM}(412) = a \times salinity + b$, where a is the slope, and b is the intercept.

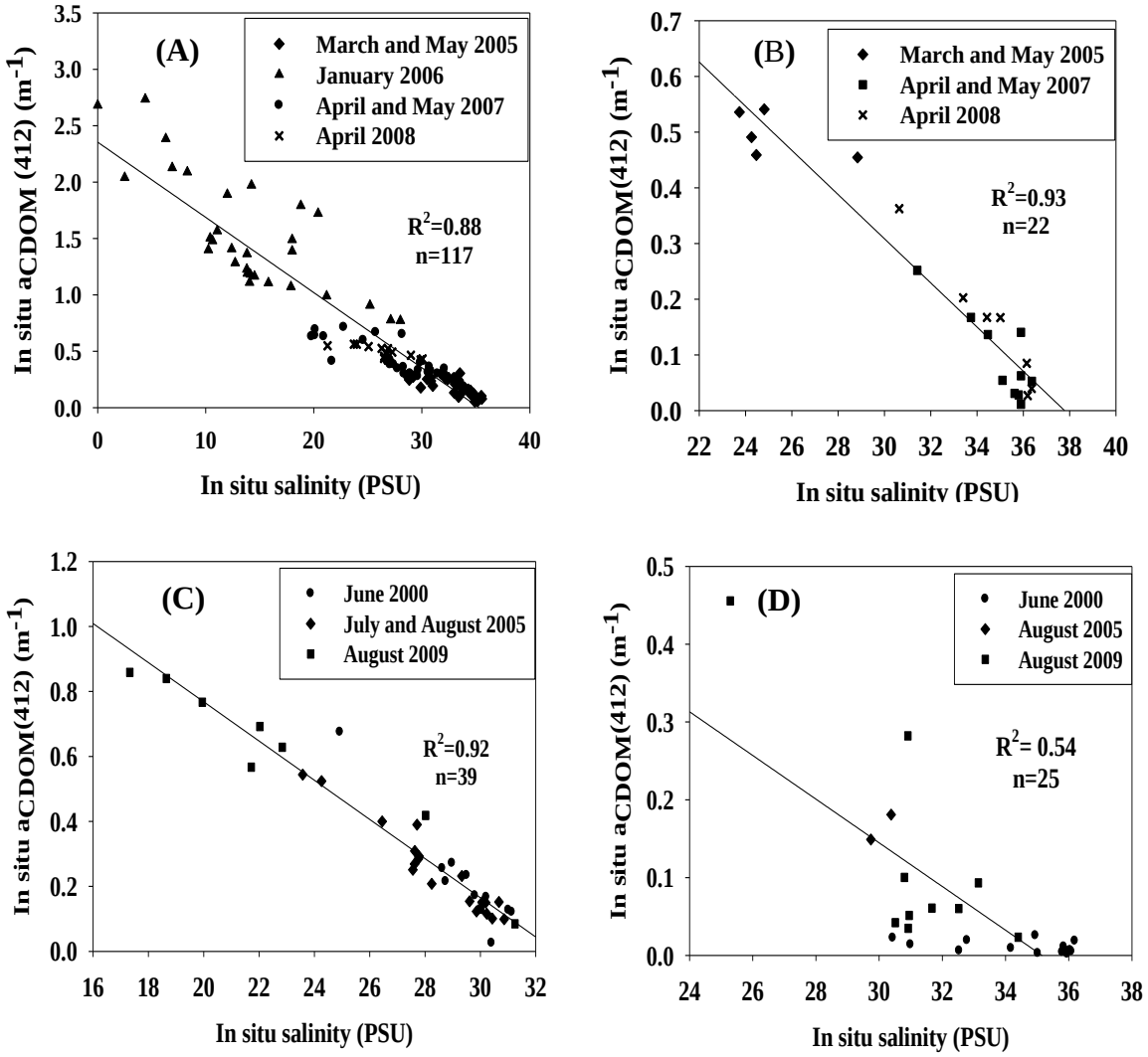

Figure 3.3: Correlation between $a_{CDOM}(412)$ and salinity (A) for the spring-winter period over the zone 1, (B) for the spring-winter period over the zone 2, (C) for summer over the zone 1, (D) for the summer over the zone 2.

3.3.2 Spatial distribution of CDOM based on modeled salinity

The CDOM-salinity relationships obtained for different zones and seasons (Table 3.3) were applied to the salinity simulated by the NCOM model. The accuracy of NCOM model for simulating salinity was examined by comparing modeled and in situ salinity for available salinity data (Figure 3.4). Error statistics such as Bias, Root Mean Square Error (RMSE), Scatter Index (SI), and Correlation Coefficient (R^2) used were calculated using equations given by:

$$\text{Bias} = \frac{1}{N}\sum_{i=1}^{N}(y_i - x_i) \quad (3.3)$$

$$\text{RMSE} = \sqrt{\frac{1}{N}\sum_{i=1}^{N}(y_i - x_i)^2} \quad (3.4)$$

$$\text{SI} = \frac{1}{\bar{x}}\sqrt{\frac{1}{N}\sum_{i=1}^{N}[(y_i - \bar{y}) - (x_i - \bar{x})]^2} \quad (3.5)$$

where y_i denotes NCOM-simulated values, x_i denotes field measured values , $\bar{y}$ is the average of NCOM-simulated value, and $\bar{x}$ is the average of in situ values. N is number of samples. Error statistics (Bias=0.28, RMSE= 3.5, SI=0.12, and R^2= 0.73 for n=225) indicated satisfactory performance of the NCOM model in simulating salinity.

CDOM-salinity relationships (Table 3.3) were used on modeled salinity to obtain NCOM-derived CDOM absorption maps (e.g., Figure 3.5A, B). These were compared to SeaWiFS-derived CDOM absorption maps based on the D'Sa et al. (2006) algorithm. Based on availability of clear satellite imagery for the study area, modeled outputs for 18 October 2005 at 7:00 PM and 23 July 2005 at 7:00 PM were selected as representatives for non-summer and summer periods, respectively. Figures 3.5A-3.5C and 3.6A-3.6C show NCOM simulated salinity maps, NCOM-derived CDOM maps and SeaWiFS-derived CDOM absorption for both selected times. The simulated salinity on October 18, 2005 at 7:00 PM (Figure 3.5A) shows that the entire study area except some regions adjacent to the mouths of the Mississippi and the Atchafalya

Rivers were influenced by high salinity values (~30 on average). The low salinity regions were limited to areas around the Mississippi birdfoot delta, Southwest Pass, Barataria Bay, Terrebonne Bay, Atchafalaya Bay and Vermilion Bay.

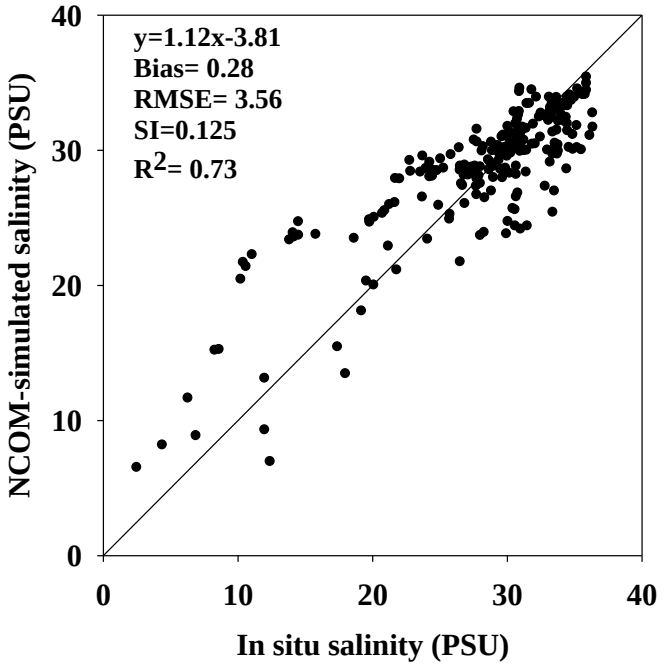

Figure 3.4: Comparison of in situ salinity with NCOM simulated salinity. Diagonal line is the 1-to-1 line.

Due to the inverse and linear relationship between CDOM and salinity determined for the study area, high salinity values implies low CDOM, while high CDOM is expected for the low salinity coastal regions. This is illustrated in Figure 3.5B showing a map of surface CDOM absorption derived from NCOM simulated salinity. A comparison of the model-derived surface CDOM and SeaWiFS-derived CDOM for 18 October 2005 at 6:30:42 PM (Figure 3.5C) shows similar patterns of CDOM distributions. Entrainment of CDOM from the Southwest Pass of the Mississippi River toward the inner-shelf in the simulated map appeared similar to the SeaWiFS-derived image as was the pattern at the mouth of the Atchafalaya Bay.

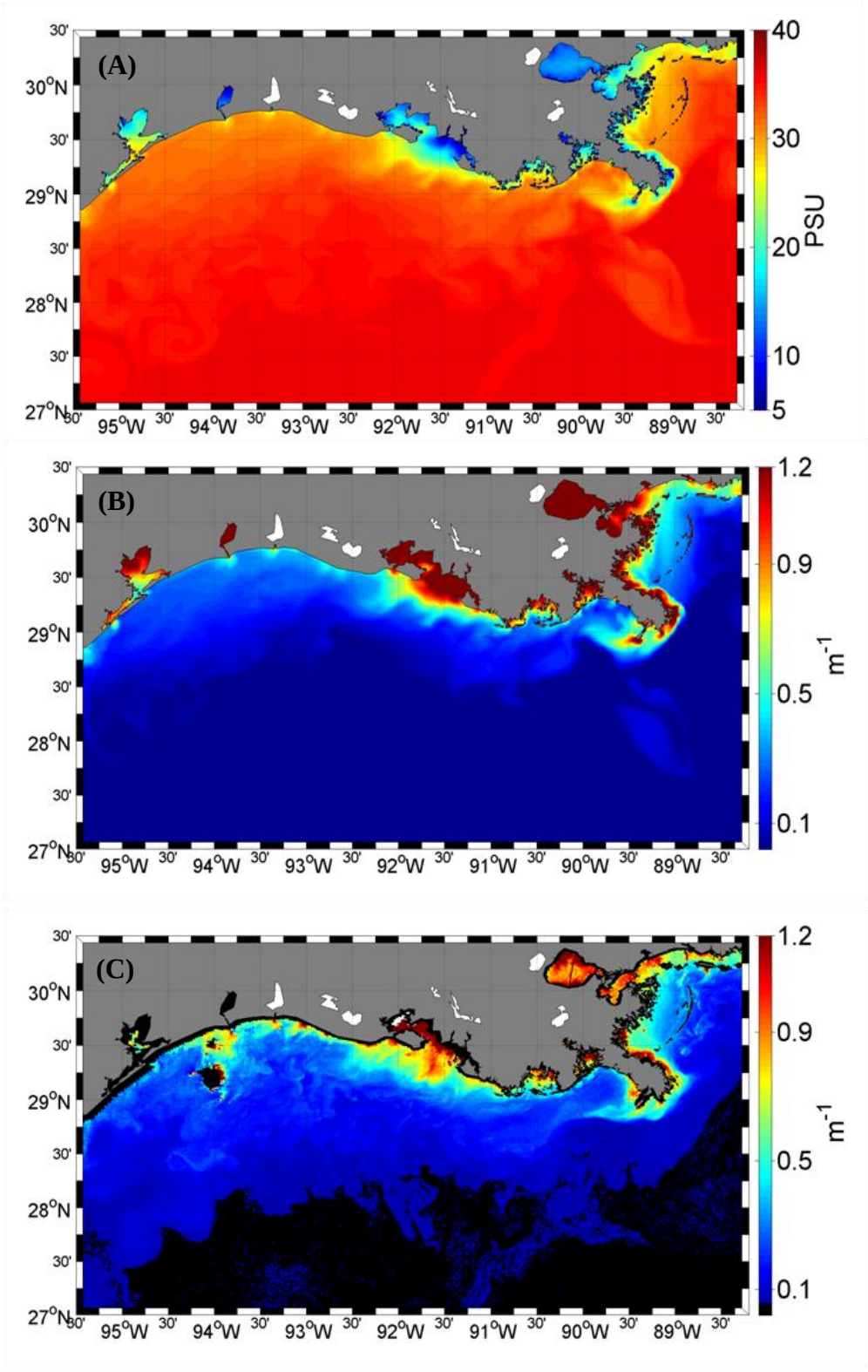

Figure 3.5: (A) NCOM-simulated salinity map for 18 October 2005, at 7:00:00 PM, (B) NCOM-derived CDOM absorption map for 18 October 2005, at 7:00:00 PM, and (C) SeaWiFS-derived CDOM absorption map for 18 October 2005, at 6:30:24 PM.

NCOM simulated salinity was selected for 23 July 2005 at 7:00:00 PM as representative for the summer along with SeaWiFS imagery for the same day (Figure 3.6). The NCOM simulated salinity (Figure 3.6A) depicts low salinity filaments extending outward from South Pass of the Mississippi River delta. This pattern appears as high surface CDOM in the vicinity of South Pass towards the shelf break until it disperses, and mixes with high salinity offshore waters. Model simulation also shows the CDOM-laden low salinity waters spreading east of the Mississippi birdfoot delta toward the eastern shelf (Figure 3.6B). Although the simulated CDOM exhibits high consistency with satellite image (Figure 3.6C), especially along the coastal areas, satellite-derived CDOM overestimates in the very near shore waters could be due to interference from seawater constituents such as suspended sediments and algal biomass.

The ability of the model to simulate CDOM was investigated by comparing NCOM-derived CDOM with in situ measurements for the spring-winter and the summer periods (Figure 3.7A and 3.7B, respectively). NCOM data used for matchup comparisons were acquired from simulations in May, March, July and August (2005) concurrent with in situ data and were independent of the data used for the investigation of CDOM conservative behavior. Results show that the NCOM-derived CDOM was quantitatively in agreement with field data. For the spring-winter, average measured and modeled $a_{CDOM}(412)$ was 0.44 m^{-1}, and 0.48 m^{-1}, respectively with Bias= 0.03; RMSE= 0.099; SI= 0.21, and R^2= 0.52. In the summer, the average values of $a_{CDOM}(412)$ were 0.2 m^{-1} and 0.18 m^{-1} obtained from field measurement and NCOM, respectively with Bias= -0.016, RMSE= 0.059, SI= 0.28, and R^2= 0.51. These results provide support for NCOM's ability to determine surface CDOM in our study area. In order to provide integrated maps, the obtained CDOM-salinity relationships were applied to regions outsides the zone 1and 2; therefore, the result for these regions should be used with caution.

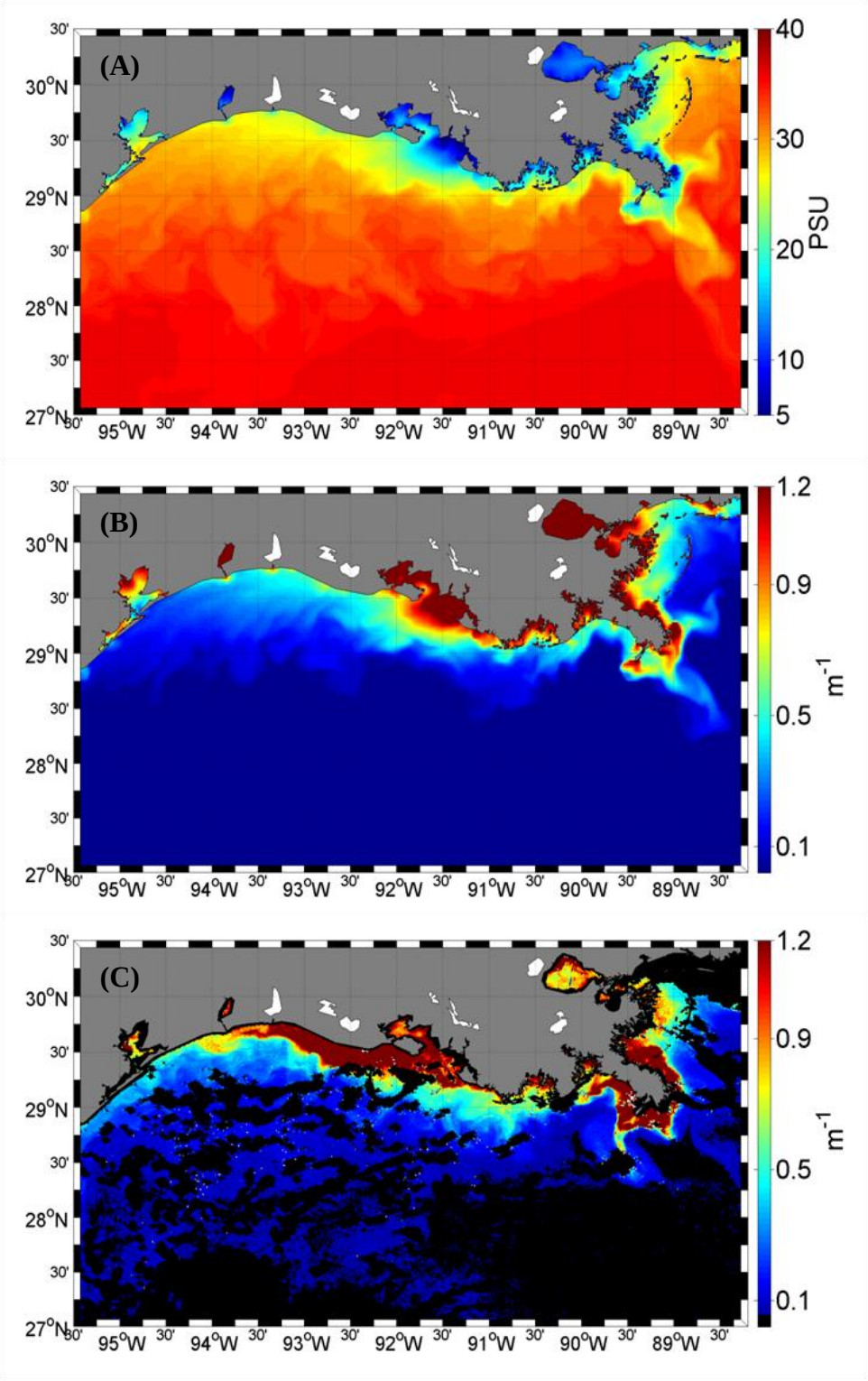

Figure 3.6: (A) NCOM-derived salinity map for 23 July 2005, at 7:00:00 PM, (B) NCOM-derived CDOM absorption map for 23 July 2005, at 7:00:00 PM, and (C) SeaWiFS-derived CDOM map for 23 July2005, at 6:51:23 PM.

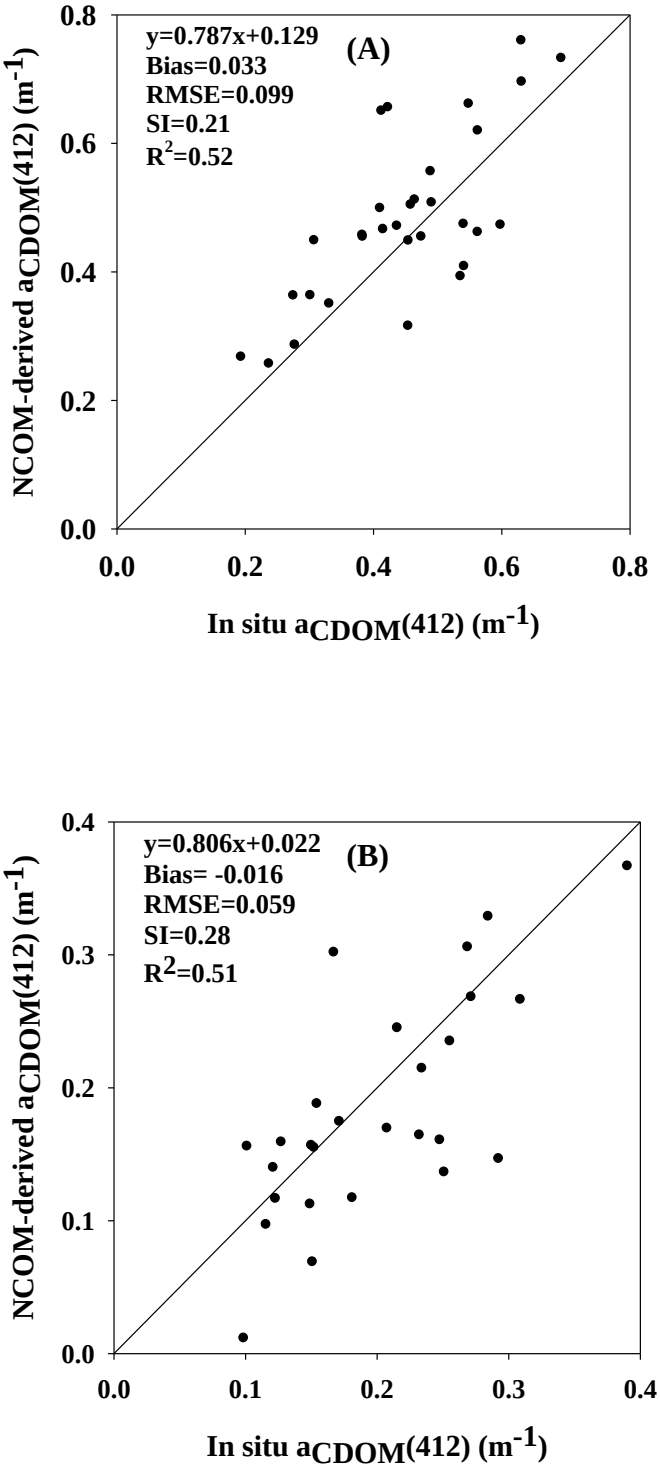

Figure 3.7: Match-up comparison between NCOM-derived CDOM and in situ CDOM (A) for the spring-winter period, and (B) for the summer.

3.3.3 Effect of advection on CDOM distribution

Advection by currents is the main physical process affecting the distribution of CDOM after being discharged to the marine environment by rivers (here the Mississippi and the Atchafalaya Rivers) (Boss et al., 2001). A seasonal reversal in the direction of currents along with the seasonal variations in rivers' discharge and CDOM levels lead to a spatial and temporal variability in surface CDOM distribution pattern. In order to study CDOM distribution in relation to horizontal advection, surface CDOM derived by NCOM (as described in section 3.3.2) were superimposed on simulated current patterns. The patterns were investigated for periods corresponding to the cold front, as well as the down-coast and the up-coast regimes. A high consistency was observed between CDOM distribution and current patterns for different time periods in 2005. Results for three specific time periods corresponding to each of the above-mentioned patterns are presented and discussed.

Figure 3.8 depicts CDOM distribution overlaid by simulated currents for May 5, 2005 at 6:00 PM showing a representative down-coast current. The general current direction over the inner-shelf is westward with the average current velocity of 0.5 m/s. Approaching the shelf-break, current velocity increases to approximately 1 m/s. A large anticyclonic eddy offshore of the birdfoot delta generated eastward currents at the shelf-break. In general, the persistent direction of shelf currents to the west entrained CDOM from coastal areas toward the inner-shelf. Currents characteristics during May were further studied by examining time series NCOM currents at points 1 and 2 (Figure 3.9A and 3.9D) located south of the Mississippi birdfoot delta and off the Terrebonne Bay, respectively (see Figure 3.1 for location). At point 1, westward and southwestward currents were dominant for first five days of May (Figure 3.9A), while southeastward to northeastward currents were prevalent for the rest of the month. Point 2

exhibited longer periods of down-coast current patterns with intermittent changes in current direction southward which were induced by a cold front intrusion. CDOM-rich waters west of the Mississippi birdfoot delta and in front of the Atchafalaya Bay (CDOM concentration of 1.2 m^{-1} or more) were advected by westward shelf currents. The high surface CDOM south of the birdfoot delta was not entrained toward the outer-shelf as the current pattern implies an east to west CDOM advection. CDOM absorption was relatively high (0.8-1 m^{-1}) over the area between Southwest Pass on the Mississippi delta and Barataria Bay or Louisiana Bight. Current pattern demonstrates that CDOM-laden waters were trapped in this region as a result of an anticyclonic gyre generated by the rotation of the Mississippi River plume that originated off Southwest Pass (Figure 3.10).

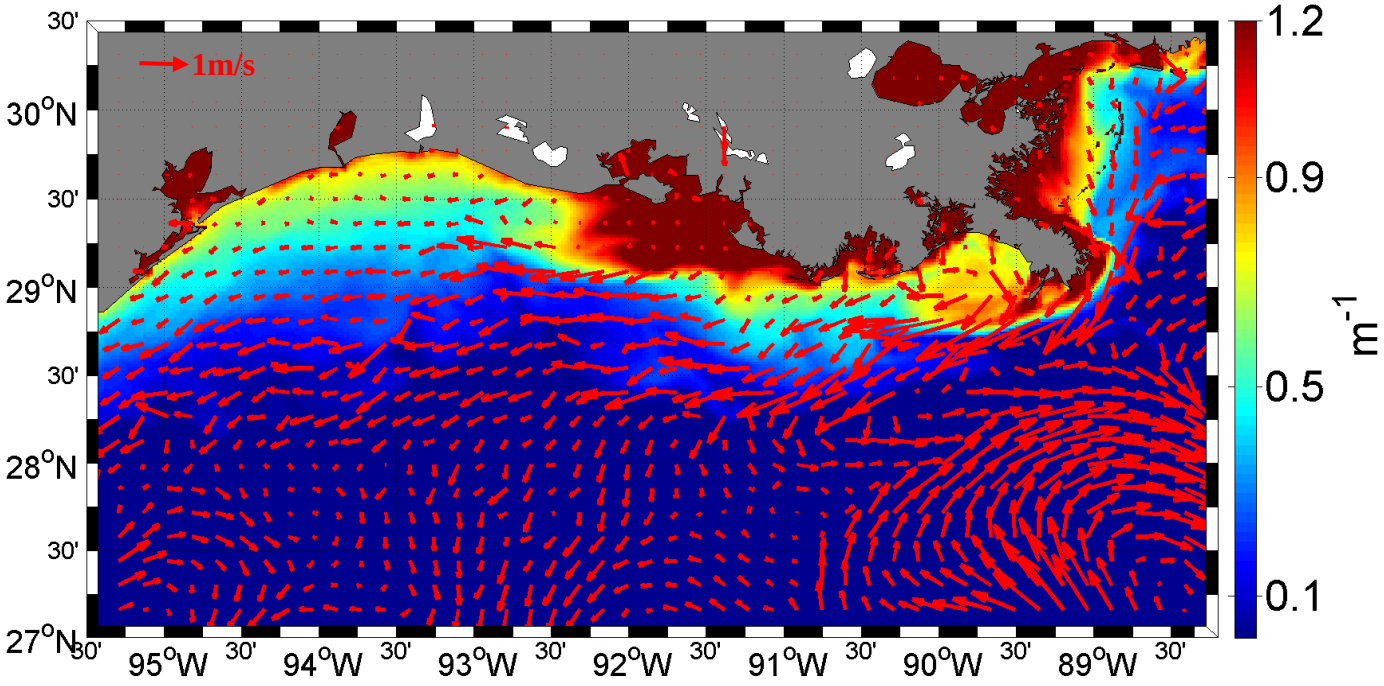

Figure 3.8: Model-simulated current pattern for 5 May 2005, at 6:00:00 PM (color bar indicates CDOM absorption coefficient (m^{-1})).

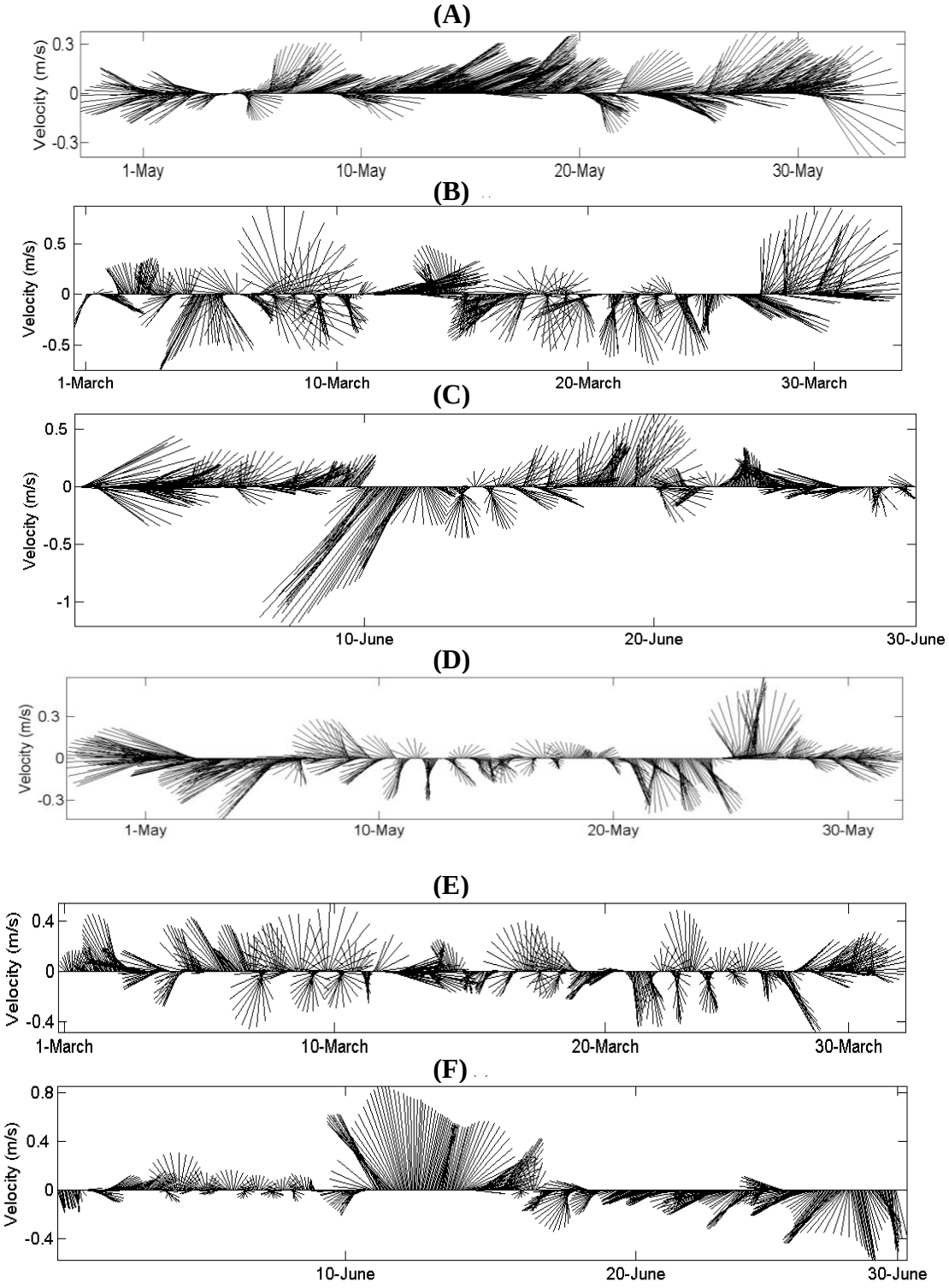

Figure 3.9: Time series of current (A) at the point 1 for May 2005, (B) at the point 1 for March 2005, (C) at the point 1 for June 2005, (D) at the point 2 for May 2005, (E) at point 2 for March 2005, and (F) at the point 2 for June 2005 (see Figure 3.1 for points 1 and 2 location).

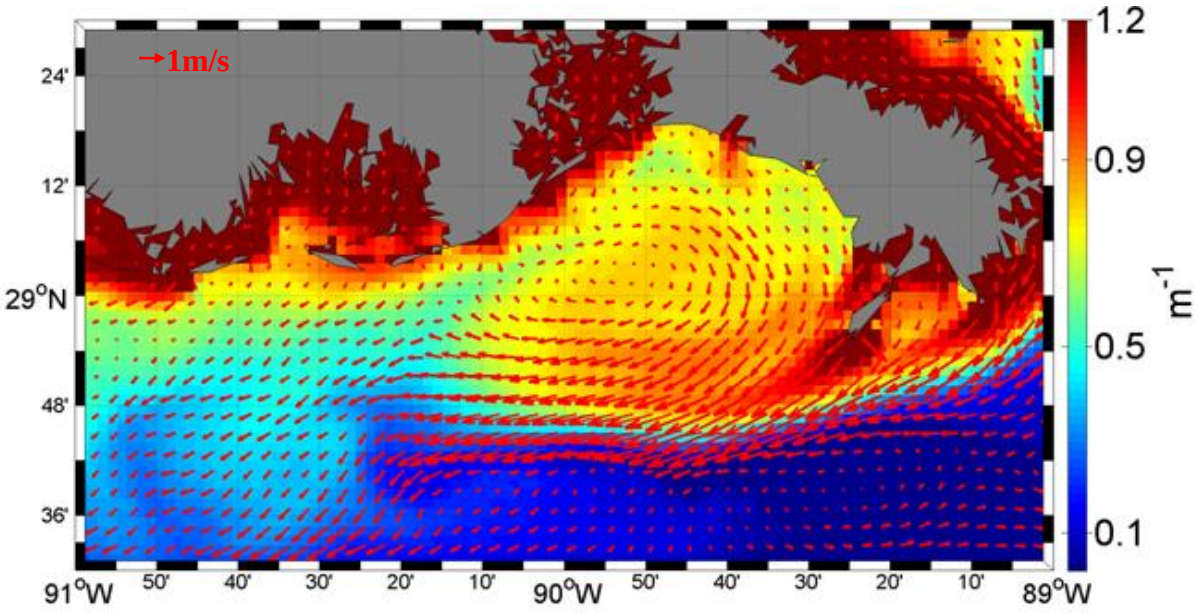

Figure 3.10: Anti-cylonic gyre pattern in the Lousiana Bight on May 5, 2005, at 6:00:00 PM (color bar indicates CDOM absorption coefficient (m^{-1})).

Figure 3.11 illustrates NCOM-simulated CDOM pattern overlaid with NCOM-simulated current vectors associated with a cold front on March 11, 2005, at 12:00 PM. The intrusion of cold front disturbed the consistent westward down-coast current system. During the selected time, the outbreak of a cold front associated with northwesterly winds caused southward to southeastward currents with a velocity of 0.2 to 0.8 (m/s) over the inner Louisiana-Texas shelf. Currents were generally directed eastward over the outer shelf due to the impact of mesoscale eddies. Time series of currents for both point 1 (Figure 3.9B) and point 2 (Figure 3.9E) during this month showed significant southward current directions as a result of cold front outbreaks reaching a maximum velocity of 0.8 and 0.6 m/s for points 1 and 2, respectively. The corresponding CDOM pattern was highly tied to the current pattern. The general southward direction of induced current over the inner-shelf advected CDOM-laden waters toward the outer-shelf. CDOM-rich waters (CDOM absorption of 1.2 m^{-1} and greater) from the Atchafalaya-Vermilion and Terrebonne-Timbalier Bays were flushed out by the cold front intrusion and were injected into the inner-shelf. The same process advected CDOM from estuaries and coastal areas

in the eastern Texas shelf southward. Typical surface advective influence on CDOM distribution for the summer (22 June 2005, at 12 AM) is illustrated in Figure 3.12.

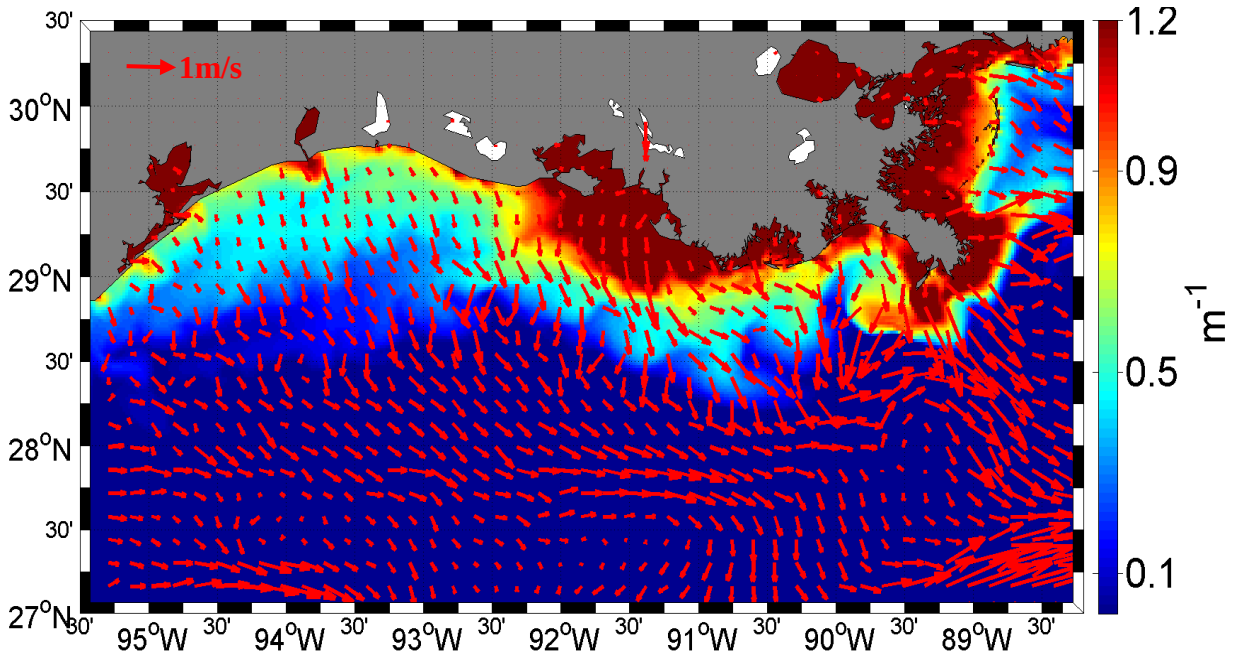

Figure 3.11: Current pattern for March 11, 2005 at 12 PM (color bar indicates CDOM absorption coefficient (m^{-1})).

Shelf currents are observed to be disorganized with a general eastward direction that is consistent with an up-coast current regime. Shelf-break currents to the south and southwest of the birdfoot delta were eastward and influenced by a meso-scale clockwise eddy located offshore of the Mississippi Canyon at latitude 27º 30´ N. The average inner-shelf current velocity at this time was ~0.3 m/s. Vector representation of currents at point 1 (Figure 3.9C) during June showed a general up-coast pattern with current velocity up to 0.8 m/s. There was a general eastward current direction for the first nine days of June, but later strong southwest currents with velocities up to 1.5 (m/s) were formed and affected the shelf area for two days. The direction of southward currents changed to northeastward as a result of the up-coast current regime on June 22. As observed, current pattern at point 1 was complex. The complex current pattern at this point was the result of seasonal wind pattern, Loop Current eddies, as well as the influence of the

Mississippi River plume (Nowlin et al., 2000; Walker et al., 2005; Martínez-López and Zavala-Hidalgo, 2009). Point 2 experienced small current velocities during the first ten days of June (less than 0.2 m/s); within the next seven days strong northwestward to northeastward currents (maximum velocity of 1 (m/s)) induced by mesoscale eddies were dominant at this location. The current velocities declined by June 20 and by the end of June increased and were directed southward with velocity of 0.5 m/s under the influence of a mesoscale eddy located offshore of the Mississippi Canyon at the latitude of 27º 30´ N. Over the eastern Texas shelf CDOM was widely spread over the shelf presumably as a result of Ekman transport induced by westerly and southwesterly winds. An increase in current velocity (up to 0.6 m/s) in front of the Atchafalaya Bay advected CDOM-laden water over the Louisiana shelf. In addition, an increase of current velocity south of Barataria Bay entrained CDOM southward.

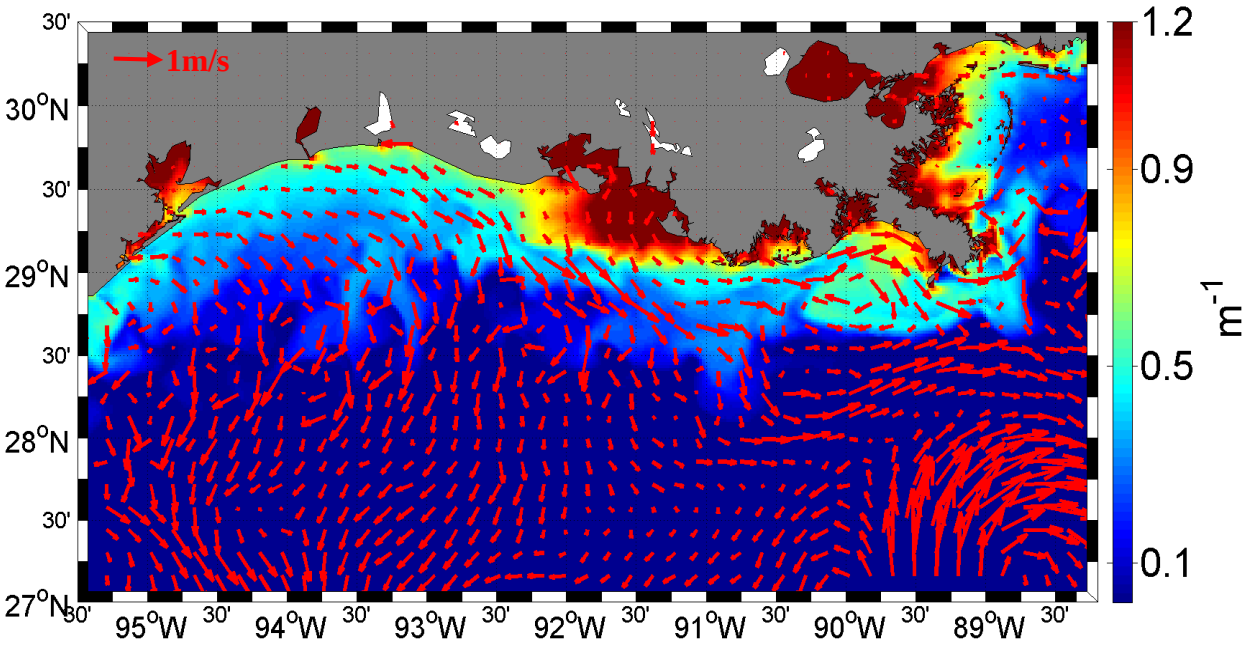

Figure 3.12: Current pattern for 22 June 2005, at 12 AM (color bar indicates CDOM absorption coefficient (m^{-1})).

3.4 Discussion

3.4.1. CDOM and salinity behavior

CDOM can be used as a passive proxy to track fresh water masses, and salinity (Ferrari and Dowell, 1998; D'Sa et al., 2002; Binding and Bowers, 2003; D'Sa and Miller, 2003). The robust negative linear relationship between salinity and CDOM demonstrates a conservative behavior of these two parameters modulated by seasonality of river discharge. The dependency of CDOM on salinity was demonstrated in section 3.3.1 for two different zones during the spring-winter and the summer periods. As depicted, CDOM and salinity were highly correlated in zone 1 for the spring-winter and summer periods suggesting CDOM distribution was regulated by mixing (Chen et al., 2007). Elevated levels of CDOM associated with low salinity waters in zone 1 indicate allochthonous sources of CDOM (Toming et al., 2009). In addition, high concentration of CDOM introduced by the Mississippi and the Atchafalaya River runoff to the inner-shelf can mask all variations induced by removal and addition processes such as photobleaching and microbial activities, respectively (Chen et al., 2004; D'Sa and DiMarco, 2009). In fact, Walker et al. (2005) suggested 75% of the Mississippi River discharge is advected to the shelf region west of the Mississippi birdfoot delta. It indicates that this area is highly affected by CDOM-rich water from the Mississippi River. Solar illumination and water column stratification during the summer causes photochemical decomposition of CDOM which disturbs the inverse linear relationship between CDOM and salinity. However, the CDOM-salinity relationship for zone 1 in summer exhibited a strong inverse linear relationship (i.e. conservative behavior). This could be attributed to the masking effect of the Mississippi and the Atchafalaya discharge (D'Sa and DiMarco, 2009). Furthermore, the required time scale for CDOM photoxidation is days to weeks which is larger than the time needed for river-laden CDOM to affect the inner-shelf and coastal areas (Vodacek et al., 1997; Hitchcock et al., 2004).

A different seasonal behavior in terms of the CDOM-salinity relationship was observed in zone 2. A strong conservative behavior of CDOM and salinity during the spring-winter period (R^2=0.93) was observed. In contrast, the summer time relationship suggested a poor conservative behavior of CDOM (R^2=0.54), which indicated the removal of CDOM presumably by photodegradation. The footprint of CDOM photodegradation can be identified in Figure 3.3D by data points which were scattered downward with respect to linear CDOM-salinity relationship. The strength of photobleching over this offshore zone in the summer was accentuated due to lack of masking impact of river's discharge which is less prominent over the zone 2 during the summer time. In addition, an increase in salinity over the zone 2 may increase CDOM's photoreactivity (Osburn and Morris, 2003).

The above mentioned conservative relationships between CDOM and salinity over the zones 1 and 2 resulted in high accuracy CDOM concentration maps using simulated salinity. The similarity between CDOM's distribution maps obtained from model and SeaWiFS sensor suggests that the approach for producing CDOM synoptic map using simulated salinity and CDOM-salinity conservation concept is an appropriate method. However, discrepancies between modeled and SeaWiFS-derived surface CDOM concentration are observed in estuaries and very shallow waters. These could be due to errors in atmospheric correction and interference by the optically active seawater constituents which may impair the performance of the sensor (Le Fouest et al., 2006; D'Sa, 2008). In addition, this can be attributed to the model deficiency in simulating salinity in coastal areas which may lead to a lower accuracy of CDOM estimation in these regions. NCOM-derived CDOM maps can be utilized as a supplemental data to fill temporal and spatial gaps in the satellite-derived CDOM map. The spatial gap is mostly due to cloud coverage, lack of swath, and sun glint.

3.4.2 Advection and CDOM distribution

The profound impact of advection on CDOM distribution over the study area was concluded based on the results presented in section 3.3. Extension of CDOM-laden waters toward the inner -shelf and outer-shelf during different current regimes clearly demonstrated the impact of horizontal advection on CDOM distribution. Cold front passages strongly contribute to the CDOM advection over the Louisiana shelf by inducing generally southward currents. This pattern can flush CDOM-laden water out of the bays toward the shelf. Walker and Hammack (2000) estimated 30-50% of the bay volume leaves during cold front passages. Feng (2009) reported that strong cold fronts could flush more than 40% of the bay waters to the shelf within a period of less than 40 hours. It implies that cold fronts are the major events causing outward flushing of the bays (Feng, 2009). The significant influence of northerly and northwesterly winds on flushing water out of the bays has been studied by satellite imageries and numerical models (Walker and Hammack, 2000; Cobb et al., 2008). Thus, relatively high southward current velocities over the shelf associated with the cold fronts also advect CDOM. Figure 3.13B illustrates CDOM distribution overlaid with isobaths over the inner and outer shelves for 11March, 2005, at 12 AM. Due to southward advection caused by the cold front, elevated CDOM was spread up to 60 m isobath off the Terrebonne Bay, 30 m isobath off the Atchafalaya Bay, and 40 m isobath off the eastern Texas coast. Westward directed down-coast currents contribute less to advection of CDOM toward the outer shelf compared to the cold front-induced currents. While cold front-induced currents advect CDOM to ~50 m isobath (on average), down-coast current regimes transport CDOM to ~30 m isobath (on average) (Figure 3.13A and 3.13B).

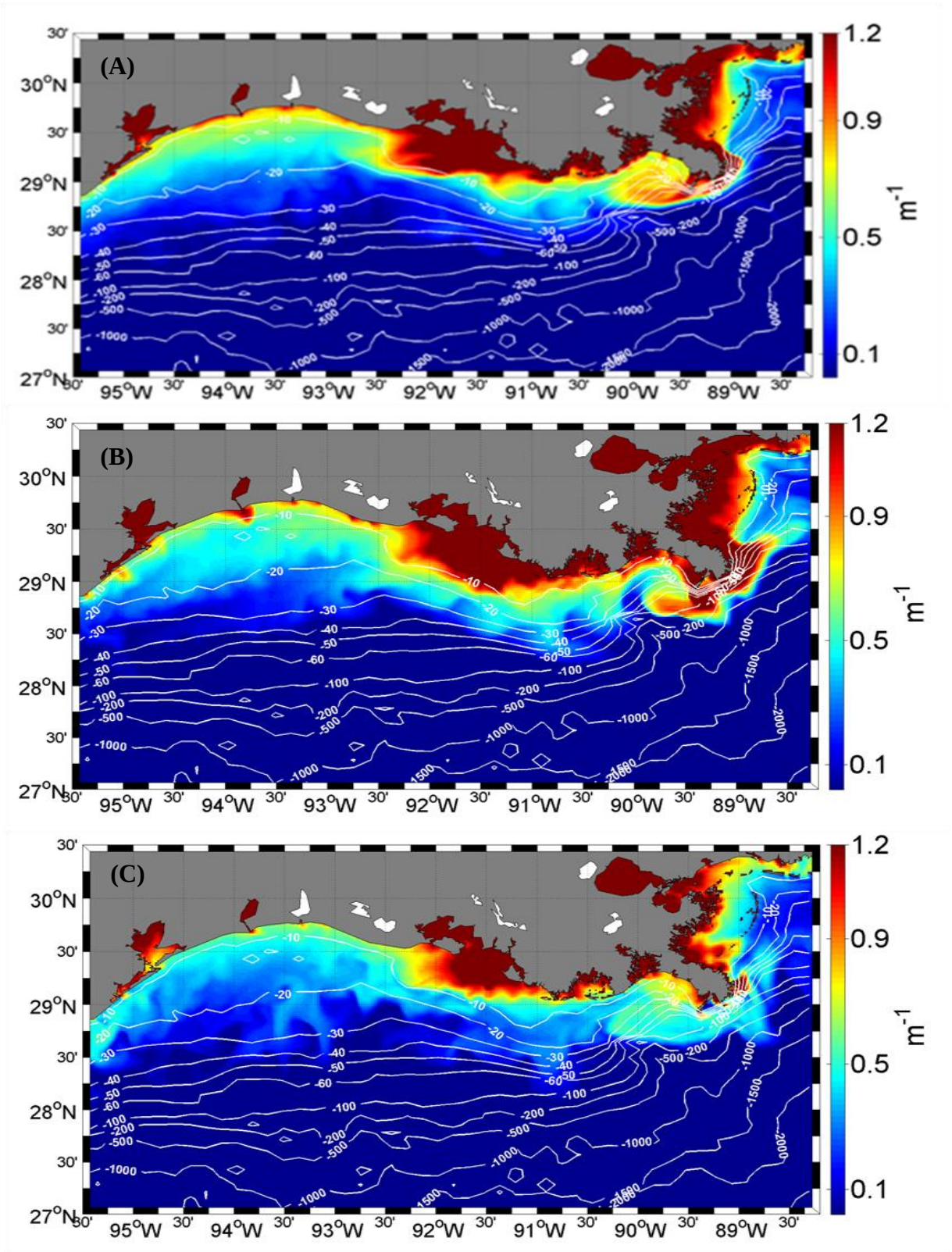

Figure 3.13: Surface CDOM absorption map derived from NCOM (A) on May 5, 2005 at 6 PM (B) on March 11, 2005 at 12 PM and (C) on June 22, 2005 at 12 AM.

The down-coast advection regime may lead to the formation of a relatively high concentration of CDOM zone parallel to the Louisiana and eastern Texas coast. This is in agreement with the persistent westward or down-coast current regime which forms continuous advection to the west (Belabbassi, 2005; Walker, 2005; Allahdadi et al., 2012). The other impact of horizontal advection on CDOM concentration is modulating salinity and stratification by transporting fresh water discharge from rivers to the shelf. In the Louisiana Bight, a clockwise quasi-permanent gyre traps freshwater discharge from the Mississippi Southwest Pass and results in an increase in stratification (Rouse and Coleman, 1976; Walker and Rabalais, 2006) and CDOM concentration.

Significant increases in buoyancy and stratification over the inner-shelf due to advection of the Mississippi River discharge has been reported by Wiseman et al., (1997). Although, the up-coast current regime is not as organized as that of the down-coast current, CDOM can be advected farther offshore. As shown in figure 3.13C, CDOM is entrained up to 60 m isobath off the Terrebonne Bay, 50 m isobath off the Atchafalaya Bay, and 50 m isobath off the eastern Texas coast. This distribution could be due to Ekman transport induced by westerly and southwesterly winds which are prevalent during up-coast current season. In addition, intrusion of meso-scale eddies can contribute to more offshore entrainment of CDOM.

During summer, the general pattern of up-coast current transports salty water from western Gulf of Mexico and Texas to the Louisiana shelf (Li et al., 1997; Belabbassi, 2006). The advection of salty water may also disturb the conservative relationship between CDOM and salinity in summer.

3.5 Summary and Conclusion

The joint application of numerical modeling and remote sensing provides us a valuable tool to investigate CDOM dynamics with high spatial and temporal resolution. Accordingly, an approach to provide synoptic maps of surface CDOM concentration for the northern Gulf of Mexico using simulated salinity was suggested. The main requirement for implementing this approach was converting salinity to CDOM. This can be met when CDOM covaries inversely with salinity. Field data of CDOM and salinity for different oceanographic cruises were utilized to examine the seasonal and spatial dependence of CDOM on salinity. The conservative behavior was met for both inner-shelf and outer-shelf zones during the spring-winter period, while the summer conservative behavior can only be met over inner-shelf zone due to the masking influence of rivers' runoff on destructive impacts of photodegradation. The resulting CDOM-salinity relationships were applied to NCOM-simulated salinity to produce CDOM maps for different time steps over the study area. The derived surface CDOM distribution maps were compared with surface CDOM absorption maps derived from SeaWiFS data (based on the D'Sa et al. (2006) algorithm), and a satisfactory agreement was observed. Also, the remarkable agreement between in situ and NCOM-derived $a_{CDOM}(412)$ was shown by a quantitative evaluation reveals the model's ability to predict CDOM with hourly temporal resolution. Some disparities which were seen between these two maps especially in estuaries and shallow water regions could be attributed to the model's drawback in simulation of salinity in these regions. Contaminated CDOM signal by the optically active water's constituents can induce further discrepancies.

NCOM simulated currents were further applied to investigate CDOM advection over the study area by overlaying simulated current over the NCOM-derived CDOM maps.

Advection impact on CDOM distribution was demonstrated through a detailed comparison for the up-coast and the down-coast current regimes with the corresponding NCOM-derived CDOM patterns. Southward currents induced by cold front outbreaks advect CDOM-laden waters from coastal bays to the inner and outer shelf, while the persistent westward down-coast current regime have less contribution to CDOM advection toward the outer shelf. This pattern forms a continuous CDOM advection along Louisiana and eastern Texas coasts. Seaward CDOM advection during up-coast current regime is significant due to the Ekman transport and the intrusion of meso-scale eddies.

This study demonstrated the suitability of the approach to generate high resolution CDOM maps based on simulated salinity. As the base of this approach is a conservative behavior of CDOM and salinity, it is possible to reverse it. Hence salinity can be obtained using satellite data. This would be desired, when simulated salinity data are not available or reliable.

CHAPTER 4: SUMMARY AND CONCLUSIONS

CDOM comprising mainly of a mixture of humic and fulvic acids is an important organic substance affecting bio-chemical parameters in aquatic environments. CDOM is introduced to the coastal waters by rivers' runoff, while in the open ocean autochthonous sources such as autotrophic and heterotrophic processes are dominant.

Regulating light attenuation through absorption is an important function of CDOM which has been studied extensively for the northern Gulf of Mexico. The absorption of light by CDOM regulates the ultraviolet (UV) light penetration, hence CDOM can protect living tissues from the damaging impact of UV light. Inorganic nutrients are influenced by CDOM as CDOM carries nitrogen and phosphorous from coastal waters to open ocean. CDOM also plays an important role as an intermediate parameter to study dissolved organic carbon (DOC) and dissolved organic matter (DOM). Hence, it is critical to study the dynamics of CDOM in the marine environment. Application of satellite ocean-color data to study the spatial and temporal variability of CDOM in coastal and oceanic waters is recognized as an important tool. This study thus, is primarily focused on evaluating and developing proper algorithms for retrieving CDOM and DOC from remotely sensed data from different ocean color sensors in the northern Gulf of Mexico. In order to develop algorithms for retrieving CDOM from satellite ocean color sensors' data, field measured data of CDOM concentration should be correlated against proper remote sensing reflectance's (R_{rs}) ratio extracted from a satellite database. Field CDOM data were obtained from spectrophotometric analysis of filtered water samples gathered during different field campaigns. The algorithm evaluation and development was implemented for three different sensors including SeaWiFS, MODIS, and MERIS. As two CDOM-retrieving algorithms (D'Sa et al. (2006) and Mannino et al. (2008)) were available for retrieving CDOM from SeaWiFS, these two algorithms were evaluated using available field data. Match-up comparison showed high

accuracy of the D'Sa et al. (2006) algorithm for CDOM retrieval based on SeaWiFS remote sensing reflectance band ratios. CDOM algorithms were also extended to MODIS and MERIS sensors with field CDOM data correlated against appropriate remote sensing reflectance band ratios obtained from each sensor. The resulting relationships were evaluated based on independent field data demonstrating the satisfactory performance of developed relationships for CDOM retrieval.

To construct an algorithm for DOC estimation, conservative seasonal relationships between CDOM and DOC were required. The correlations were investigated for the summer and non-summer seasons over the study area. The resulting relationships were combined with CDOM-R_{rs} equations for all three sensors and DOC- R_{rs} relationships were developed to retrieve DOC from satellite ocean color data. Some sources of algorithms' deficiency with respect to field data were investigated by examining measurement locations, seasonality, and sensors' limitation. The main conclusions of this part of the study were:

- DOC is highly correlated with CDOM in our study area, indicating that DOC behaves conservatively ($R^2 = 0.9$).
- Our evaluation results revealed that the D'Sa et al. (2006) algorithm performs well in retrieving CDOM and DOC from SeaWiFS.
- The MERIS sensor performs better than MODIS in retrieving CDOM and DOC.

Although satellites are widely used for studying CDOM in the aquatic environments, some constraints associated with satellite sensors limit their application. Temporal resolution is one of the most limiting factors. For all three investigated sensors there are daily pass over the northern Gulf of Mexico. Hence, no CDOM data can be obtained other than passing time. Cloud coverage and sun glint exacerbate it as no appropriate data can be retrieved during a cloudy sky or when sun glint contaminates signals. To overcome these limitations, an approach was presented to

retrieve CDOM from simulated salinity by a circulation ocean model in the third chapter. Simulated salinity over the northern Gulf of Mexico derived from the NCOM model was selected to develop this approach. Since for most coastal areas and some open ocean areas there are strong inverse linear relationships between salinity and CDOM concentration, salinity was selected as a proxy for CDOM. The relationships were examined for two inner-shelf and outer-shelf areas over the northern Gulf of Mexico during summer and spring-winter seasons. Applying these relationships to NCOM-simulated salinity enabled CDOM maps to be derived with high temporal resolution. The resulting CDOM distribution was compared with satellite derived CDOM distributions and field measured CDOM concentrations. NCOM model also provided current data which is appropriate to study the effect of advection on CDOM dynamics. NCOM-derived CDOM maps were overlaid on current from model simulation for different current regime occurring in the northern Gulf of Mexico including down-coast, up-coast and cold front induced regimes. The conclusions are briefly presented as follows:

- CDOM behaves conservatively with respect to salinity, except for the summer in the outer shelf.
- NCOM-derived CDOM matches with satellite-derived CDOM qualitatively.
- NCOM-derived CDOM matches with in situ CDOM quantitatively.
- CDOM distribution follows simulated current pattern over the inner-shelf and outer-shelf during down-coast, up-coast, and cold front regime.

In other to improve CDOM and DOC retrieval by satellite ocean color sensors more field seasonal data are required for thorough assessment of empirical algorithms as well as CDOM-DOC relationships. The approach introduced for estimation of CDOM using simulated salinity

could be utilized to estimate DOC using numerical models. In addition, CDOM-salinity relationship could be applied to ocean color data to retrieve salinity map.

REFERENCES

ALLAHDADI, M.N., JOSE, F., and PATIN, C., 2012, Seasonal Hydrodynamics along the Louisiana Coast: Implications for Hypoxia Spreading. Journal of Coastal Research (in press).

ALLISON, D. B., STRAMSKI, D., and MITCHELL, B. G., 2010, Seasonal and interannual variability of particulate organic carbon within the Southern Ocean from satellite ocean color observations. Journal of Geophysical Research-Oceans, 115, 18.

ARRIGO, K. R., and BROWN, C. W., 1996, Impact of chromophoric dissolved organic matter on UV inhibition of primary productivity in the sea. Marine Ecology-Progress Series, 140, 207-216.

AZAM, F., FENCHEL, T., FIELD, J. G., GRAY, J. S., MEYERREIL, L. A., and THINGSTAD, F., 1983, The ecological role of water-column microbes in the sea. Marine Ecology-Progress Series, 10, 257-263.

BARRON, C. N., KARA, A. B., MARTIN, P. J., RHODES, R. C., and SMEDSTAD, L. F., 2006, Formulation, implementation and examination of vertical coordinate choices in the Global Navy Coastal Ocean Model (NCOM). Ocean Modelling, 11, 347-375.

BELABBASSI, L., 2006, Examination of the relationship of river water to occurrences of bottom water with reduced oxygen concentration in the northern Gulf of Mexico. PhD thesis. Texas A&M University, USA.

BENNER, R., OPSAHL, S., CHINLEO, G., RICHEY, J. E., and FORSBERG, B. R., 1995, Bacterial carbon metabolism in the Amazon River system. Limnology and Oceanography, 40, 1262-1270.

BIANCHI, T. S., PENNOCK, J. R., AND TWILLEY, R. R. (Ed.), 1999, Biogeochemistry of Gulf of Mexico Estuaries, 370-372 (New York: John Wiley and Sons).

BIANCHI, T. S., FILLEY, T., DRIA, K., and HATCHER, P. G., 2004, Temporal variability in sources of dissolved organic carbon in the lower Mississippi River. Geochimica Et Cosmochimica Acta, 68, 959-967.

BIANCHI, T. S., DIMARCO, S. F., SMITH, R. W., and SCHREINER, K. M., 2009, A gradient of dissolved organic carbon and lignin from Terrebonne-Timbalier Bay estuary to the Louisiana shelf (USA). Marine Chemistry, 117, 32-41.

BINDING, C. E., AND BOWERS, D. G., 2003, Measuring the salinity of the Clyde Sea from remotely sensed ocean colour. Estuarine Coastal and Shelf Science, 57, 605-611.

BLOUGH, N.V., and ZEPP, R.G., 1990, Effects of solar ultraviolet radiation on biogeochemical dynamics in aquatic environments. Woods Hole Oceanographic Institution Technical Report, WHOI-90-09.

BLOUGH, N. V., ZAFIRIOU, O. C., and BONILLA, J., 1993, Optical-absorption spectra of waters from the Orinoco river outflow - terrestrial input of colored organic matter to the Caribbean. Journal of Geophysical Research-Oceans, 98, 2271-2278.

BLOUGH, N.V., and GREEN, S.A., 1995, Spectroscopic characterization and remote sensing of non-living organic matter. In: The role of non-living organic matter in the Earth's carbon cycle, R. G. Zepp and C. Sonntag (Ed.), 23-45 (Chichester, England: John Wiley & Sons).

BLOUGH, N. V., and ZEPP, R.G., 1995, Reactive oxygen species in natural waters. In: Active oxygen: Reactive oxygen species in chemistry, C.S. Foote et al. (Ed.), 280-333(London: Chapman and Hall).

BLOUGH, N.V., and DEL VECCHIO, R., 2002, Chromophoric DOM in the coastal environment. In: Biogeochemistry of Marine Dissolved Organic Matter, D.A. Hansell and C.A. Carslon (Ed.), 509–578 (San Diego: Academic Press).

BOSS, E., PEGAU, W. S., ZANEVELD, J. R. V., and BARNARD, A. H., 2001, Spatial and temporal variability of absorption by dissolved material at a continental shelf. Journal of Geophysical Research-Oceans, 106, 9499-9507.

BOWERS, D. G., and BRETT, H. L., 2008, The relationship between CDOM and salinity in estuaries: An analytical and graphical solution. Journal of Marine Systems, 73, 1-7.

BRANCO, A. B., and KREMER, J. N., 2005, The relative importance of chlorophyll and Colored Dissolved Organic Matter (CDOM) to the prediction of the diffuse attenuation coefficient in shallow estuaries. Estuaries, 28, 643−652.

BRICAUD, A., MOREL, A., and PRIEUR, L., 1981. Absorption by dissolved organic matter in the sea (yellow substance) in the UV and visible domains. Limnology and Oceanography, 26, 43–53

BURDIGE, D. J., KLINE, S. W., and CHEN, W. H., 2004, Fluorescent dissolved organic matter in marine sediment pore waters. Marine Chemistry, 89, 289-311.

BUSHAW, K. L., ZEPP, R. G., TARR, M. A., SCHULZJANDER, D., BOURBONNIERE, R. A., HODSON, R. E., MILLER, W. L., BRONK, D. A., and MORAN, M. A., 1996, Photochemical release of biologically available nitrogen from aquatic dissolved organic matter. Nature, 381, 404-407.

CARDER, K. L., STEWARD, R. G., HARVEY, G. R., and ORTNER, P. B., 1989, Marine humic and fulvic-acids - their effects on remote-sensing of ocean chlorophyll. Limnology and Oceanography, 34, 68-81.

CARDER, K.L., HAWES, S.K., BAKER, K.A., SMITH, R.C., STEWARD, R.G., and MITCHELL, B.G., 1991, Reflectance model for quantifying chlorophyll a in the presence of productivity degradation products. Journal of Geophysical Research, 96, 20,599-20,611.

CARDER, K. L., CHEN, F. R., LEE, Z. P., HAWES, S. K., and KAMYKOWSKI, D., 1999, Semianalytic Moderate-Resolution Imaging Spectrometer algorithms for chlorophyll a and absorption with bio-optical domains based on nitrate-depletion temperatures. Journal of Geophysical Research-Oceans, 104, 5403-5421.

CARLSON, C.A., DUCHLOW, H.W., and SLEETER, T.D., 1996, Stocks and dynamics of bacterioplankton in the Northwestern Sargasso Sea. Deep Sea Research, 43, 491-515.

CARLSON, C. A., 2002, Production and Removal Processes. In Biogeochemistry of Marine Dissolved Organic Matter, D.A. Hansell and C.A. Carslon (Ed.), 91- 151 (San Diego: Academic Press).

CAUWET, G., 2002. DOM in the coastal zone. In Biogeochemistry of Marine Dissolved Organic Matter, D.A. Hansell and C.A. Carslon (Ed.), 579-612 (San Diego: Academic Press).

CHAI, F., DUGDALE, R.C., PENG, T.-H., WILKERSON, F. P., and BARBER , R. T.,2002, One dimensional ecosystem model of the Equatorial Pacific upwelling system, Part I: Model development and silicon and nitrogen cycle. Deep Sea Research, 49, 2713–2745.

CHAI, F., and BOSS, E., 2010, Physical-Biological-Optics Model Development and Simulation for the Pacific Ocean and Monterey Bay, California. Available at: http://www.onr.navy.mil/reports/FY10/eochai.pdf

CHEN, N., BIANCHI, T. S., and BLAND, J. M., 2003, Implications for the role of pre- versus post-depositional transformation of chlorophyll-a in the Lower Mississippi River and Louisiana shelf. Marine Chemistry, 81, 37-55.

CHEN, R. F., BISSETT, P., COBLE, P., CONMY, R., GARDNER, G. B., MORAN, M. A., WANG, X. C., WELLS, M. L., WHELAN, P., and ZEPP, R. G., 2004, Chromophoric dissolved organic matter (CDOM) source characterization in the Louisiana Bight. Marine Chemistry, 89, 257-272.

CHEN, R. F., and GARDNER, G. B., 2004, High-resolution measurements of chromophoric dissolved organic matter in the Mississippi and Atchafalaya River plume regions. Marine Chemistry, 89, 103-125.

CHEN, Z., HU, C., COMNY, R. N., MULLER-KARGER, F., AND SWARZENSKI, P., 2007, Colored dissolved organic matter in Tampa Bay, Florida. Marine Chemistry, 104, 98-109.

COBB, M., KEEN, T.R., and WALKER, N.D., 2008, Modeling the circulation of the Atchafalaya Bay system. Part2: river plume dynamics during cold fronts. Journal of Coastal Research, 24, 1048-1062.

COBLE, P. G., HU, C., JR GOULD, R. W., CHANG, G., and A. M. WOOD., 2004, Colored dissolved organic matter in the coastal ocean. Oceanography, 17, 50-59.

COBLE, P. G., 2007, Marine optical biogeochemistry: The chemistry of ocean color. Chemical Reviews, 107, 402-418.

COCHRANE, J. D., and KELLY, F. J., 1986, Low-Frequency Circulation on the Texas-Louisiana Continental-Shelf. Journal of Geophysical Research, 91, 10645-10659.

CONMY, R. N., COBLE, P. G., CHEN, R. F., and GARDNER, G. B., 2004, Optical properties of colored dissolved organic matter in the Northern Gulf of Mexico. Marine Chemistry, 89, 127-144.

CONMY, R. N., 2008, Temporal and spatial patterns in optical properties of colored dissolved organic matter on Florida's Gulf coast: shelf to stream to aquifer. Ph.D. thesis,University of South Florida.

COOPER, L. W., BENNER, R., MCCLELLAND, J. W., PETERSON, B. J., HOLMES, R. M., RAYMOND, P. A., HANSELL, D. A., GREBMEIER, J. M., and CODISPOTI, L. A., 2005, Linkages among runoff, dissolved organic carbon, and the stable oxygen isotope composition of seawater and other water mass indicators in the Arctic Ocean. Journal of Geophysical Research-Biogeosciences, 110.

CORBETT, C.A., 2007, Colored Dissolved Organic Matter (CDOM) Workshop summary. Available online at: http://scholarcommons.usf.edu/basgp_report/2.

CROUT, R. L., WISEMAN, W. J., and CHUANG, W. S., 1984, Variability of Wind-Driven Currents, West Louisiana Inner Continental-Shelf - 1978-1979. Contributions in Marine Science, 27, 1-11.

D'ALIMONTE, D., 2004, Determination of CDOM and NPPM absorption coefficient spectra from coastal water remote sensing reflectance. Geoscience and Remote Sensing, 42, 1770 - 1777

D'SA, E. J., STEWARD, R. G., VODACEK, A., BLOUGH, N. V., and PHINNEY, D., 1999, Determining optical absorption of colored dissolved organic matter in seawater with a liquid capillary waveguide. Limnology and Oceanography, 44, 1142-1148.

D'SA, E. J., HU, C., MULLER-KARGER, F. E., and CARDER, K. L., 2002, Estimation of colored dissolved organic matter and salinity fields in case 2 waters using SeaWiFS: Examples from Florida Bay and Florida Shelf. Proceedings of the Indian Academy of Sciences-Earth and Planetary Sciences, 111, 197-207.

D'SA, E. J., and MILLER, R. L., 2003, Bio-optical properties in waters influenced by the Mississippi River during low flow conditions. Remote Sensing of Environment, 84, 538-549.

D'SA, E.J., and Miller R. L., 2005, Bio-optical properties of coastal waters. In Remote Sensing of Coastal Aquatic Environments, R.L. Miller et al. (Ed.), 129-155 (Netherland: Springer).

D'SA, E. J., MILLER, R. L., and DEL CASTILLO, C., 2006, Bio-optical properties and ocean color algorithms for coastal waters influenced by the Mississippi River during a cold front. Applied Optics, 45, 7410-7428.

D'SA, E. J., MILLER, R. L., and MCKEE, B. A., 2007, Suspended particulate matter dynamics in coastal waters from ocean color: Application to the northern Gulf of Mexico. Geophysical Research Letters, 34.

D'SA, E. J., 2008, Colored dissolved organic matter in coastal waters influenced by the Atchafalaya River, USA: effects of an algal bloom. Journal of Applied Remote Sensing, 2.

D'SA, E. J., and KO, D.S., 2008, Short-term influences on suspended particulate matter distribution in the northern Gulf of Mexico: Satellite and model observations. Sensors, 4249-4264.

D'SA, E. J., and KOROBKIN, M., 2008, Colored dissolved organic matter in the northern Gulf of Mexico using ocean color: seasonal trends in 2005. Proceedings of SPIE 7105, 710505.

D'SA, E. J., and DIMARCO, S. F., 2009, Seasonal variability and controls on chromophoric dissolved organic matter in a large river-dominated coastal margin. Limnology and Oceanography, 54, 2233-2242.

DEL CASTILLO, C. E., 2005, Remote sensing of organic matter in coastal waters. In remote sensing of coastal aquatic environments, Miller, R. L., and et al.(Ed.), 157-180.

DEL CASTILLO, C. E., and MILLER, R. L., 2008, On the use of ocean color remote sensing to measure the transport of dissolved organic carbon by the Mississippi River plume. Remote Sensing of Environment, 112, 836-844.

DEL VECCHIO, R., and BLOUGH, N. V., 2004, Spatial and seasonal distribution of chromophoric dissolved organic matter and dissolved organic carbon in the Middle Atlantic Bight. Marine Chemistry, 89, 169-187.

DEL VECCHIO, R., and BLOUGH, N.V., 2005, Influence of ultraviolet radiation on the chromophoric dissolved organic matter in natural waters. In: Environmental UV Radiation: Measurement and Assessment. Impact on Ecosystem and Human Health and

predictive models, Ghetti, F., Bornman, J.F. (Eds.), Nato Science Series: IV. Earth and Environmental Sciences, 57, 360. (Netherland: Springer).

DEL VECCHIO, R., and BLOUGH, N. V., 2006, Influence of Ultraviolet Radiation on the Chromophoric Dissolved Organic Matter in Natural Waters. In Environmental UV Radiation: Impact on Ecosystems and Human Health and Predictive Models, F. Ghetti, G. Checcucci, and J. F. Bornman(Ed.) 203-216 (Netherland: Springer).

DINNEL, S. P., and WISEMAN, W. J., 1986, Fresh-water on the Louisiana and Texas shelf. Continental Shelf Research, 6, 765-784.

DUCKLOW, H. W., CARLSON, C. A., BATES, N. R., KNAP, A. H., and MICHAELS, A. F., 1995, Dissolved organic-carbon as a component of the biological pump in the north-atlantic ocean. Philosophical Transactions of the Royal Society of London Series B-Biological Sciences, 348, 161-167.

FENG, Z., 2009, Hydrodynamic response to cold fronts along the Louisiana coast. Master of Science thesis. Louisiana State University, USA.

FERRARI, G.M., M.D. DOWELL, S. GROSSI, and C. TARGA, 1996, Relationship between the optical properties of chromophoric dissolved organic matter and total concentration of dissolved organic carbon in the southern Baltic Sea region. Marine Chemistry, 55, 299–316.

FERRARI, G. M., and DOWELL, M. D., 1998, CDOM absorption characteristics with relation to fluorescence and salinity in coastal areas of the southern Baltic Sea. Estuarine Coastal and Shelf Science, 47, 91-105.

FERRARI, G. M., 2000, The relationship between chromophoric dissolved organic matter and dissolved organic carbon in the European Atlantic coastal area and in the West Mediterranean Sea (Gulf of Lions). Marine Chemistry, 70, 339-357.

FICHOT, C. G., and BENNER, R., 2011, A novel method to estimate DOC concentrations from CDOM absorption coefficients in coastal waters. Geophysical Research Letters, 38.

FLOGE, S. A., and WELLS, M. L., 2007, Variation in colloidal chromophoric dissolved organic matter in the Damariscotta Estuary, Maine. Limnology and Oceanography, 52, 32-45.

FOGG, G. E., 1983, The ecological significance of extracellular products of phytoplankton photosynthesis. Botanica Marina, 26, 3-14.

FUHRMAN, J. A., 1999, Marine viruses and their biogeochemical and ecological effects. Nature, 399, 541-548.

GALLEGOS, C. L., 2005, Optical water quality of a blackwater river estuary: the Lower St. Johns River, Florida, USA. Estuarine Coastal and Shelf Science, 63, 57-72.

GANDHI, H., WIEGNER, T.N., OSTROM, P.H., KAPLAN, L.A., and OSTROM, N.E., 2004, Isotopic (^{13}C) analysis of dissolved organic carbon in stream water using an elemental analyzer coupled to a stable isotope mass spectrometer. Rapid Communications in Mass Spectrometry, 18, 903-906.

GAO, H., and ZEPP, R.G., 1998, Factors influencing photoreactions of dissolved organic matter in a coastal river of the southeastern United State. Environmental Science and Technology, 32, 2940-2946.

GARVER, S. A., and SIEGEL, D.A., 1997, Inherent optical property inversion of ocean color spectra and its biogeochemical interpretation: 1. Time series from the Sargasso Sea. Journal of Geophysical research, 102, 18,607-18,625.

GEORGAS, N., LI, W., and BLUMBERG, A. F., 2010, Estuarine and coastal CDOM forecasts using a predictive fate and transport model. Available online at: http://archive.stevens.edu/ses/cms/fileadmin/cms/pdf/4.4Georgas.pdf

GORDON, H. R., BROWN, O.B., and JACOBS, M.M., 1975, Computed relations between inherent and apparent optical properties of a flat homogeneous ocean. Applied Optics, 14, 417-427.

GORDON, H. R., CLARK, D. K., BROWN, J. W., BROWN, O. B., EVANS, R. H., and BROENKOW, W. W., 1983, Phytoplankton pigment concentrations in the middle Atlantic Bight - comparison of ship determinations and CZCS estimates. Applied Optics, 22, 20-36.

GORDON, H. R., and MOREL, A. Y., 1983, Remote assessment of ocean color for interpretation of satellite visible imagery: A Review (New York: Springer-Verlag).

GORDON, H.R., 1989, Can the Lambert-Beer law be applied to the diffuse attenuation coefficient of ocean water? Limnology Oceanography, 34(8), 1389-1409.

GRIFFIN, C. G., FREY, K. E., ROGAN, J., and HOLMES, R. M., 2011, Spatial and interannual variability of dissolved organic matter in the Kolyma River, East Siberia, observed using satellite imagery. Journal of Geophysical Research-Biogeosciences, 116.

GUEGUEN, C., GUO, L. D., and TANAKA, N., 2005, Distributions and characteristics of colored dissolved organic matter in the Western Arctic Ocean. Continental Shelf Research, 25, 1195-1207.

GUO, L. D., and SANTSCHI, P. H., 1997, Isotopic and elemental characterization of colloidal organic matter from the Chesapeake Bay and Galveston Bay. Marine Chemistry, 59, 1-15.

GUO, W., STEDMON, C.A., HAN, Y., WU, F., YU, X., and HU, M., 2007, The conservative and non-conservative behavior of chromophoric dissolved organic matter in Chinese estuarine waters. Marine Chemistry, 107, 357-366.

HANSELL, D. A., and CARLSON, C. A., 2001, Biogeochemistry of total organic carbon and nitrogen in the Sargasso Sea: Control by convective overturn. Deep Sea Research, II 48, 1649–1667.

HANSELL, D.A., 2002, DOC in the Global Ocean Carbon Cycle. In Biogeochemistry of Marine Dissolved Organic Matter, D.A., Hansell, and C.A. Carlson (Ed.), 685-716 (Academic Press, San Diego)

HERNES, P. J., and BENNER, R., 2003, Photochemical and microbial degradation of dissolved lignin phenols: Implications for the fate of terrigenous dissolved organic matter in marine environments. Journal of Geophysical Research-Oceans, 108.

HITCHCOCK, G. L., CHEN, R. F., GARDNER, G. B., and WISEMAN, W. J., 2004, A Lagrangian view of fluorescent chromophoric dissolved organic matter distributions in the Mississippi River plume. Marine Chemistry, 89, 225-239.

HOCHMAN, H. T., MULLERKARGER, F. E., and WALSH, J. J., 1994, Interpretation of the coastal zone color scanner signature of the Orinoco River plume. Journal of Geophysical Research-Oceans, 99, 7443-7455.

HØJERSLEV, N.K., HOLT, N., and AARUP, T., 1996, Optical measurements in the North Sea-Baltic sea transition zone. I. On the Origin of the deep water in the Kattegat. Continental Shelf Research, 16 (10), 1329-1342.

HU, C., MULLER-KARGER, F. E., BIGGS, D. C., CARDER, K. L., NABABAN, B., NADEAU, D., and VANDERBLOEMEN, J., 2003, Comparison of ship and satellite bio-optical measurements on the continental margin of the NE Gulf of Mexico. International Journal of Remote Sensing, 24, 2597-2612.

HU, C., LEE, Z., MULLER-KARGER, F.E., CARDER, K.L., and WALSH, J.J., 2006. Ocean color reveals phase shift between marine plants and yellow substance. IEEE Geoscience and Remote Sensing Letters, 3, 262-266.

INTERNATIONAL OCEAN COLOUR COORDINATING GROUP (IOCCG), 1999, Considerations for Complementary Missions. Reports of the International Ocean Colour Coordinating Group, No.2, IOCCG, Dartmouth, Canada, Yoder, J.A (Ed.).

INTERNATIONAL OCEAN COLOUR COORDINATING GROUP (IOCCG), 2006, Remote Sensing of Inherent Optical Properties: Fundamentals, Tests of Algorithms and Applications. Reports of the International Ocean Colour Coordinating Group, No. 5, IOCCG, Dartmouth, Canada, Z.P. Lee (Ed.).

JAROSZ, E., 1997, Summer flow regime on the Louisiana inner shelf. M.S. thesis, Louisiana State University, USA.

JIAO, N., HERNDL, G. J., HANSELL, D. A., BENNER, R., KATTNER, G., WILHELM, S. W., KIRCHMAN, D. L., WEINBAUER, M. G., LUO, T., CHEN, F., and AZAM, F., 2010, Microbial production of recalcitrant dissolved organic matter: long-term carbon storage in the global ocean. Nat Rev Micro, 8, 593-599.

JERLOV, N.G., 1968, Optical Oceanography, Elsevier Oceanography series, (Amsterdam: Elsevier).

JERLOV, N.G., 1953, Influence of suspended and dissolved matter on the transparency of sea water. Tellus 5, 59-65.

JERLOV, N. G. (Ed.), 1976, Marine Optics, (New York: Elsevier).

JENSEN, T., MARTIN, P., ROWLEY, C., CAMPELL, T., ALLARD, R., SMITH, T., and SMALL. J., 2010, Recent development in the Navy Coastal Ocean Model and its application as the ocean component in regional coupled forecast models. Available online at:http://www.ccpo.odu.edu/~tezer/IWMO_2010/PRESENTATIONS/WEDNESDAY_pdf/Jensen_NCOM.pdf.

JOHANNESSEN, S. C., MILLER, W. L., and CULLEN, J. J., 2003, Calculation of UV attenuation and colored dissolved organic matter absorption spectra from measurements of ocean color. Journal of Geophysical Research-Oceans, 108.

JOLLIFF, J. K., WALSH, J. J., HE, R. Y., WEISBERG, R., STOVALL-LEONARD, A., COBLE, P. G., CONMY, R., HEIL, C., NABABAN, B., ZHANG, H. Y., HU, C. M., and MULLER-KARGER, F. E., 2003, Dispersal of the Suwannee River plume over the West Florida shelf: Simulation and observation of the optical and biochemical consequences of a flushing event. Geophysical Research Letters, 30.

JUMARS, P. A., PENRY, D. L., BAROSS, J. A., PERRY, M. J., and FROST, B. W., 1989, Closing the microbial loop - dissolved carbon pathway to heterotrophic bacteria from incomplete ingestion, digestion and absorption in animals. Deep-Sea Research Part A-Oceanographic Research Papers, 36, 483-495.

KAHRU, M., and MITCHELL, B. G., 2001, Seasonal and nonseasonal variability of satellite-derived chlorophyll and colored dissolved organic matter concentration in the California Current. Journal of Geophysical Research-Oceans, 106, 2517-2529.

KALLE, K., 1966, the problem of gelbstoff in the sea. Oceanography Marine Biology Annals Review, 4, 91-104.

KALLIO, K., 2000, Remote sensing as a tool for monitoring lake water quality. In Hydrological and limnological aspects of lake monitoring, P. Heinonen, G. Ziglio and A. van der Beken (Ed.), 237-245 (Chichester, England: John Wiley & Sons).

KEIL, R. G., and KIRCHMAN, D. L., 1994, Abiotic transformation of labile protein to refractory protein in sea-water. Marine Chemistry, 45, 187-196.

KIEBER, D. J., MCDANIEL. J., and MOPPER, K., 1989, Photochemical source of biological substrates in sea water: implications for carbon cycling. Nature, 341, 637-639.

KIRK, J. T. O., 1976, Yellow substance (gelbstof) and its contribution to the attenuation of photosynthetically active radiation in some inland and coastal south-eastern Australian waters. Australian Journal of Marine and freshwater research, 27, 67-71.

KIRK, J. T. O.(Ed.), 1994, Light and Photosynthesis in the Aquatic Ecosystems (Cambridge: University Press).

KIRK, P, G. J., ORRICO. C., MOLINE, M. A., OLIVER, M., and SCHOFIELD, O. M., 2003, Continuous hyperspectral absorption measurements of colored dissolved organic material in aquatic systems. Applied Optics, 42, 6564-6568.

KISHINO, M., TANAKA, A., OISHI, T., DOEFFER, R., and SCHILLER, H., 2001, Temporal and spatial variability of chlorophyll a, suspended solids, and yellow substance in the Yellow Sea and East China Sea using ocean color sensors. Proceeding. SPIE, 4154, 179-187.

KLUG, J. L., and COTTINGHAM, K. L., 2001, Interactions among environmental drivers: Community responses to changing nutrients and dissolved organic carbon. Ecology, 82, 3390-3403.

KO, D.S., R.H. PRELLER, and P.J. MARTIN, 2003, An Experimental Real-Time Intra Americas Sea Ocean Nowcast/Forecast System for Coastal Prediction. Proceedings, AMS 5th Conference on Coastal Atmospheric and Oceanic Prediction and Processes, 97-100.

KO, D.S.; MARTIN, P.J. ; ROWLEY, C.D., and PRELLER, R.H., 2008, A real-time coastal ocean prediction experiment for MREA04. Journal of Marine Systems, 69, 17-28.

MARTIN, P.J., 2000, Description of the Navy Coastal Ocean Model Version 1.0. Technical Report NRL/FR/7322-00-9962, 42.

KOWALCZUK, P., 1999, Seasonal variability of yellow substance absorption in the surface layer of the Baltic Sea. Journal of Geophysical Research-Oceans, 104, 30047-30058.

KOWALCZUK, P., ZABLOCKA, M., SAGAN, S., and KULINSKI, K., 2010, Fluorescence measured in situ as a proxy of CDOM absorption and DOC concentration in the Baltic Sea. Oceanologia, 52, 431-471.

LAANEN, M., 2007, Yellow Matters-Improving the remote sensing of coloured Dissolved Organic Matter in inland freshwater. Ph.D. thesis, University of Amsterdam.

LEE, Z. P., CARDER, K. L., and ARNONE, R. A., 2002, Deriving inherent optical properties from water color: a multiband quasi-analytical algorithm for optically deep waters. Applied Optics, 41, 5755-5772.

LE FOUEST, V., ZAKARDJIAN, B., SAUCIER, F. J., and CIZMELI, S. A., 2006, Application of SeaWIFS- and AVHRR-derived data for mesoscale and regional validation of a 3-D high-resolution physical-biological model of the Gulf of St. Lawrence (Canada). Journal of Marine Systems, 60, 30-50.

LI, Y., NOWLIN, W. D., JR., and REID, R. O., 1997, Mean hydrographic fields and their interannual variability over the Texas-Louisiana continental shelf in spring, summer and fall. Journal of Geophysical Research, 102, 23.

LOHRENZ, S. E., DAGG, M. J., and WHITLEDGE, T. E., 1990, Enhanced primary production at the plume oceanic interface of the Mississippi River. Continental Shelf Research, 10, 639-664.

LOHRENZ, S., FAHNENSTIEL, G. L., REDALIJE, D. G., LANG, G. A., DAGG, M. J., WHITLEDGE, T. E., and DORTCH, Q., 1999, Nutrients, irradiance and mixing as factors regulating primary primary production in coastal waters impacted by the Mississippi River plume. Continental Shelf Research, 19, 1113-1141.

MAIER, R. M., PEPPER, I. I., and GERBER, C.P. (Ed.), 2009, Environmental microbiology (Amsterdam: Elsevier Academic Press).

MANNINO, A., RUSS, M. E., and HOOKER, S. B., 2008, Algorithm development and validation for satellite-derived distributions of DOC and CDOM in the US Middle Atlantic Bight. Journal of Geophysical Research-Oceans, 113, 1-19.

MARITORENA, S., SIEGEL, D. A., and PETERSON, A., 2002, Optimization of a semi-analytical ocean color model for global scale applications. Applied Optics, 41, 2705-2714.

MARTIN, P.J., 2000, A description of the Navy Coastal Ocean Model Version 1.0. NRL Report NRL/FR/7322-00-9962, Naval Research Laboratory, SSC, MS 39529, 42.

MARTINEZ-LOPEZ, B., and ZAVALA-HIDALGO, J., 2009, Seasonal and interannual variability of cross-shelf transports of chlorophyll in the Gulf of Mexico. Journal of Marine Systems, 77, 1-20.

MAYBACK, M., 1982, Carbon, nitrogen, and phosphorus transport by world rivers. American Journal of science, 282, 401-450.

MCKNIGHT, D.M., and AIKEN, G.R., 1998, Sources and age of aquatic humus. In Aquatic humic substances, Hessen, D.O., Tranvik, L.J (Ed.), 9-39 (Berlin: Springer).

MILLER, W.L., and ZEPP R.G., 1995, photochemical production of dissolved inorganic carbon from terrestrial organic matter: Significance to the oceanic organic carbon cycle. Geophysical Research letters, 22, 412-420.

MILLER, W.L., MORAN, M.A., SHELDON, W.M., ZEPP, R.G., and OPSAHL, S., 2002, Determination of apparent quantum yield spectra for the formation of biologically labile photoproducts. Limnology and Oceanography, 47, 343-352.

MOBLEY, C.D. (Ed.), 1994, Light and Water: Radiative Transfer in Natural Waters, (San Diego: Academic Press).

MOBLEY, C.D., D. STRAMSKI, BISSET, W. P., and E. BOSS., 2004, Optical modeling of ocean waters: Is the case-1 case-2 still useful?. Oceanography, 17, 60-67.

MOPPER, K., ZHOU, X. L., KIEBER, R. J., KIEBER, D. J., SIKORSKI, R. J., and JONES, R. D., 1991, Photochemical degradation of dissolved organic-carbon and its impact on the oceanic carbon-cycle. Nature, 353, 60-62.

MORAN, M.A., WICKS, R.J., and HODSON, R, E., 1991, Exprot of dissolved organic matter from a mangrove swap ecosystem: evidence from natural fluorescence, dissolved lignin phenols, and bacterial secondary production. Marine Ecology Progress Series, 76, 175-185.

MORAN, M. A., and ZEPP, R. G., 1997, Role of photoreactions in the formation of biologically labile compounds from dissolved organic matter. Limnology and Oceanography, 42, 1307-1316.

MORAN, M.A., SHELDON JR, W. M., and ZEPP, R.G., 2000, Carbon loss and optical property changes during long-term photochemical and biological degradation of estuarine dissolved organic matter. Limnology and Oceanography, 45, 1254-1264.

MOREL, A., and PRIEUR, L., 1977, ANALYSIS OF VARIATIONS IN OCEAN COLOR. Limnology and Oceanography, 22, 709-722.

MOREL, A., and GENTILI, B., 1993, Diffuse reflectance of oceanic waters. II. Bidirectional aspects. Applied Optics, 32, 6864-6879.

NAIK, P., D'SA, E. J., GRIPPO, M., CONDREY, R., and FLEEGER, J., 2011, Absorption properties of shoal-dominated waters in the Atchafalaya Shelf, Louisiana, USA. International Journal of Remote Sensing, 32, 4383-4406.

NELSON, N. B., SIEGEL, D. A., and MICHAELS, A. F., 1998, Seasonal dynamics of colored dissolved material in the Sargasso Sea. Deep-Sea Research Part I-Oceanographic Research Papers, 45, 931-957.

NELSON, N.B., and SIEGEL, D.A., 2002. Chromophoric DOM in the open ocean. In Biogeochemistry of Marine Dissolved Organic Matter, Hansell, D.A., Carlson, C.A. (Ed.), 547-578 (San Diego: Academic Press).

NELSON, N. B., SIEGEL, D. A., CARLSON, C. A., SWAN, C., SMETHIE, W. M., and KHATIWALA, S., 2007, Hydrography of chromophoric dissolved organic matter in the North Atlantic. Deep-Sea Research Part I-Oceanographic Research Papers, 54, 710-731.

NOWLIN, W.D., JOCHENS, A.E., DIMARCO, S.F., REID, R.O., and HOWARD, M.K., 2005, Low-frequancy circulation over the Texas-Louisiana shelf. In Circulation in the Gulf of Mexico: Observations and models. Geophysical Monograph Series, AGU, 161, 219-240.

OEY, L. Y., 1995, Eddy-forced and wind-forced shelf circulation. Journal of Geophysical Research-Oceans, 100, 8621-8637.

OGAWA, H., and TANOUE, E., 2003, Dissolved organic matter in oceanic waters. Journal of Oceanography, 59, 129-147.

OPSAHL, S., and BENNER, R., 1998, Photochemical reactivity of dissolved lignin in river and ocean waters. Limnology and Oceanography, 43, 1297-1304.

O'REILLY, J. E., MARITORENA, S., MITCHELL, B.G., SIEGEL, D.A., CARDER, K. LA., KAHRU, M., and MCCLAIN, C., 1998, Ocean color chlorophyll algorithm for SeaWiFS. Journal of Geophysical Research, 103, 24,937-24,953.

O'REILLY, J.E. and 21 co-authors, 2000, Ocean color chlorophyll *a* algorithms for SeaWiFS, OC2, and OC4: Version 4. In: O'Reilly, J.E. and 24 co-authors: SeaWiFS postlaunch calibration and validation analyses, part 3. NASA Tech. Memo. 2000-206892, *Vol. 11*, S.B.Hooker and E.R. Firestone, Eds., NASA Goddard Space Flight Center, Greenbelt, Maryland, 9-23.

OSBURN, C. L., and MORRIS, D. P., 2003, Photochemistry of chromophoric dissolved organic matter in natural waters, In UV Effects in Aquatic Organisms and Ecosystems, Hebling, W. E. and Zagarese, H. E. (Ed.), 500 (Royal Society of Chemistry).

OSBURN, C. L., RETAMAL, L., and VINCENT, W. F., 2009, Photoreactivity of chromophoric dissolved organic matter transported by the Mackenzie River to the Beaufort Sea. Marine Chemistry, 115, 10-20.

PAKULSKI, J. D., BENNER, R., AMON, R., EADIE, B., and WHITLEDGE, T., 1995, Community metabolism and nutrient cycling in the Mississippi River plume - evidence

for intense nitrification at intermediate salinities. Marine Ecology-Progress Series, 117, 207-218.

POLIMENE, L., PINARDI, N., ZAVATARELLI, M., ALLEN, J.I., GIANI, M., and VICHI, M., 2007, A numarical simulation study of dissolved organic carbon accumulation in the northern Adriadic Sea. Journal of Geophyscial Research,112.

POPE, R.M., and FRY. E.S., 1997, Absorption spectrum (380-700 nm) of pure water. II. Integrating cavity measurements. Applied Optics, 36, 8710-8723.

POWELL, R. T., and WILSON-FINELLI, A., 2003, Photochemical degradation of organic iron complexing ligands in seawater. Aquatic Sciences, 65, 367-374.

RABALAIS, N. N., WISEMAN, W. J., TURNER, R. E., SENGUPTA, B. K., and DORTCH, Q., 1996, Nutrient changes in the Mississippi River and system responses on the adjacent continental shelf. Estuaries, 19, 386-407.

REYES-PESARESI. P., 2010, Dynamics of chromophoric dissolved organic matter, CDOM, in coastal tropical waters. PhD thesis. University of Puerto Rico,USA.

ROESLER, S. R., and PERRY, M. J., 1995, In situ phytoplankton absorption, fluorescence emission, and particulate backscattering spectra determined from reflectance. Journal of Geophysical Research, 100, 13,279-13,294.

ROCHELLE-NEWALL, E. J., and FISHER, T. R., 2002, Production of chromophoric dissolved organic matter fluorescence in marine and estuarine environments: an investigation into the role of phytoplankton. Marine Chemistry, 77, 7-21.

ROUSE, L. J., 1998, Circulation and hydrographic structure in the vicinity of the Mississippi River delta. In: An Observational Study of the Mississippi-Atchafalaya Coastal Plume: Final Report, S.P. Murray (Ed.), New Orleans: U.S. Department of the Interior, Minerals Management Service, Gulf of Mexico OCS Study MMS 98-0040, 513.

ROUSE, L. J., and COLEMAN, J. M., 1976, Circulation observations in the Louisiana Bight using LANDSAT imagery. Remote Sensing of Environment, 5, 635-642.

SALISBURY, J. E., CAMPBELL, J. W., LINDER, E., MEEKER, L. D., MULLER-KARGER, F. E., and VOROSMARTY, C. J., 2004, On the seasonal correlation of surface particle fields with wind stress and Mississippi discharge in the northern Gulf of Mexico. Deep-Sea Research Part Ii-Topical Studies in Oceanography, 51, 1187-1203.

SCHAEFFER, B. A., CONMY, R. N., AUKAMP, J., CRAVEN, G., and FERER, E. J., 2011, Organic and inorganic matter in Louisiana coastal waters: Vermilion, Atchafalaya, Terrebonne, Barataria, and Mississippi regions. Marine Pollution Bulletin, 62, 415-422.

SHANK, G. C., ZEPP, R. G., WHITEHEAD, R. F., and MORAN, M. A., 2005, Variations in the spectral properties of freshwater and estuarine CDOM caused by partitioning onto river and estuarine sediments. Estuarine Coastal and Shelf Science, 65, 289-301.

SHANK, G. C., and EVANS, A., 2011, Distribution and photoreactivity of chromophoric dissolved organic matter in northern Gulf of Mexico shelf waters. Continental Shelf Research, 31, 1128-1139.

SHANMUGAM, P., 2011, A new bio-optical algorithm for the remote sensing of algal blooms in complex ocean waters. Journal of Geophysical Research-Oceans, 116.

SHARP, J.H., 1997, Marine dissolved organic carbon: are the older values correct? Marine Chemistry, 56, 265 – 277.

SHULMAN, I., MOLINE, M. A., PENTA, B., ANDERSON, S., OLIVER, M., and HADDOCK, S. H. D., 2011, Observed and modeled bio-optical, bioluminescent, and physical properties during a coastal upwelling event in Monterey Bay, California. Journal of Geophysical Research-Oceans, 116.

SIEGEL, D. A., MARITORENA, S., NELSON, N. B., HANSELL, D. A., and LORENZI-KAYSER, M., 2002, Global distribution and dynamics of colored dissolved and detrital organic materials. Journal of Geophysical Research-Oceans, 107.

SINGH, S., D'SA, E., and SWENSON, E., 2010, Seasonal variability in CDOM absorption and fluorescence properties in the Barataria Basin, Louisiana, USA. Journal of Environmental Sciences-China, 22, 1481-1490.

STEINBERG, C. E. W.(Ed.), 2003, Ecology of humic substances in freshwater, (Verlag New York: Springer).

STEINBERG, D. K., NELSON, N. B., CARLSON, C. A., and PRUSAK, A. C., 2004, Production of chromophoric dissolved organic matter (CDOM) in the open ocean by zooplankton and the colonial cyanobacterium Trichodesmium spp. Marine Ecology-Progress Series, 267, 45-56.

STEDMON, C. A., and MARKAGER, S., 2003, Behaviour of the optical properties of coloured dissolved organic matter under conservative mixing. Estuarine Coastal and Shelf Science, 57, 973-979.

STEDMON, C. A., OSBURN, C. L., and KRAGH, T., 2010, Tracing water mass mixing in the Baltic-North Sea transition zone using the optical properties of coloured dissolved organic matter. Estuarine Coastal and Shelf Science, 87, 156-162.

STEVENSON, F. J.(Ed.), 1982, Humus. chemistry, Genesis, Composition, Reaction(Canada: John Wiley&Sons).

STEWART, J. R., and BROWN, R. M., 1969, CYTOPHAGA THAT KILLS OR LYSES ALGAE. Science, 164, 1523.

STRAMSKI, D., REYNOLDS, R. A., BABIN, M., KACZMAREK, S., LEWIS, M. R., ROETTGERS, R., SCIANDRA, A., STRAMSKA, M., TWARDOWSKI, M. S., FRANZ, B. A., and CLAUSTRE, H., 2008, Relationships between the surface concentration of particulate organic carbon and optical properties in the eastern South Pacific and eastern Atlantic Oceans. Biogeosciences, 5, 171-201.

SUGIMURA, Y., and SUZUKI, Y., 1988, A high temperature catalytic oxidation me thod o f non-volatile dissolved organic carbon in seawater by direct injection o f liquid samples. Marine Chemistry, 24, 105-131.

SWAN, C. M., SIEGEL, D. A., NELSON, N. B., CARLSON, C. A., and NASIR, E., 2009, Biogeochemical and hydrographic controls on chromophoric dissolved organic matter distribution in the Pacific Ocean. Deep-Sea Research Part I-Oceanographic Research Papers, 56, 2175-2192.

SWETT, M. P., 2010, Assessment of benthic flux of dissolved organic carbon inestuaries using the eddy correlation technique. Master of scinece thesis. University of Main, USA.

TASSAN, S., and FERRARI, G. M., 2003, Variability of light absorption by aquatic particles in the near-infrared spectral region. Applied Optics, 42, 4802-4810.

THURMAN, E. M. (Ed.), 1985, Organic Geochemistry of Natural Waters, 497 (Netherland: Martinus Nijhoff/Dr W. Junk).

TOMING, K., ARST, H., PAAVEL, B., LAAS, A., and NOGES, T., 2009, Spatial and temporal variations in coloured dissolved organic matter in large and shallow Estonian waterbodies. Boreal Environment Research, 14, 959-970.

TWARDOWSKI, M. S., and DONAGHAY, P. L., 2001, Separating in situ and terrigenous sources of absorption by dissolved materials in coastal waters. Journal of Geophysical Research-Oceans, 106, 2545-2560.

TWARDOWSKI, M. S., BOSS, E., SULLIVAN, J. M., and DONAGHAY, P. L., 2004, Modeling the spectral shape of absorption by chromophoric dissolved organic matter. Marine Chemistry, 89, 69-88.

TWARDOWSKI, M. S., LEWIS, M., BARNARD, A. and ZANEVELD, J. R. V., 2005, In-water instrumentation and platforms for ocean color remote sensing applications. In: Remote Sensing of Coastal Aquatic Environments, R. Miller, C. Del Castillo and B. McKee (Ed.), 69–100 (Springer: Netherlands).

URBAN-RICH, J., 1999, Release of dissolved organic carbon from copepod fecal pellets in the Greenland Sea. Journal of Experimental Marine Biology and Ecology, 232, 107-124.

UHER, G., HUGHES, C., HENRY, G., and UPSTILL-GODDARD, R. C., 2001, Non-conservative mixing behavior of colored dissolved organic matter in a humic-rich, turbid estuary. Geophysical Research Letters, 28, 3309-3312.

VAN DER LEEDEN, F., TROISE, F.L., and TODD, D.K. (Eds), 1990, The Water Encyclopedia, pp. 126 (Chelsea, MI: Lewis).

VODACEK, A., HOGE, F. E., SWIFT, R. N., YUNGEL, J. K., and PELTZER, E. T., and BLOUGH, N. V., 1995, the use of in-situ and airborne fluorescence measurements to determine btv absorption-coefficients and doc concentrations in surface waters. Limnology and Oceanography, 40, 411-415.

VODACEK, A., BLOUGH, N. V., DEGRANDPRE, M. D., PELTZER, E. T., and NELSON, R. K., 1997, Seasonal variation of CDOM and DOC in the Middle Atlantic Bight: Terrestrial inputs and photooxidation. Limnology and Oceanography, 42, 674-686.

WALKER, N. D., 1996, Satellite assessment of Mississippi River plume variability: Causes and predictability. Remote Sensing of Environment, 58, 21-35.

WALKER, N. D., and HAMMACK, A. B., 2000, Impacts of winter storms on circulation and sediment transport: Atchafalaya-Vermilion Bay Region, Louisiana, U.S.A. Journal of Coastal Research, 16, 996-1010.

WALKER,N. D., 2005, Wind and eddy-related shelf/slope circulation processes and coastal upwelling in the northwestern Gulf of Mexico, in circulation in the Gulf of Mexico:observation and models. Geophysical Monograph Series, 161, 295-313.

WALKER, N. D., WISEMAN, W. J., ROUSE, L. J., and BABIN, A., 2005, Effects of river discharge, wind stress, and slope eddies on circulation and the satellite-observed structure of the Mississippi River plume. Journal of Coastal Research, 21, 1228-1244.

WALKER, N. D., and RABALAIS, N. N., 2006, Relationships among satellite chlorophyll a, river inputs, and hypoxia on the Louisiana continental shelf, gulf of Mexico. Estuaries and Coasts, 29, 1081-1093.

WETZEL, R. G., HATCHER, P. G., and BIANCHI, T. S., 1995, Natural photolysis by ultraviolet irradiance of recalcitrant dissolved organic matter to simple substrates for rapid bacterial metabolism. Limnology and Oceanography, 40, 1369-1380.

WILLIAM, P. M., and DRUGGEL, E.R.M., 1988, Dissolved organic matter in the ocean: Comments on a controversy. Oceanography, 1, 14-17.

WISEMAN, W.J., BANE, J.M., MURRAY, S.P., and TUBMAN, M.W., 1976, Small-scale temperature and salinity structure over the inner shelf west of the Mississippi River delta. Memo. Soc. Roy.Sci. Hiege, 6, 277 – 285.

WISEMAN, W. J., and KELLY, F. J., 1994, Salinity variability within the Louisiana coastal current during the 1982 flood season. Estuaries, 17, 732-739.

WISEMAN, W. J., and GARVINE, R. W., 1995, PLUMES AND COASTAL CURRENTS NEAR LARGE RIVER MOUTHS. Estuaries, 18, 509-517.

WISEMAN, W. J., RABALAIS, N. N., TURNER, R. E., DINNEL, S. P., and MACNAUGHTON, A., 1997, Seasonal and interannual variability within the Louisiana coastal current: stratification and hypoxia. Journal of Marine Systems, 12, 237-248.

XING, Y., 2010, Characterization of dissolved organic carbon in prairie surface waters using Fourier transform infrared spectroscopy. Mater of science thesis, University of Saskatchewan.

YENTSCH, C. S., LAPOINTE, B. E., POULTON, N., and PHINNEY, D. A., 2008, Anatomy of a red tide bloom off the southwest coast of Florida. Harmful Algae, 7, 817-826.

YONG SUN, D., LI, Y. M., WANG, Q., LU, H., LE, C. F., HUANG, C. C., and GONG, S.Q., 2011, A neural-network model to retrieve CDOM absorption from *in situ* measured hyperspectral data in an optically complex lake: Lake Taihu case study. International Journal of Remote Sensing, 32, 4005-4022.

ZAVALA-HIDALGO, J., MOREY, S. L., and O'BRIEN, J. J., 2003, Cyclonic eddies northeast of the Campeche Bank from altimetry data. Journal of Physical Oceanography, 33, 623-629.

ZEPP, R. G., CALLAGHAN, T., and ERICKSON, D., 1995, EFFECTS OF INCREASED SOLAR ULTRAVIOLET-RADIATION ON BIOGEOCHEMICAL CYCLES. Ambio, 24, 181-187.

ZHU, W., YU, Q., TIAN, Y. Q., CHEN, R. F., and GARDNER, G. B., 2011, Estimation of chromophoric dissolved organic matter in the Mississippi and Atchafalaya river plume regions using above-surface hyperspectral remote sensing. Journal of Geophysical Research-Oceans, 116.

ZWEIFEL, U. L., WIKNER, J., HAGSTROM, A., LUNDBERG, E., and NORRMAN, B., 1995, DYNAMICS OF DISSOLVED ORGANIC-CARBON IN A COASTAL ECOSYSTEM. Limnology and Oceanography, 40, 299-305.

VITA

Nazanin Chaichi Tehrani was born in Isfahan, Iran, in October 1979. She entered the Department of Physics at Karaj Azad University in September 1997 and received her B.Sc. degree in applied physics in July 2001. After her graduation from the Physics Department, she started her graduate studies in physical oceanography at Kish University and focused on simulation of currents and sediment transport in the Persian Gulf coasts. After completing her master studies in January 2004, Nazanin started teaching physics as an instructor at University of Applied Science and Technology in Karaj and at Qeshm Azad University. In June 2006, she joined the Water and Energy Research Company and worked on different hydrodynamics, sediment transport and coastal management projects. She entered Louisiana State University, Department of Oceanography and Coastal Science, as a master student in January 2010, and worked as a graduate research and teaching assistant. She will graduate with Master of Science Degree in Oceanography and Coastal Science in August 2012.